DIGITALCOMMONS
— @WAYNESTATE —

Wayne State University

Wayne State University Dissertations

1-1-2014

Modulation Of Water-Exchange Rates Of Lanthanide(iii)-Containing Complexes Using Polyethylene Glycol

Buddhima Nirodhi Siriwardena-Mahanama
Wayne State University,

Follow this and additional works at: http://digitalcommons.wayne.edu/oa_dissertations

Part of the Inorganic Chemistry Commons

Recommended Citation

Siriwardena-Mahanama, Buddhima Nirodhi, "Modulation Of Water-Exchange Rates Of Lanthanide(iii)-Containing Complexes Using Polyethylene Glycol" (2014). *Wayne State University Dissertations.* Paper 922.

This Open Access Dissertation is brought to you for free and open access by DigitalCommons@WayneState. It has been accepted for inclusion in Wayne State University Dissertations by an authorized administrator of DigitalCommons@WayneState.

MODULATION OF WATER-EXCHANGE RATES OF LANTHANIDE(III)-CONTAINING COMPLEXES USING POLYETHYLENE GLYCOL

by

BUDDHIMA N. SIRIWARDENA-MAHANAMA

DISSERTATION

Submitted to the Graduate School

of Wayne State University,

Detroit, Michigan

in partial fulfillment of the requirements

for the degree of

DOCTOR OF PHILOSOPHY

2014

MAJOR: CHEMISTRY

Approved by:

Advisor Date

DEDICATION

To my beloved parents and husband

ACKNOWLEDGMENTS

First and foremost, I wish to extend my sincere gratitude and thanks to my advisor, Dr. Matthew J. Allen for letting me join his group and for his guidance and support throughout the course of my research project. It was indeed a privilege to work under the guidance of such an outstanding mentor. I am thankful to my committee members, Dr. Claudio Verani, Dr. Sarah Trimpin, and Dr. Messer Ali for their valuable time and suggestions.

I also wish to thank past and present members of the Allen group including Dr. Yujiang Mei, Dr. Prabani Dissanayake, Dr. Jeremy Moore, Dr. Joel Garcia, Dr. Sashiprabha Vithanarachchi, Nipuni Gamage, Derek Averil, Akila Kuda-Wedagedara, Lauren Hopper, Zhijin Lin, Chamika Lenora, Levi Ekanger, Nikhil Barua, Lina Basal, Michael Cross, and Chengcheng Wang for their assistance, enlightening research discussions, and friendship during the course of the years I spent in the Allen group. I was truly fortunate to work in a group of talented and supportive chemists. A special thank you is extended to Jeremy for his help with HPLC and LCMS instrumentation, Derek for being a cheerful and gracious hood mate, and Lauren and Levi for proofreading two of my thesis chapters.

I am indeed grateful to the Department of Chemistry at Wayne State University for offering me the opportunity to pursue graduate studies.

I also wish to thank Dr. Bashar Ksebati for his assistance and cooperation with the use of NMR instruments, especially with variable-temperature ^{17}O-NMR experiments, Dr. Lew Hryhorczuk and Dr. Yuri Danylyuk for acquiring high-resolution mass spectrometry data, Corey Lambert for his assistance with running ICP-OES experiments, and Dr. Ellen Inutan and Dr. Chamara Senevirathne for their assistance with performing MALDI mass spectrometry.

My sincere appreciation is dedicated to Melissa Barton, Debbie McCreless, Erin Bachert

Mary Wood, Nestor Ocampo, science stores staff, business office staff, and main office staff for their support and making the Department of Chemistry a pleasant place.

I am sincerely thankful to Dr. Chatu Sirimanne for her generosity, advice, and assistance in numerous ways, all Sri Lankan friends including Asha, Chamika, Kumudumalie, Lakshika, Nalin, Prabuddha, Ravin, and Sachini for their support and friendship, friends in the Department of Chemistry for their acquaintance, and the Sri Lankan Student Association at Wayne State University for assistance given to help us settle down in the US.

I am indebted to my beloved parents Lakshman and Manil for all what they have done to make me what I am today and for their endless love, guidance, and moral support. I also wish to thank my dearest sisters, Hasanthi and Vimukthi, for their love, encouragement, and support given to me. Last, but not least, I extend my heartfelt gratitude to my loving husband, Lakmal, without whom, this dissertation could not have been possible. I am very grateful for your love, patience, understanding, wisdom, and for being the perfect husband for me.

TABLE OF CONTENTS

Dedication……………………………………………………………………………..ii

Acknowledgments..……………………………………………………………………iii

List of Tables…………………………………………………………………………. viii

List of Figures………………………………………………………………………… ix

List of Schemes……………………………………………………………………….xii

List of Abbreviations…………………………………………………………………. xiii

List of Symbols……………………………………………………………………….. xv

Chapter 1: Strategies for Optimizing Water-Exchange Rates of Lanthanide-Based Contrast Agents for Magnetic Resonance Imaging..…………………………….. 1

Introduction…………………………………………………………..……..1

Coordination-Chemistry-Based Strategies to Tune k_{ex}…….…………………………… 6

Modification of Water-Exchange Mechanism…………..……………………6

Modification of the Charge of a Ln^{III}-Containing Complex…………………. 12

Modification of Steric Hindrance at the Site of Water Coordination……….. 19

Modification of Ligand Side Chains...….……………………………………..26

Modification of TSAP/SAP Ratios for DOTA-Type Complexes……………. 30

Summary……………………………………………………………………… 36

Research approach….………………………………………………………… 37

Chapter 2: Ligand Design and Synthetic Approach…………………...…………………..... 39

Ligand Design...…...………………………………………………………………39

Synthetic Approach…………...……………………………………………………43

Experimental Procedures…………………………………………………………... 45

Applications………………………………………………………………………... 59

Chapter 3: Modulating Water-Exchange Rates of Lanthanide(III)-Containing Polyaminopolycarboxylate-Type Complexes Using Polyethylene Glycol……… 60

Introduction………………………………………………………………………60

Experimental Procedures…………………………………………………….. 63

Results and Discussion…...……………………………………………...….. 65

Analysis of Water-Coordination Number Data……………………………… 65

Analysis of Variable-Temperature ^{17}O-NMR Data………………………….. 65

Analysis of Relaxivity Data…..……………………………………………66

Analysis of Estimated Rotational Correlation Times (τ_R)…………………… 66

Conclusions………………………………………………………………………67

Chapter 4: Synthesis of Lanthanide(III)-Containing Polyethylene Glycol (PEG) Conjugates for the Investigation of the Influence of the Density of PEG on Water-Exchange Rates of Lanthanide(III)-Containing Complexes..……...……………………..68

Introduction….…………………………………………………………………...68

Synthesis of M^{III}-Containing PEG conjugates……..…………………………………71

Experimental Procedures…………………………………………………... 71

Synthesis of Eu^{III}-Containing PEG Conjugate **2.14e**…..……………………...72

Synthesis of Eu^{III}-Containing PEG Conjugates **2.17c** and **2.20c**……...………77

Synthesis of Eu^{III}-Containing Acetamide Conjugates **2.17a** and **2.20a**............83

Future Directions………………………...……………………………………… 85

Chapter 5: Summary, Conclusions, and Future Directions…..……………………………… 87

Summary…………………………………………………………………………87

Conclusions………………………………………………………………………91

Future Directions…………………...……………………………………………… 92

Appendix A: Chapter 2 NMR Spectra………………………………………………………...94

Appendix B: Chapter 2 HPLC Chromatograms……..………………………….…………. 110

Appendix C: Chapter 3 Data..…………..………...……………………….………………..117

Appendix D: Permissions……………………………………………………………….. 128

References……………………………………………………………………………..132

Abstract……………………………………………………………………………….. 141

Autobiographical Statement…………………………………………………………...143

LIST OF TABLES

Table 1.1 Water-exchange parameters obtained from ^{17}O-NMR spectroscopy and coordination numbers of complexes **1.1−1.11..**……………………………………7

Table 1.2 Water-exchange rates of complexes **1.12–1.42** determined from ^{17}O-NMR spectroscopy and CEST spectra for Gd^{III}- and Eu^{III}-containing complexes, respectively….………………………………………………………14

Table 1.3 Water-exchange rates of Gd^{III}-containing complexes **1.43–1.63** determined using ^{17}O-NMR spectroscopy………..…………..…………………………….. 21

Table 1.4 Water-exchange rates of Eu^{III}-containing DOTA-tetraamide complexes **1.40** and **1.66–1.80**…………………………………………………………………27

Table 1.5 Water-exchange rates and water-coordination numbers of Gd^{III}-containing HOPO-based (**1.4** and **1.81–1.83**) PEG conjugates..…………………………….... 30

Table 1.6 Water-exchange rates and TSAP/SAP ratios of Gd^{III}-containing complexes (**1.18–1.20** and **1.88–1.93**)……………………………..................................... 31

Table 3.1 Molecular parameters of complexes **2.13a–d**…………………………………... 65

Table 4.1 Different reaction conditions explored in the synthesis of Eu^{III}-containing PEG conjugate **2.14e**…...……………..……………………………………………74

Table 4.2 Elution time range of the two fractions collected during the purification of **2.14e** (reaction condition 4, **Table 4.1**)…..………………………………......... 74

Table 4.3 Elution time range of the three fractions collected during the purification of **2.14e** (reaction condition 4, **Table 4.1**)…....……………………………………… 76

Table 4.4 Different reaction conditions explored in the synthesis of Eu^{III}-containing PEG conjugates **2.17c** and **2.20c**….………………………...……………………79

Table 4.5 MWs of compounds present in reaction mixtures of **2.17c** or **2.20c**……...………. 82

Table 4.6 Different reaction conditions explored in the synthesis of Eu^{III}-containing PEG conjugates **2.17a** and **2.20a**…..…………………………………………….... 85

Table 4.7 MWs of compounds present in reaction mixtures of **2.17a** or **2.20a**………………85

Table 5.1 Molecular parameters of complexes **2.13a–d**…………………….………………..90

LIST OF FIGURES

Figure 1.1 Optimum water-exchange rates of T_1 and PARACEST agents……………..…….3

Figure 1.2 Representative Gd^{III}-containing complexes that undergo water exchange via dissociative (**1.1** and **1.2**), dissociative interchange (**1.9**), associative (**1.3**, **1.4**, **1.7**, **1.8**, **1.10**, and **11**), and associative interchange (**1.5** and **1.6**) processes[28–37]... 8

Figure 1.3 Ground and transition states of the water-exchange process. A. Stabilization and destabilization of the ground state lead to slower and faster water-exchange rates, respectively. B. Stabilization and destabilization of the transition state lead to faster and slower water-exchange rates, respectively..……..…………….. 9

Figure 1.4 Representative Gd^{III}- and Eu^{III}-containing complexes that relate the influence of charge (compounds **1.12**–**1.26**) and electron density of coordinating atoms (compounds **1.27**–**1.42**) to water-exchange rate[38–49]....…………..……….……… 15

Figure 1.5 Representative Gd^{III}-containing complexes **1.43**–**1.65** that relate the influence of steric hindrance at the water-coordination site to water-exchange rate[10,50–62]…20

Figure 1.6 Coordination polyhedron of Gd^{III}-containing complex **1.43**[10]…...……………… 21

Figure 1.7 Representative complexes **1.66**–**1.83** that relate the influence of bulkiness and polarity of ligand side chains to water-exchange rates[15,27,63–69]…...………… 26

Figure 1.8 Representative complexes **1.88**–**1.93** that relate the influence of TSAP/SAP ratios with water-exchange rates of DOTA-type complexes[41,70–77]………………. 31

Figure 1.9 Top-down view of (left) TSAP and (right) SAP isomers with the O–Gd^{III}–N twist angles indicated. In these views, the oxygen plane is above the Gd^{III} ion and the nitrogen plane is below the Gd^{III} ion….………..…………………........... 32

Figure 2.1 The DO3A-based ligand (**2.1**) designed to investigate the influence of length of PEG on water-exchange rates of Ln^{III}-containing complexes. This ligand system incorporates one amine-terminated arm that can be conjugated to one PEG moiety. The counteranion of ligand **2.1** is not shown for clarity…...……39

Figure 2.2 The DO3A- (**2.2**) and DO2A-based (**2.3**) systems designed to investigate the influence of density of PEG on water-exchange rates of Ln^{III}-containing complexes. Ligand **2.2** incorporates one arm that branches into two terminal amines and ligand **2.3** incorporates two amine-terminated arms. The terminal amines on ligands **2.2** and **2.3** can be conjugated to two PEG moieties. The counteranions of ligands **2.2** and **2.3** are not shown for clarity……....………….. 40

Figure 2.3 Structures of metal complexes **2.4–2.12** formed using ligands **2.1–2.3**. The counteranions of the complexes are not shown for clarity…..…………………..... 41

Figure 2.4 The structures of M^{III}-containing PEG conjugates, **2.13–2.21**, acetate, **a**, used as a control, and PEG moieties **b–e** used to investigate the influence of length and density of PEG on water-exchange rates of Ln^{III}-containing complexes. The counteranions of complexes **2.19–2.21** are not shown for clarity………....... 42

Figure 3.1 Structures of M^{III}-containing PEG conjugates **2.13a–d**, **2.14a–d**, and **2.15a–d**…. 62

Figure 4.1 The structures of M^{III}-containing PEG conjugates, **2.13–2.21**, *N*-acetoxysuccinimide, **4.1a**, used as a control, and PEG moieties **4.1c** and **4.1e** used to investigate the influence of density of PEG on water-exchange rates of Ln^{III}-containing complexes.……..………………………………………………… 70

Figure 4.2 SEC chromatograms (fluorescence response) of **2.14e** (reaction condition 4 in **Table 4.1**, top) and fractions 1 (middle) and 2 (bottom) collected using a Bio-Sil SEC 250 column (0.5 mL/min flow rate)……..…………………………...75

Figure 4.3 SEC chromatograms (fluorescence response) of fractions 1 (top) and 2 (bottom) collected using a Bio-Sil SEC 250 column (0.5 mL/min flow rate) from reaction condition 4 (**Table 4.1**) of **2.14e**…...……………………….……... 76

Figure 4.4 SEC chromatograms (fluorescence response) of fractions 1 (top) and 2 (bottom) collected from Sephadex G-25 chromatography from reaction condition 4 (**Table 4.1**)...……….…………………………………………………… 77

Figure 4.5 SEC chromatograms (fluorescence response) of **2.17c** obtained with a PL-aquagel OH column for reaction conditions 1 (top) and 4 (bottom) in **Table 4.4** in the absence and presence, respectively, of a large excess of DIEA……..… 80

Figure 4.6 SEC chromatograms (fluorescence response) of **2.17c** obtained with a PL-aquagel OH column for reaction conditions 1 (top) and 2 (bottom) in **Table 4.4** with 24 and 48 h reaction times, respectively……….……………............ 80

Figure 4.7 SEC chromatograms (fluorescence response) of **2.17c** obtained with a PL-aquagel OH column for reaction conditions 4 (top) and 5 (bottom) in **Table 4.4**………………………...……………………………………….................. 81

Figure 4.8 SEC chromatograms (fluorescence response) of **2.17c** obtained with a PL-aquagel OH column for reaction condition 3 at the end of 24 h (top), 48 h (middle), and 72 h (bottom)………..……………………………………… 82

Figure 5.1 The structures of M^{III}-containing PEG conjugates, **2.13–2.21**, acetate, **a**, used as a control, and PEG moieties **b–e** used to investigate the influence of length and density of PEG on water-exchange rates of Ln^{III}-containing complexes…...... 88

Figure 5.2 Positively charged Ln^{III}-containing complexes that can be conjugated to PEG with the potential to lead to slow water-exchange rates required for PARACEST agents…..……………………………………………………………93

LIST OF SCHEMES

Scheme 2.1 Four step retrosynthetic analysis of **2.13–2.15**. The counteranions of complexes **2.4–2.6** and ligand **2.1** are not shown for clarity……….…………. 43

Scheme 2.2 Four step retrosynthetic analysis of **2.16–2.18**. The counteranions of complexes **2.7–2.9** and ligand **2.2** are not shown for clarity……………..……… 44

Scheme 2.3 Four step retrosynthetic analysis of **2.19–2.21**. The counteranions of complexes **2.10–2.12** and ligand **2.3** are not shown for clarity…..………..…... 44

Scheme 2.4 Synthetic route to M^{III}-containing PEG conjugates **2.13a–e**, **2.14a–e**, and **2.15a–e**...…………….…………………………………………………47

Scheme 2.5 Synthetic route to M^{III}-containing PEG conjugates **2.16a–2.18a** and **2.16c–2.18c**…….…..……………………………………………………......53

Scheme 2.6 Synthetic route to M^{III}-containing PEG conjugates **2.19a–2.21a** and **2.19c–2.21c**….………………..……………………………………….....56

Scheme 4.1 Synthesis of Eu^{III}-containing PEG conjugate **2.14e** from Eu^{III}-containing complex **2.5**……….……………….……………………………..........73

Scheme 4.2 Synthesis of Eu^{III}-containing PEG conjugates **2.17c** and **2.20c** from Eu^{III}-containing complexes **2.8** and **2.11**, respectively………..………………………. 78

Scheme 4.3 Synthesis of Eu^{III}-containing acetamide conjugates **2.17a** and **2.20a** from Eu^{III}-containing complexes **2.8** and **2.11..**……..………………………………. 84

LIST OF ABBREVIATIONS

Abbreviation	**Term**
brs	broad singlet
calcd	calculated
CEST	chemical exchange saturation transfer
cyclen	1,4,7,10-tetraazacyclododecane
d	doublet
EPR	electron paramagnetic resonance
equiv	equivalents
HPLC	high performance liquid chromatography
HRESIMS	high-resolution electrospray ionization mass spectra
ICP-MS	inductively coupled plasma-mass spectrometry
ICP-OES	inductively coupled plasma-optical emission spectroscopy
Ln^{III}	lanthanide(III)
m	multiplet
MALDI	matrix assisted laser desorption ionization
MRI	magnetic resonance imaging
MW	molecular weight
MWCO	molecular weight cut off
nr	not reported
PARACEST	paramagnetic chemical exchange saturation transfer
PBS	phosphate buffered saline
PEG	polyethylene glycol
R_f	retention factor
SAP	square-antiprism
SBM	Solomon–Bloembergen–Morgan
SEC	size-exclusion chromatography
s	singlet
t	triplet
TSAP	twisted-square-antiprism
TLC	thin-layer chromatography

Abbreviation	**Term**	**Structure**
cyclen	1,4,7,10-tetraazacyclododecane	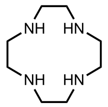
DO2A	1,4,7,10-tetraazacyclododecane-1,7-bis(acetic acid)	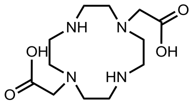
DO3A	1,4,7,10-tetraazacyclododecane-1,4,7-tris(acetic acid)	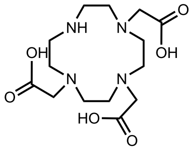
DOTA	1,4,7,10-tetraazacyclododecane-1,4,7,10-tetraacetate	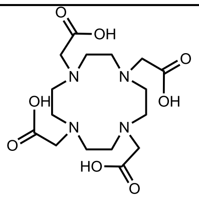
DTPA	diethylenetriamine tetraacetate	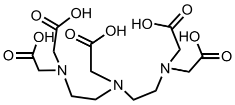
HOPO	2-hydroxypyridine-*N*-oxide	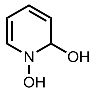

LIST OF SYMBOLS

Symbol	**Term**
μ_B	Bohr magneton
δ	chemical shift
g_L	electronic Landé *g*-factor
γ_S	electron gyromagnetic ratio
ω_S	electron Larmor frequency
r_{GdH}	electron spin-proton distance
ΔH	enthalpy change for the water-exchange process
r_1^{IS}	inner-sphere relaxivity
τ_{C1}	longitudinal correlation time
$1/T_{1e}$	longitudinal electron spin relaxation rate
T_{1e}	longitudinal electron spin relaxation time
$1/T_1^{\mathrm{DD}}$	longitudinal relaxation rate of coordinated water protons through dipole–dipole interactions
$1/T_1^{\mathrm{SC}}$	longitudinal relaxation rate of coordinated water protons through scalar coupling
$1/T_1$	longitudinal relaxation rate of water protons
T_{1m}	longitudinal relaxation time of coordinated water protons
T_1	longitudinal relaxation time of water protons
r_1	longitudinal relaxivity
B	magnetic field strength
γ_I	nuclear gyromagnetic ratio
r_1^{Obs}	observed longitudinal relaxivity
r_1^{OS}	outer-sphere relaxivity
ΔH_pp	peak-to-peak line width
ω_I	proton Larmor frequency
k_{ex} or $1/\tau_m$	rate of exchange between coordinated- and bulk-water molecules
τ_m	residency lifetime of coordinated water molecules
τ_R	rotational correlation time
S	total electron spin of paramagnetic metal ion
τ_{C2}	transverse correlation time
$1/T_{2e}$	transverse electron spin relaxation rate
T_{2e}	transverse electron spin relaxation time
μ_0	vacuum permeability
$\Delta V^\ddagger$	volume of activation for the water-exchange process
q	water-coordination number

CHAPTER 1. Strategies for Optimizing Water-Exchange Rates of Lanthanide-Based Contrast Agents for Magnetic Resonance Imaging

Parts of this chapter were adapted with permission from Siriwardena-Mahanama B.N.; Allen, M.J. *Molecules* **2013**, *18*, 9352–9381; published by MDPI, 2013.

Introduction

This chapter describes coordination-chemistry-based strategies from the past decade used to tune the water-exchange rates of lanthanide-based T_1-shortening and paramagnetic chemical exchange saturation transfer (PARACEST) contrast agents for magnetic resonance imaging (MRI) as well as the implications of these strategies on the development of new contrast agents, and will provide context to the research discussed in subsequent chapters.

MRI is a non-invasive imaging modality that is widely used in clinical medicine and biomedical research to generate three-dimensional images with a high spatial resolution (~1 mm^3) and excellent tissue penetration.[1] Conventional MRI generates contrast through differences in water proton density and the longitudinal and transverse relaxation times of water protons. These differences provide information regarding the chemical and physical nature of an imaged specimen. However, a key challenge associated with MRI is the low inherent contrast that is often observed.[2] To overcome this challenge, paramagnetic substances known as contrast agents are used to catalytically shorten the longitudinal (T_1) and transverse (T_2) relaxation times of nearby water protons.[2–4] This shortening leads to improved image contrast between regions that differ in the amount of contrast agent present. Contrast agents that shorten both longitudinal and transverse relaxation times to approximately the same degree are called T_1-shortening agents. Agents that shorten transverse relaxation times to a much greater extent than longitudinal relaxation times are called T_2-shortening agents. In general, T_1-shortening agents give rise to increased signal intensity and are referred to as positive contrast agents, and T_2-shortening agents give rise to a decreased signal intensity and are referred to as negative contrast agents.[5] Of these two types of agents, T_1-shortening agents are often favored because the darker images produced by T_2-shortening agents can be difficult to differentiate from background.[6] Consequently, the research described in this thesis will focus on T_1-shortening agents.

The most widely used clinical contrast agents are $\mathrm{Gd^{III}}$-containing acyclic or macrocyclic polyaminopolycarboxylate-based chelates. The efficiency of these $\mathrm{Gd^{III}}$-containing complexes as contrast agents is described by their ability to shorten the relaxation times of nearby water protons and is expressed as relaxivity, r_1, with units of $\mathrm{mM^{-1}\ s^{-1}}$. The relaxivity of $\mathrm{Gd^{III}}$-based contrast agents is governed by magnetic field strength and several structural, dynamic, and electronic parameters of the agents including the number of coordinated water molecules, q; the rate of exchange between coordinated and bulk water, k_{ex}; the distance between the $\mathrm{Gd^{III}}$ ion and coordinated water protons, r_{GdH}; the longitudinal and transverse electron spin relaxation times T_{1e} and T_{2e}, respectively; and the rotational correlation time of the agent, τ_R. The contributions of these molecular parameters to relaxivity are described by the Solomon–Bloembergen–Morgan (SBM) equations, and have been discussed in detail elsewhere.[7–9]

Based on the SBM equations, an optimum relaxivity of approximately 40 $\mathrm{mM^{-1}\ s^{-1}}$ per coordinated water molecule is expected at the clinically relevant field strength of 1.5 T for $\mathrm{Gd^{III}}$-containing contrast agents.[8,9] However, the observed relaxivity of clinically approved contrast agents is much lower (~4–5 $\mathrm{mM^{-1}\ s^{-1}}$) than the theoretical optimum value.[10] The low observed relaxivity suggests that the molecular parameters that govern the relaxivity of these agents need to be tuned. A great deal of research has been employed to tune the molecular parameters that influence relaxivity using coordination chemistry. For example, relaxivity increases as a function of water-coordination number, and water-coordination number is a molecular parameter that can be tuned through modification of ligands. However, the tuning of water-coordination number is limited by issues beyond relaxivity: increasing water-coordination number beyond two often compromises complex stability, which has a detrimental impact on toxicity. Another molecular parameter that can be tuned using coordination chemistry is rotational correlation time, where slow rotation leads to high relaxivity. Attempts to slow rotation through interactions with high-molecular weight species have been successful, but the maximum effect of high molecular weight interactions are not observed due to internal motion, slow water-exchange rates, or both. Therefore, tuning water-exchange rate becomes crucial in designing efficient T_1-shortening agents (**Figure 1.1**).

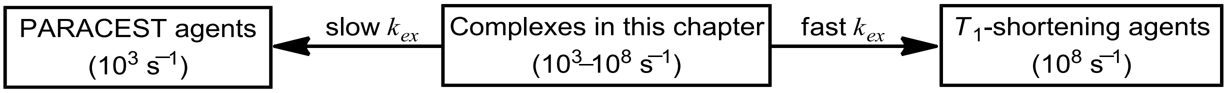

Figure 1.1. Optimum water-exchange rates of T_1 and PARACEST agents.

The optimum water-exchange rate for small-molecular T_1-shortening agents is ~10^8 s^{-1} at 1.5 T, based on the SBM equations, and this rate is roughly two orders of magnitude faster than the water-exchange rates of current clinical agents (~10^6 s^{-1}).[8–10] It is also important to note that water exchange provides the lower limit for proton exchange, but at physiologically relevant pH values, proton and water exchange are roughly the same.[9,11] Consequently, this chapter focuses on water-exchange rates and not proton-exchange rates.

In addition to T_1-shortening agents, a relatively new class of contrast agents that function based on the transfer of magnetization by chemical exchange of protons has gained much attention in the last two decades. These agents are referred to as chemical exchange saturation transfer (CEST) agents. One limitation of CEST agents is the small signal produced from direct presaturation of bulk water that occurs coincidentally during presaturation of exchangeable protons. This limitation can be overcome with the use of paramagnetic lanthanide(III) (Ln^{III})-containing complexes (in this chapter, Ln^{III} = Ce^{III}, Pr^{III}, Nd^{III}, Sm^{III}, Eu^{III}, Tb^{III}, Dy^{III}, Ho^{III}, Er^{III},

Tm^{III}, or Yb^{III}) that are able to shift the resonance frequency of exchangeable protons away from that of bulk water, and these complexes are called paramagnetic chemical exchange saturation transfer (PARACEST) contrast agents. Reviews of PARACEST agents in general can be found elsewhere.[12–14] The exchangeable protons on PARACEST agents can be O–H or N–H protons on a multidentate ligand or protons from Ln^{III}-coordinated water molecules that undergo chemical exchange with bulk water. This chapter focuses on water-exchange-based agents that are relevant to the research described in the rest of this thesis.

PARACEST agents give rise to a decrease in the bulk water magnetization as a result of the transfer of saturated magnetization from exchangeable protons (coordinated water molecules for the purpose of this chapter) to bulk water after selective presaturation of the coordinated-water protons. The efficiency of PARACEST agents is measured in terms of the magnitude of percent saturation transfer. For transfer of saturated magnetization to occur, the difference in resonance frequency between the two exchanging pools of protons, $\Delta\omega$, needs to be greater than or equal to the rate of exchange between the two pools of exchanging protons, k_{ex}.[15] Paramagnetic Ln^{III}-containing complexes can display $\Delta\omega$ values that are about an order of magnitude greater than those observed for diamagnetic systems that undergo magnetization transfer.[12,16] Large values of $\Delta\omega$ are advantageous because they enable selective presaturation of exchangeable protons without direct saturation of bulk water. For $\Delta\omega$ to be greater than or equal to the k_{ex}, PARACEST agents require slow water-exchange rates ($\sim 10^3$ s^{-1}) to maximize efficiency (**Figure 1.1**). However, most PARACEST agents developed to date display water-exchange rates that are about an order of magnitude faster ($\sim 10^4$ s^{-1}) than the optimum water-exchange rate.[17]

Tuning water-exchange rate is of great importance to achieve maximum efficiencies for both T_1-shortening and PARACEST agents; however, these classes of agents require tuning in opposite directions: T_1-shortening agents require fast rates and PARACEST agents require slow rates. The need to tune water-exchange rates over a broad range from slow ($\sim 10^3$ s^{-1}) to fast ($\sim 10^8$ s^{-1}) has led to an enormous focus on coordination-chemistry-based strategies to tune and on analytical techniques to measure the rates and mechanisms of exchange. Determination of the rates and mechanisms of water exchange of Ln^{III}-containing complexes has provided a general understanding of the influence of the structure of Ln^{III}-containing complexes on water-exchange rates. The water-exchange rates of Ln^{III}-containing complexes are often determined from the temperature-dependence of the transverse relaxation rates of ^{17}O-enriched water measured by variable-temperature ^{17}O-NMR spectroscopy. The mechanism of water exchange is determined from the volume of activation ($\Delta V^{\ddagger}$) obtained from the pressure-dependence of the transverse relaxation rate of ^{17}O-enriched water determined using variable-pressure ^{17}O-NMR spectroscopy. Experimental details for these measurements have been described elsewhere[18–20] and, therefore, are not included in this chapter. Because water-exchange rates depend on temperature, comparisons made among water-exchange rates in this chapter are only between rates measured at the same temperature. All water-exchange rates reported in the text have been determined at 25 °C unless otherwise noted.

The importance and determinants of water-exchange rate of Gd^{III}-based T_1-shortening agents were reviewed at the end of the last century.[21] In addition, the importance of water-exchange rates was reviewed recently with respect to responsive T_1-shortening and PARACEST agents.[22] The following text describes coordination-chemistry-based strategies explored over the last decade to tune the water-exchange rates of T_1-shortening and PARACEST agents and the implications of these strategies for improving the efficiency of both types of contrast agents.

Coordination-Chemistry-Based Strategies to Tune k_{ex}

Coordination-chemistry-based strategies that have been used to tune the water-exchange rates of Ln^{III}-containing complexes for T_1-shortening and PARACEST agents include modification of (1) the mechanism of water exchange; (2) the charge of the Ln^{III}-containing complex; (3) the steric hindrance at the site of water coordination; (4) the ligand side chains; and (5) the ratio of twisted-square-antiprism (TSAP) to square-antiprism (SAP) isomers for 1,4,7,10-tetraazacyclododecane-1,4,7,10-tetraacetate (DOTA)-type complexes. In addition to the five strategies listed above, the identity of the Ln^{III} ion in a complex also influences the magnitude of water-exchange rates.[23–27] However, this chapter focuses on strategies useful to both T_1-shortening and PARACEST agents, and therefore, a description of the influence of Ln^{III} ion on water-exchange rates is not included because Ln^{III} ions other than Gd^{III} are not useful for T_1-shortening agents. The following text is divided into separate sections that describe the five strategies listed above in terms of their implications to T_1-shortening and PARACEST agents. Although these strategies are separated in this text to enable structure–function comparisons to be made, it is important to note that these strategies are interrelated and cannot be completely isolated from each other.

Modification of Water-Exchange Mechanism

The mechanism of water exchange is an important determinant of the magnitude of water-exchange rates of Ln^{III}-containing complexes. In this section, the relationship between the mechanism of water exchange and water-exchange rate will be discussed using complexes **1.1**–**1.11** (**Table 1.1** and **Figure 1.2**). Water exchange in Ln^{III}-containing complexes proceeds via dissociative, associative, or interchange mechanisms. In a dissociative mechanism, dissociation of the coordinated water is rate limiting and precedes coordination of the incoming water molecule. In an associative mechanism, coordination of the incoming water molecule is rate limiting and precedes the dissociation of the coordinated water molecule. The interchange mechanisms are where transition states are not observed. Interchange mechanisms are divided in to dissociative interchange and associative interchange mechanisms depending on the relative contributions from bond breaking and forming: higher bond-breaking contributions lead to dissociative interchange and higher bond-forming contributions lead to associative interchange. Ln^{III}-containing complexes with coordination numbers of nine tend to undergo dissociative or dissociative interchange mechanisms of exchange, and complexes with coordination numbers of eight tend to undergo associative or associative interchange mechanisms of exchange.

Table 1.1. Water-exchange parameters obtained from ^{17}O-NMR spectroscopy and coordination numbers of complexes **1.1**−**1.11**.

Complex number	k_{ex} ($\times 10^6$ s^{-1})	$\Delta V^\ddagger$ (cm^3 mol^{-1})	q	Coordination number	Mechanism	Reference
1.1	4.1	10.5	1	9	dissociative	31
1.2	3.3	12.5	1	9	dissociative	31
1.2	7.0 (37 °C)	nr	1	9	dissociative	38
1.3	380	nr	2	8	associative[a]	30
1.4	130	nr	2	8	associative[a]	30
1.5	53	–5	2	8	associative interchange	29
1.6	102	–1.5	2	8	associative interchange	33
1.7	27	nr	1	8	associative[a]	34
1.8	170	nr	1	8	associative[a]	22
1.9	700	8.3	0.6	8 and 9	dissociative interchange	36
1.10	804	–3.3	8	8	associative	31
1.11	220	nr	1.4	9 and 10	associative[a]	37

nr = not reported, [a]associative, but no $\Delta V^\ddagger$ data given.

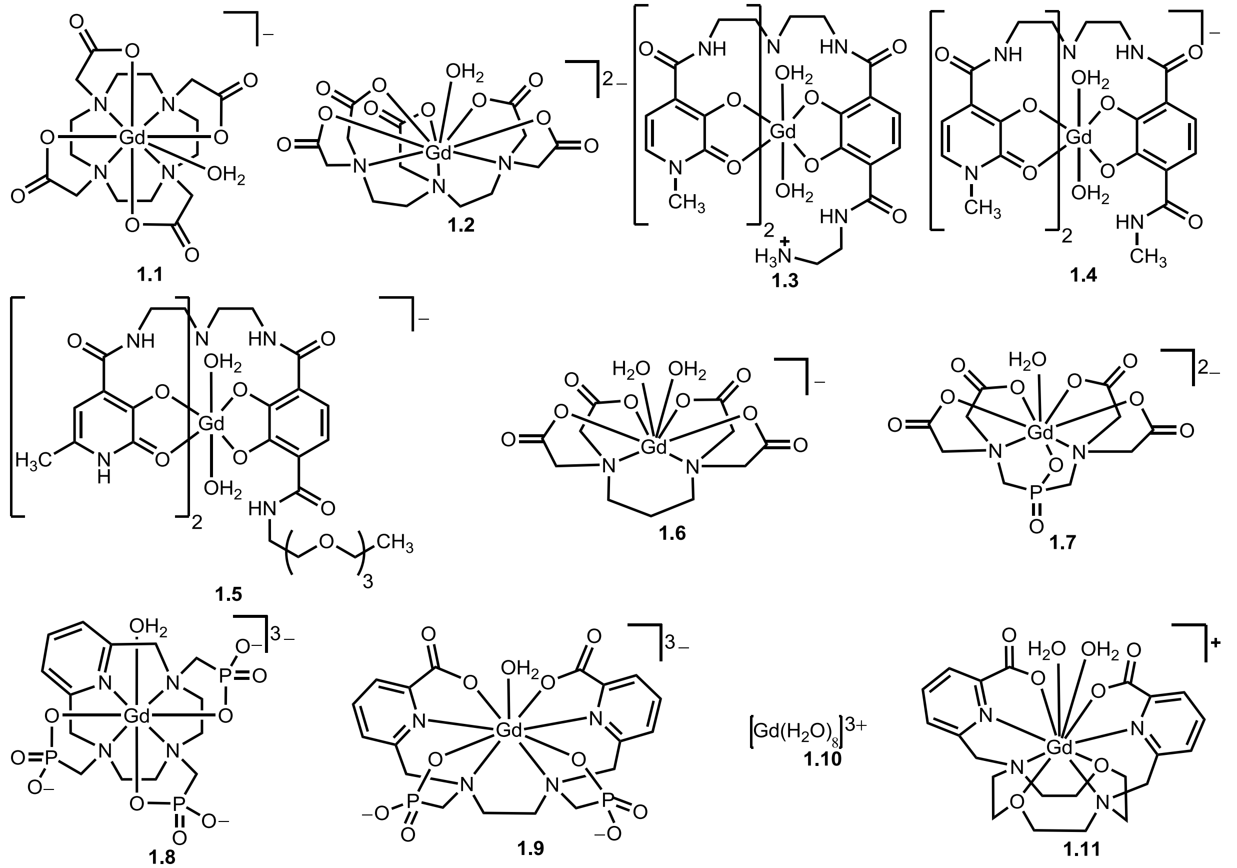

Figure 1.2. Representative Gd^{III}-containing complexes that undergo water exchange via dissociative (**1.1** and **1.2**), dissociative interchange (**1.9**), associative (**1.3**, **1.4**, **1.7**, **1.8**, **1.10**, and **11**), and associative interchange (**1.5** and **1.6**) processes.[28–37]

In aqueous solution, Ln^{III} aqua ions usually have water-coordination numbers of eight or nine, with large lanthanides (La^{III} to Nd^{III}) tending toward water-coordination number nine, medium-sized lanthanides (Sm^{III} to Gd^{III}) existing mostly in equilibrium between water-coordination numbers eight and nine, and small lanthanides (Tb^{III} to Lu^{III}) likely having water-coordination numbers of eight. Many polyaminopolycarboxylate-based ligands occupy eight coordination sites of Ln^{III} ions allowing space for the coordination of one water molecule. Because these types of complexes have coordinatively saturated (nine coordinate) ground states, they tend to undergo dissociative water exchange through a relatively unstable eight-coordinate transition state. Dissociative exchange often leads to slow water-exchange rates due to the large energy difference between the nine-coordinate ground state and the eight-coordinate transition state, and the rates of exchange could be increased by stabilizing the eight-coordinate transition state or destabilizing the nine-coordinate ground state. On the other hand, water-exchange rates could be decreased by stabilizing the nine-coordinate ground state or destabilizing the eight-coordinate transition state (**Figure 1.3**).

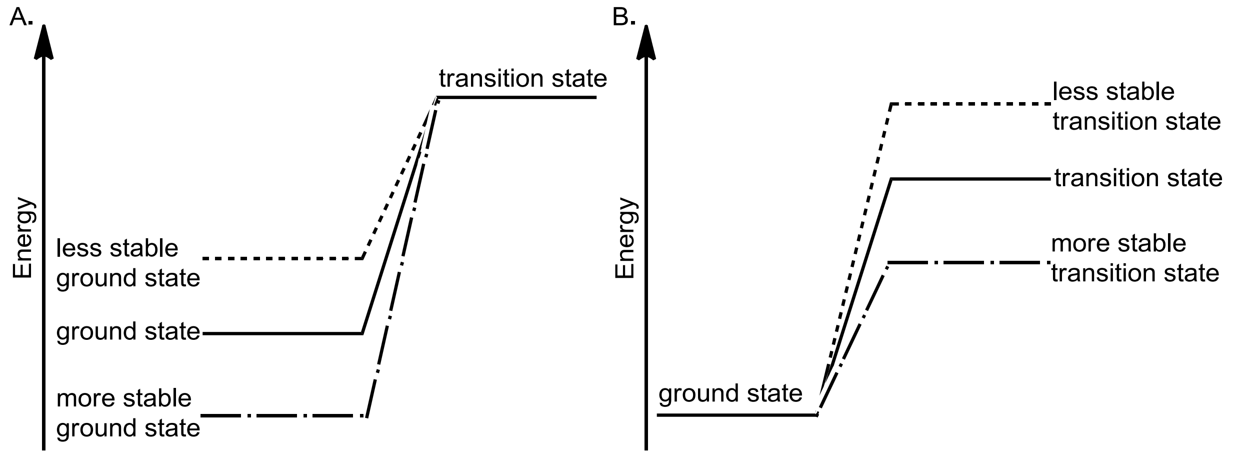
A.
Energy
transition state
less stable ground state
ground state
more stable ground state
B.
Energy
less stable transition state
transition state
more stable transition state
ground state

Figure 1.3. Ground and transition states of the water-exchange process. A. Stabilization and destabilization of the ground state lead to slower and faster water exchange-rates, respectively. B. Stabilization and destabilization of the transition state lead to faster and slower water-exchange rates, respectively.

Different from nine-coordinate complexes, eight-coordinate Ln^{III}-containing complexes used as contrast agents tend to have six or seven coordination sites occupied by a multidentate ligand, enabling the coordination of one or two water molecules in the inner coordination sphere of the Ln^{III} ion. Due to the coordinatively unsaturated ground state, eight-coordinate complexes tend to undergo associative water exchange through a nine-coordinate transition state. Because the energy gaps between eight-coordinate ground states and nine-coordinate transition states tend to be small, associative exchange mechanisms often display fast water-exchange rates.[28] Therefore, with eight-coordinate complexes, stabilization of the nine-coordinate transition state is a potential method to increase water-exchange rates, and stabilization of the eight-coordinate ground state is likely to decrease water-exchange rates.

Nine-coordinate polyaminopolycarboxylate complexes **1.1** and **1.2** display water-exchange rates on the order of 10^6 s^{-1}, and eight-coordinate complexes (compounds **1.3**–**1.8**) display relatively fast water-exchange rates (10^7–10^8 s^{-1}). These differences in water-exchange rates can be attributed in part to the differences in the mechanism of water exchange. The water-exchange rates of hydroxypyridonate (HOPO)-based complexes **1.3–1.5**, reported by Raymond and co-workers, are closer to the optimum water-exchange rate (10^8 s^{-1}) of T_1-shortening agents at 1.5 T than those of clinically approved polyaminopolycarboxylate-based complexes **1.1** and **1.2**.[28–31] Similar to HOPO-based complexes, the fast water-exchange rates observed for polyaminopolycarboxylate-based complexes **1.6** and **1.7** and phosphonate-containing complex **1.8** can be attributed in part to an associative exchange mechanism.[32–34]

As mentioned earlier, water-exchange rates can be increased by stabilizing the transition state formed during the exchange process. This idea is exemplified by the 3-fold faster water-exchange rate of complex **1.3** relative to complex **1.4**.[30] This difference in water-exchange rate is likely due to the accommodation of a third water molecule in the inner-coordination sphere through intra-molecular hydrogen bonding between the primary amine of complex **1.3** and a third water molecule. Stabilization of the nine-coordinate transition state through intra-molecular hydrogen bonding is likely the cause of the faster water-exchange rate for complex **1.3**.[30] In another example, linear complex **1.9**, despite undergoing dissociative exchange, displays a water-exchange rate that is 210-times greater than the rate for linear complex **1.2** and is nearly as fast as the Gd^{III}-aqua complex, **1.10**. This extremely fast water-exchange rate is likely due to the existence of both eight- and nine-coordinate species in solution as observed by variable-temperature UV–vis spectroscopy of the Eu^{III} analog of complex **1.9**, implying that the eight-coordinate transition state is stabilized.[35,36] In a similar study, but on a macrocyclic complex, Tóth and co-workers demonstrated that macrocyclic complex **1.11** displayed a water-exchange rate that is 54-times faster than the rate of macrocyclic complex **1.1**, because of an equilibrium between two hydration states (q = 1 and q = 2) with coordination-numbers nine and ten based on variable-temperature UV–vis spectroscopy. Complex **1.11** likely undergoes associative exchange based on the large negative activation entropy (–35 J mol^{-1} K^{-1}); however, the authors did not report the volume of activation for complex **1.11**.[37]

The fast water-exchange rates (10^7–10^8 s^{-1}) of complexes **1.3**–**1.9** and **1.11** are desirable starting points for the design of T_1-shortening agents. Designing eight-coordinate complexes with the ability to undergo associative exchange and complexes in which eight- and nine-coordinate species are in equilibrium with one another is desirable to attain fast water-exchange rates for T_1-shortening agents. In addition to complexes that undergo associative exchange, complexes that undergo dissociative exchange, but with stable eight-coordinate transition states are likely to display fast water-exchange rates desirable for T_1-shortening agents. However, stabilizing the eight-coordinate transition state can be challenging for most polyaminopolycarboxylate-based ligands because these ligands tend to favor complexes with coordination number nine. On the other hand, the fast water-exchange rates of complexes **1.3**–**1.9** and **1.11** and the relatively slower exchange rates (10^6 s^{-1}) of nine-coordinate polyaminopolycarboxylate-based complexes **1.1** and **1.2** are orders of magnitude too fast to be useful for PARACEST agents. Therefore, designing coordinatively saturated nine-coordinate complexes that undergo dissociative exchange is a useful starting point for the development of PARACEST agents. Moreover, stabilizing the nine-coordinate ground state, for example through hydrogen-bond interactions, would lead to a larger energy gap between the ground and transition states, potentially leading to slow water-exchange rates. Stabilization of the nine-coordinate ground state leads to slow water-exchange rates, which at first glance seems opposite to the fast water-exchange rate observed for complex **1.3** when the nine-coordinate transition state was stabilized. However, the opposite trends in water-exchange rates can be rationalized based on the difference in the mechanism of exchange: *dissociative* mechanisms have slow water-exchange rates with stable nine-coordinate *ground states*, and *associative* mechanisms have fast water-exchange rates with stable nine-coordinate *transition states*.

Modification of the Charge of a Ln^{III}-Containing Complex

The charge of Ln^{III}-containing complexes is another important determinant of the magnitude of water-exchange rate, and this section describes the influence of complex charge and electron density of the coordinating atoms on water-exchange rate using complexes **1.12**–**1.42** as examples (**Table 1.2** and **Figure 1.4**). It is important to note that modification of charge toward positively charged complexes is expected to lead to increased proton-exchange rates;[11] however, discussion of proton-exchange rates is beyond the scope of this chapter. Also, the differences in water-exchange rates described in this section are explained in terms of charge density only, although the charge density at the Ln^{III} center closely correlates with Lewis acidity of the Ln^{III} ion. The influence of the charge of a complex on water-exchange rates is exemplified by the 2- to 8-times slower water-exchange rate that is observed for monoamide complexes **1.12** and **1.13** and bisamide complex **1.14** compared to the all carboxylate complex **1.2**.[38,39] Not only is the charge of a Ln^{III}-containing complex important for tuning water-exchange rates, but the charge density at the Ln^{III} center is equally important. The atoms directly coordinating to a Ln^{III} ion tend to have the greatest impact on the charge density at the Ln^{III} center. Modifying the coordinating atoms can change the charge density, thereby altering the water-exchange rate. For example, a slowing of water-exchange rates is observed in macrocyclic amide derivatives **1.15**–

1.17 relative to the all-carboxylate macrocyclic complex **1.1**.[40] This slowing of water-exchange rates occurs due to the higher positive charge density at the Gd^{III} center, regardless of the increasing negative charge of the phosphonate side chains in the series **1.15**–**1.17**. The slowing of water-exchange rates in amide-containing complexes is proportional to the number of amide groups that coordinate to the Ln^{III} ion.

In general, faster water-exchange rates are observed in complexes with less positive charges. For example, an 18- and 4.5-fold difference in water-exchange rate was observed between negatively charged complexes **1.18** and **1.19** and structurally similar, but neutral complex **1.20**.[41] Another example demonstrated that the water-exchange rate of negatively charged Gd^{III}-containing 1,4,7,10-tetraazacyclododecane-1,4,7-triacetate (DO3A) derivative **1.21** with a monodentate phosphonate group displayed a water-exchange rate that is 170-times faster than that of the neutral DO3A derivative **1.22** with a bidentate ethoxyacetate moiety.[42] The difference in water-exchange rate between negatively charged and neutral complexes is possibly due to the difference in charge between the two complexes but is likely also due to the change in the functional groups (discussed in subsequent sections on influence of steric hindrance and ligand side chains on water-exchange rates). Based on the correlation between fast water-exchange rates and positive charges, complexes with less positive charge at the Gd^{III} center are desirable for designing Gd^{III}-containing T_1-shortening agents with fast water-exchange rates.

Table 1.2. Water-exchange rates of complexes **1.12**–**1.42** determined from ^{17}O-NMR spectroscopy and CEST spectra for Gd^{III}- and Eu^{III}-containing complexes, respectively.

Complex	k_{ex} ($\times 10^6$ s^{-1})	Ln^{III} ion	Reference
1.12	1.9	Gd^{III}	39
1.13	1.3	Gd^{III}	39
1.14	0.85 (37 °C)	Gd^{III}	38
1.15	0.77	Gd^{III}	40
1.16	0.16	Gd^{III}	40
1.17	0.038	Gd^{III}	40
1.18	80	Gd^{III}	41
1.19	20	Gd^{III}	41
1.20	4.4	Gd^{III}	41
1.21	78.7	Gd^{III}	42
1.22	0.457	Gd^{III}	42
1.23	0.98	Gd^{III}	43
1.24	0.60	Gd^{III}	43
1.25	14.1	Gd^{III}	44
1.26	6.29	Gd^{III}	44
1.27	17.6	Gd^{III}	45
1.28	7.4	Gd^{III}	45
1.29	1.7	Gd^{III}	46
1.30	0.66	Gd^{III}	46
1.31	0.0069	Eu^{III}	47
1.32	0.0051	Eu^{III}	47
1.33	0.0037	Eu^{III}	47
1.34	0.0033	Eu^{III}	47
1.35	0.0031	Eu^{III}	47
1.36	0.0028	Eu^{III}	47
1.37	0.018	Eu^{III}	48
1.38	0.012	Eu^{III}	48
1.39	0.005	Eu^{III}	48
1.40	0.00290	Eu^{III}	49
1.41	0.00253	Eu^{III}	49
1.42	0.00211	Eu^{III}	49

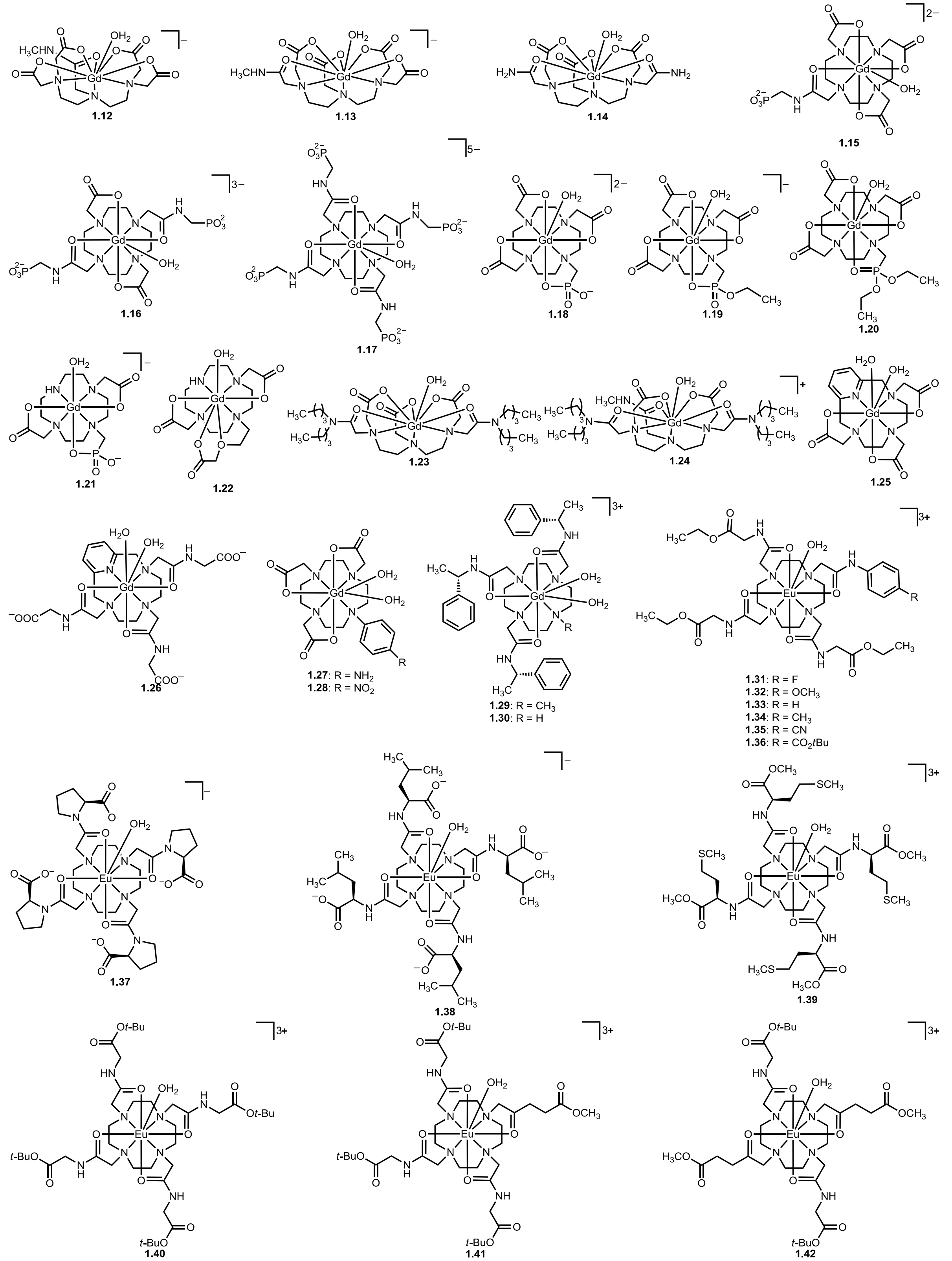
1.12
1.13
1.14
1.15
1.16
1.17
1.18
1.19
1.20
1.21
1.22
1.23
1.24
1.25
1.26
1.27: R = NH2
1.28: R = NO2
1.29: R = CH3
1.30: R = H
1.31: R = F
1.32: R = OCH3
1.33: R = H
1.34: R = CH3
1.35: R = CN
1.36: R = CO2tBu
1.37
1.38
1.39
1.40
1.41
1.42

Figure 1.4. Representative Gd^{III}- and Eu^{III}-containing complexes that relate the influence of charge (compounds **1.12**–**1.26**) and electron density of coordinating atoms (compounds **1.27**–**1.42**) to water-exchange rate.[38–49]

On the other hand, reducing the water-exchange rate is desirable when designing PARACEST agents, and complexes with high positive charges on the Ln^{III} ion tend to lead to slow water-exchange rates. As mentioned earlier, the observed 8.2-fold difference in water-exchange rate between negatively charged linear complex **1.2** and the analogous neutral linear complex **1.14** at 37 °C is an example of slowing of water-exchange rates with higher overall positive charge and higher positive charge on the Ln^{III} ion.[38] Similarly, a 1.6-fold difference in water-exchange rate was observed between neutral, linear complex **1.23** and the analogous positively charged complex **1.24**.[43] Complexes **1.23** and **1.24** are structurally similar but have different charges; consequently, the slowing of water-exchange rate can be attributed at least partially to the difference in charge between **1.23** and **1.24**. In another example, a 2.2-fold difference in water-exchange rate was observed between neutral, macrocyclic Gd^{III}-containing complex **1.25** and neutral glycine derivative **1.26**.[44] Although complexes **1.25** and **1.26** are both neutral, the charge distribution on the complexes is different. Complex **1.26** has the negative ligand-based charges farther away from the Gd^{III} ion than in complex **1.25**, resulting in a lower density of positive charge close to the Gd^{III} ion in complex **1.25** relative to **1.26**. This difference in charge density at the Gd^{III} center likely is responsible for the differences in water-exchange rates between complexes **1.25** and **1.26**. Observations that slow water-exchange rates occur with more positive charges suggest that complexes with more positive charges are potentially useful in designing PARACEST agents with slow water-exchange rates.

To further probe the influence of charge density near a Ln^{III} ion on water-exchange rates, the electronic effects of coordinating atoms have been studied. As an example, Aime and co-workers demonstrated that the water-exchange rates of neutral DO3A-type complexes can be varied by altering the electronic properties of coordinating macrocyclic nitrogen atoms.[45] In this example, complexes **1.27** and **1.28** differ in the substituent on the *para*-position of the phenyl group attached to a coordinating macrocyclic nitrogen atom. A 2.4-fold faster water-exchange rate was observed with complex **1.27**, with an electron-donating amino group, relative to complex **1.28**, with an electron-withdrawing nitro group.[45] Moreover, the influence of electron-donating methyl groups on water-exchange rates of triamide derivatives of DO3A-type complexes has also been investigated. Complex **1.29** that contains an electron-donating methyl substituent displayed a 2.6-fold faster water-exchange rate than non-methyl-containing analog **1.30**.[46] The relatively fast water-exchange rates in complexes **1.27** and **1.29** compared to **1.28** and **1.30** can be attributed to the electron density on the macrocyclic nitrogen atoms. This density can neutralize some of the positive charge on the Ln^{III} ion resulting in weak interactions with water and facilitate the dissociation of coordinated water from the Ln^{III} ion. In addition to electron density, steric hindrance at the water-coordination site caused by the methyl group in complex **1.29** (described in the subsequent section that discusses influence of steric hindrance on water-exchange rates) is likely another contributing factor to the faster water-exchange rate of complex **1.29** relative to complex **1.30**.

The influence of the electron density of macrocyclic nitrogen donors on water-exchange rates is similar to the influence of electron density on arm donors. In one study, Sherry and co-workers investigated the series of complexes **1.31**–**1.36** containing substituents with different electronic properties, and demonstrated that water-exchange rate can be tuned by varying the electron density on the coordinating amide group. In this study, mesomeric electron-donating groups (OCH_3) led to fast exchange rates, and mesomeric electron-withdrawing groups (CO_2*t*-Bu and CN) led to slow exchange. However, the opposite trend was reported for inductively donating (CH_3) and withdrawing (F) groups.[47] In another example, a series of three complexes (compounds **1.37**–**1.39**) was investigated, where complexes **1.37** and **1.38** displayed 3.6- and 2.4-times faster water-exchange rates, respectively, relative to complex **1.39**. This observation was expected based on the calculated Mulliken charges on the coordinating carbonyl oxygen atoms. In this series of complexes, the negative charge on the coordinating carbonyl oxygen atoms ranges from most negative in complex **1.37** to least negative in complex **1.39**.[48] The idea that lower charge density on the coordinating atom leads to slower water-exchange rates was expanded to investigate the suitability of ketones to achieve slow water-exchange rates desirable for PARACEST agents.[49] In this study of complexes **1.40**–**1.42**, water-exchange rates were 1.1- to 1.4-times faster in complex **1.40** relative to complexes **1.41** and **1.42**, respectively. These observations are consistent with water-exchange rate being dependent on the number of poorly electron donating ketone-donor arms in the complex.

Based on the studies described in this section, negatively charged complexes with carboxylate and phosphonate donors lead to fast water-exchange rates compared to positively charged complexes with amide donors. Moreover, water-exchange rates become faster as a function of the negative charge of the complex, low positive charge density at the $\mathrm{Ln^{III}}$ center, or both. These features that lead to fast water-exchange rates are desirable for the design of T_1-shortening agents. The opposite is true for PARACEST agents, where positively charged complexes with amide and ketone donors tend to be useful as PARACEST agents because complexes with high positive charges favor slow water-exchange rates. However, complexes with poorly donating amide and ketone groups tend to display lower stability relative to negatively charged complexes with strong carboxylate donors, and stability of these complexes is critical in designing contrast agents.

Modification of Steric Hindrance at the Site of Water Coordination

Another parameter that influences water-exchange rates is the degree of steric hindrance at the water-coordination site. This parameter is related to mechanism of exchange (discussed in the first section) and isomer ratio (described in the last section); increased steric hindrance leads to faster water-exchange rates in complexes that undergo dissociative water exchange because crowding the water-coordination site favors dissociation of the coordinated water molecule, which is the rate-limiting step. The influence of steric hindrance at the site of water coordination on water-exchange rate is described in this section using complexes **1.43–1.65** (**Figure 1.5** and **Table 1.3**).

Merbach and coworkers demonstrated that complex **1.43**, an analog of macrocyclic complex **1.1** with an extended macrocyclic backbone that is one carbon longer than the macrocyclic backbone of complex **1.1**, has a 66-fold faster water-exchange rate relative to complex **1.1**. The difference in water-exchange rates was attributed to the increased steric encumbrance at the site of water coordination that results from the difference between the five-membered and six-membered rings formed between the macrocycles and the Ln^{III} ions.[10] The argument of increased steric hindrance is supported by the differences in the Gd^{III}–$O_{carboxylate}$ distances and the $O_{carboxylate}$–Gd^{III}–$O_{carboxylate}$ angles (**Figure 1.6**). Although complexes **1.1** and **1.43** have similar Gd^{III}–O_{water} distances of 2.45 and 2.48 Å, respectively, they have markedly different Gd^{III}–$O_{carboxylate}$ distances of 0.70 and 0.83 Å, respectively. These data indicate that the negatively charged carboxylate plane is closer to the axially coordinated water molecule in complex **1.43** than in complex **1.1**. This argument is further supported by the differences in the $O_{carboxylate}$–Gd^{III}–$O_{carboxylate}$ angles (136.7 and 142.7° for complex **1.43** vs 146° for **1.1**) implying that the carboxylate plane around the Gd^{III} ion is more compact in complex **1.43** than in complex **1.1**.[10]

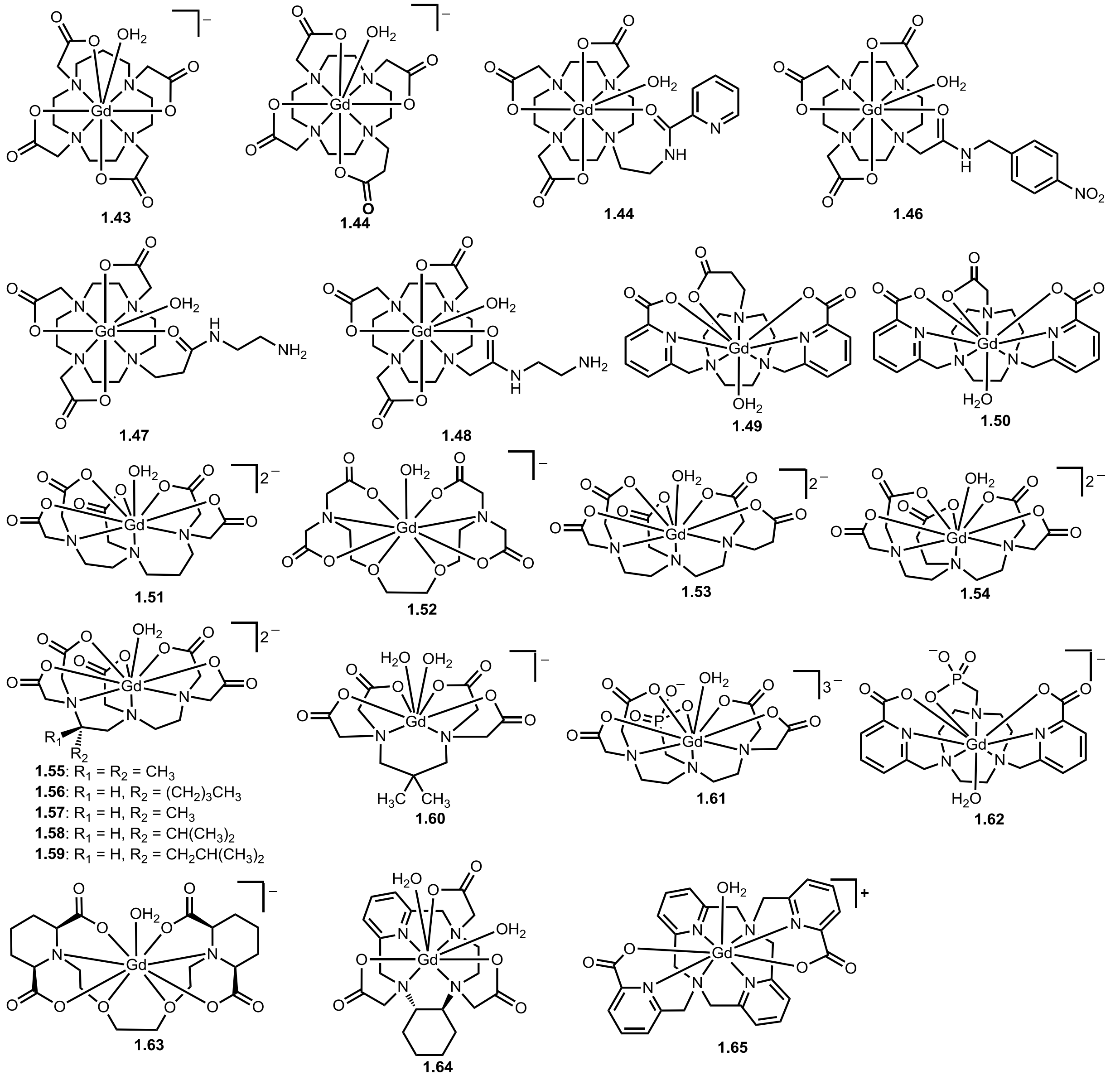
1.43
1.44
1.44
1.46
1.47
1.48
1.49
1.50
1.51
1.52
1.53
1.54
1.55: R1 = R2 = CH3
1.56: R1 = H, R2 = (CH2)3CH3
1.57: R1 = H, R2 = CH3
1.58: R1 = H, R2 = CH(CH3)2
1.59: R1 = H, R2 = CH2CH(CH3)2
1.60
1.61
1.62
1.63
1.64
1.65

Figure 1.5. Representative Gd^{III}-containing complexes **1.43–1.65** that relate the influence of steric hindrance at the water-coordination site to water-exchange rate.[10,50–62]

Table 1.3. Water-exchange rates of Gd^{III}-containing complexes **1.43**–**1.63** determined using ^{17}O-NMR spectroscopy.

Complex	k_{ex} (×10^6 s^{-1})	Reference
1.43	270	10
1.44	61	50
1.45	110	51
1.46	1.6	52
1.47	81.2	53
1.48	1.1	53
1.49	86	54
1.50	0.6	54
1.51	330	55
1.52	31	56
1.53	80	50
1.54	31	50
1.55	18 (37 °C)	57
1.56	12 (37 °C)	57
1.57	11 (37 °C)	57
1.58	10 (37 °C)	57
1.59	9.26 (37 °C)	57
1.60	43	58
1.61	11	59
1.62	34	54
1.63	59	60
1.64	29	61
1.65	63	62

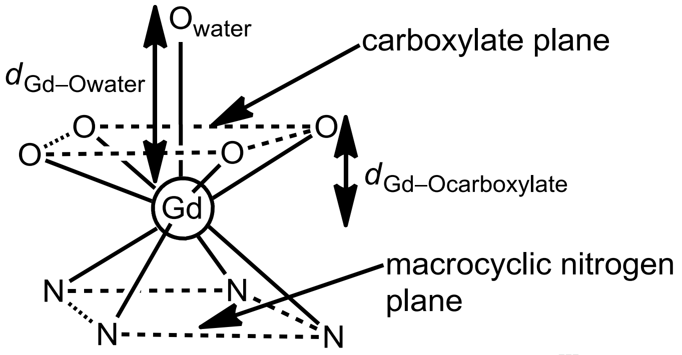
O_{water}
d_{Gd–Owater}
carboxylate plane
O
O
O
O
Gd
d_{Gd–Ocarboxylate}
macrocyclic nitrogen plane
N
N
N
N

Figure 1.6. Coordination polyhedron of Gd^{III}-containing complex **1.43**.[10]

The steric difference between five and six-membered rings in chelation also can be observed in the arms of the complexes. Complex **1.44**, with an extended carboxylate arm that is one carbon longer than the arms in complex **1.1**, displayed a 15-fold faster water-exchange rate than complex **1.1**. This difference is likely due to the increased steric hindrance at the site of water coordination, similar to the system with an extended macrocycle.[50] Based on the water-exchange rates of **1.43** and **1.44**, extending the macrocyclic backbone has a more pronounced effect in increasing the water-exchange rates of DOTA-type complexes compared to extending one of the arms.

In another example, DOTA-monoamide derivative **1.45**, with an amide group separated by an ethylene bridge from the macrocyclic nitrogen, displayed a water-exchange rate that is 69-times faster than the analogous DOTA-monoamide complex **1.46**.[51,52] The fast water-exchange rate of **1.45** is likely due to the steric hindrance at the water-coordination site, imposed by the seven membered chelate formed by the ethylene bridge between the macrocyclic nitrogen and the amide oxygen compared to the five membered chelate in DOTA-monoamide complex **1.46**. A similar trend in water-exchange rates was observed between DOTA-monoamide complexes **1.47** and **1.48** where complex **1.47** displayed a water-exchange rate that is 74-times faster than that of complex **1.48**.[53] The faster water-exchange rate of complex **1.47** relative to complex **1.48** is possibly due to the steric constraints at the site of water-coordination caused by the six membered chelate in **1.47** relative to the five membered chelate in **1.48**. Similar to the fast water-exchange rates observed for DOTA-monoamide derivatives **1.45** and **1.47**, a 143-fold difference in water-exchange rate was observed between triaza-macrocyclic complex **1.49** with a propionate arm and the analogous triaza-macrocyclic complex **1.50** with an acetate arm. The difference in water-exchange rate between complexes **1.49** and **1.50** was reportedly due to the increased steric hindrance at the site of water coordination caused by the extended propionate arm.[54] These studies suggest that the steric environment caused by ring size is generalizable to different sizes of macrocyclic ligand backbones.

The work on elongation of the macrocyclic backbones was extended into linear diethylene triamine pentaacetate (DTPA)-type systems by Merbach and coworkers. In one study, complex **1.51**, which is structurally similar to complex **1.2** but with an extra carbon in the nitrogen backbone, displayed a 100-fold faster water-exchange rate relative to that of complex **1.2**. The faster water-exchange rate of **1.51** relative to **1.2** was reported to be due to the steric hindrance caused by the extra carbon in the backbone of **1.51**.[55] In another example, complex **1.52** with an ether-based oxy-ethylene bridge in the backbone led to a water-exchange rate that is 9.4-times faster than that of complex **1.2**. The difference in water-exchange rate between **1.2** and **1.52** can be attributed to the 3% longer Gd–O$_{\text{water}}$ distance in **1.52** compared to **1.2**, possibly due to steric hindrance caused by the ethylene bridge on the backbone of **1.52**, which facilitates the dissociation of the coordinated water molecule.[56] However, because there are multiple structural differences between complexes **1.2** and **1.52**, it is likely that no single difference is responsible for the entire change in water-exchange rate.

In addition to extending the linear backbone, DTPA-type complexes with extended arms have been synthesized to study the influence of arm extensions on water-exchange rates. For example, a 24-fold difference in water-exchange rate was observed between DTPA analog **1.53** with an extended carboxylate arm and the parent complex **1.2**.[50] Furthermore, with DTPA-type complexes, the position of the extended carboxylate arm (whether terminal or central) also influences the water-exchange rate. Complex **1.53**, with a terminal extended carboxylate arm, has a water-exchange rate that is 2.6-times faster than that of complex **1.54** with a central extended carboxylate arm.[50] This observation implies that the extension of terminal carboxylates causes more steric hindrance at the site of water coordination and leads to faster water-exchange rates compared to extension of the central carboxylate arm. Unlike with macrocyclic complexes, extension of the nitrogen backbone with linear complexes generally has a higher impact on water-exchange rates than extending one of the carboxylate arms.

In addition to extending multidentate ligand backbones and arms, the influence of steric crowding caused by backbone substitution on the water-exchange rates was studied using the series of linear complexes **1.55**–**1.59**.[57] In this series, the complexes differ from one another in the alkyl-group substitution on the ethylene carbons. The dialkyl substituted complex **1.55** has a water-exchange rate that is 2.6-times faster than complex **1.2** at 37 °C, and monoalkyl substituted complexes **1.56**–**1.59** display water-exchange rates that are 1.3- to 1.7-times faster than the parent unsubstituted complex **1.2** at 37 °C. The faster water-exchange rates of the alkyl substituted complexes relative to parent complex **1.2** are likely due to the increased steric hindrance in the inner-coordination sphere.[57] A similar study demonstrated that dimethyl-substituted complex **1.60** had a 1.3-fold faster water-exchange rate than parent complex **1.6**.[58] A confounding point with complex **1.6** is that it has two different reported water-exchange rates (102×10^6 s^{-1} and 33×10^6 s^{-1})[33,58], and the 1.3-fold difference in rates is not observed if the wrong value is used when comparing complexes **1.6** and **1.60**. As with the other systems, this result is likely due to the increased steric hindrance from the methyl substitution.

In addition to using alkyl groups to investigate the influence of steric crowding on water-exchange rates, complexes containing bulky phosphonate arms display faster water-exchange rates relative to complexes with no phosphonates. This difference in rates is likely at least partially due to the steric hindrance at the site of water-coordination caused by the large size of the phosphonate groups. For example, phosphonate-containing complex **1.61** displayed a water-exchange rate that is 3.5-times faster than that of the parent complex **1.2**.[59] In another example, phosphonate-containing triaza-macrocyclic complex **1.62** displayed a 57-fold faster water-exchange rate relative to the non-phosphonate-containing analog **1.50**.[54]

Rigidifying the backbone of polyaminopolycarboxylate-based ligands is another strategy that often results in faster water-exchange rates, possibly due to enhanced steric crowding caused by substituents used to rigidify the ligand backbone. For example, backbone rigidification in complex **1.63** using two piperidine moieties led to a 1.9-fold faster water-exchange rate than non-rigid complex **1.52**.[60] In another example, complex **1.64** with a cyclohexylene-bridge-containing rigidified macrocycle led to a water-exchange rate that was 2.4-fold faster than that of non-rigid **1.25**.[61] Another example demonstrated that a rigid macrocyclic ligand framework based on diazapyridinophane (complex **1.65**) displayed a 15-fold faster water-exchange rate than complex **1.1**.[62] The faster water-exchange rates of rigidified complexes **1.63**–**1.65** with respect to non-rigid analogs **1.52**, **1.25**, and **1.1** are likely due to a variety of differences, but one of the influences is the increased steric hindrance brought about by the cyclic functionalities that enhance the rigidity of the backbone.

Increasing steric hindrance at the site of water coordination—using strategies including extension of ligand backbone or arms, incorporating bulky phosphonates, introducing bulky alkyl groups on the ligand backbone, and rigidification of the ligand backbone—leads to complexes with fast water-exchange rates; therefore, these strategies are desirable in T_1-shortening agents. However, it is important to note that extension of ligand backbone and arms often leads to less stable complexes relative to analogous complexes without backbone and arm extensions, and stability is a critical consideration in the design of contrast agents. On the other hand, releasing steric encumbrance at the site of water coordination using less sterically demanding coordinating groups leads to complexes with slow water-exchange rates that might be desirable for use as PARACEST agents.

Modification of Ligand Side Chains

The water-exchange rates of Ln^{III}-containing complexes tend to depend on the chemical nature of ligand side chains including bulkiness, polarity, and charge as has been described to some extent in the previous sections. This section focuses on the influence of ligand side chains on water-exchange rate using complexes **1.4** (**Figure 1.2**), **1.40** (**Figure 1.4**) and **1.66–1.83** (**Figure 1.7** and **Tables 1.4** and **1.5**).

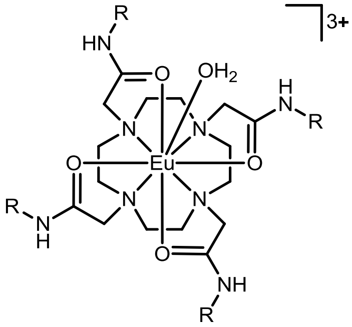

1.66: R = H
1.67: R = CH_2Ph
1.68: R = $CH(CH_3)Ph$
1.69: R = $CH_2CO_2CH_2CH_3$
1.70: R = CH_2CO_2*n*Bu
1.71: R = $CH_2CO_2CH_2Ph$
1.72: R = 4-heptyl
1.73: R = 3-pentyl
1.74: R = *t*-Bu
1.75: R = *i*-Pr
1.76: R = $C(CH_3)_2CO_2^-$
1.77: R = CH_3
1.78: R = $CH_2PO(OCH_2CH_3)_2$
1.79: R = $C(CH_3)_2CO_2CH_2CH_3$
1.80: R = $CH_2PO_3^{2-}$

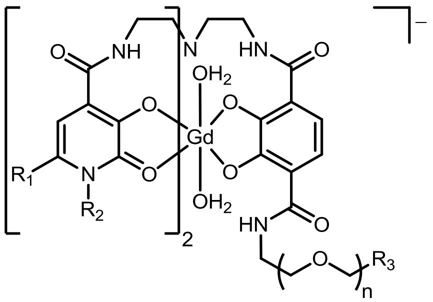

1.81: $R_1 = R_3 = CH_3$, R_2 = H, n = 12
1.82: $R_1 = R_3$ = H, $R_2 = CH_3$, n = 44
1.83: $R_1 = R_3$ = H, $R_2 = CH_3$, n = 123

Figure 1.7. Representative complexes **1.66–1.83** that relate the influence of bulkiness and polarity of ligand side chains to water-exchange rates.[15,27,63–69]

For example, a series of Eu^{III}-tetraamide-based complexes (**1.40** and **1.66–1.71**) was synthesized to investigate the influence of ligand side chains in terms of water-accessible surface area (calculated from molecular modeling) on water-exchange rates.[63] The complexes in the series likely undergo dissociative water exchange based on their nine coordinate ground state structures. Based on the findings of this study, the water-exchange rate decreased with decreasing water-accessible surface area (**1.66** > **1.40** > **1.67** > **1.68** > **1.69** > **1.70** = **1.71**).[63] The rationale used to explain these data is that large water-accessible surfaces give rise to a large amount of second-sphere hydration, subsequently decreasing the activation energy for the water-exchange process. Moreover, any substituent that facilitates the access of incoming water molecules through second-sphere hydration was reported to lead to fast water-exchange rates. On the other hand, substituents on the ligand side chains that hinder the access of incoming water molecules lead to slow water-exchange rates.[63]

Table 1.4. Water-exchange rates of Eu^{III}-containing DOTA-tetraamide complexes **1.40** and **1.66**–**1.80**.

Complex	k_{ex} ($\times 10^6$ s^{-1})	Side chain	Method	Reference
1.40	0.007	CH_2CO_2t-Bu	NMR spectroscopy[c]	63
1.66	0.01	H	NMR spectroscopy[c]	63
1.66	0.0083[a]	H	^{1}H-NMR spectroscopy	65
1.67	0.005	CH_2Ph	NMR spectroscopy[c]	63
1.68	0.004	$CH(CH_3)Ph$	NMR spectroscopy[c]	63
1.69	0.003	$CH_2CO_2CH_2CH_3$	NMR spectroscopy[c]	63
1.69	0.0013[a]	$CH_2CO_2CH_2CH_3$	^{1}H-NMR spectroscopy	27
1.70	0.002	CH_2CO_2nBu	NMR spectroscopy[c]	63
1.71	0.002	$CH_2CO_2CH_2Ph$	NMR spectroscopy[c]	63
1.72	>1[a]	4-heptyl	CEST	15
1.73	0.059[a]	3-pentyl	CEST	15
1.74	0.10[a]	*t*-Bu	CEST	15
1.75	0.02[a]	*i*-Pr	CEST	15
1.76	0.0096[a]	$C(CH_3)_2CO_2^-$	CEST	15
1.77	0.0064[a]	CH_3	^{1}H-NMR spectroscopy	65
1.78	0.00077[a]	$CH_2PO(OCH_2CH_3)_2$	^{1}H-NMR spectroscopy	66
1.79	0.0048[a]	$C(CH_3)_2CO_2CH_2CH_3$	CEST	15
1.80	0.015[b]	$CH_2PO_3^{2-}$	^{1}H-NMR spectroscopy	27

[a]for the square-antiprism (SAP) isomer in CH_3CN, [b]in water, [c]the authors did not specify ^{1}H or ^{17}O

In addition to studying the influence of water-accessible surface area on water-exchange rates, a recent study correlated the steric bulk of ligand side chains and water-exchange rates using complexes **1.72**–**1.75**. Based on this study, large amounts of steric bulk on ligand side chains resulted in fast water-exchange rates.[15] However, this trend cannot be generalized to any bulky group because there are other factors involved including polarity of the side chains. The relationship between steric bulk of ligand side chains and water-exchange rate is similar to that observed in the previous section, where water-exchange rate increased with steric hindrance imposed at the site of water-coordination. Furthermore, at least a 17-times faster water-exchange rate was observed for more bulky heptyl-containing complex **1.72** relative to less bulky pentyl-containing complex **1.73**, and a 3.7-fold faster water-exchange rate was observed for complex **1.74** (with more bulky *tert*-butyl substituents) relative to **1.75** (with less bulky isopropyl substituents).[15] To explain these observations, it was suggested that side chains with bulky substituents interact with one another through steric interactions making the coordinated water exposed to bulk water.[15] The exposure of coordinated water to bulk water facilitates water exchange leading to fast water-exchange rates.

Because the steric bulk and polarity of side chains are intertwined, complexes **1.74** and **1.76** were used to isolate the effects of steric bulk and polarity. Despite being similar in terms of steric bulk, complexes **1.74** and **1.76** display different water-exchange rates (**Table 1.4**), suggesting that the polarity of the side chains influences the magnitude of water-exchange rates. Complex **1.74** displayed a 10-fold faster water-exchange rate than complex **1.76** with polar carboxylate groups. This difference in water-exchange rate can be attributed to the ability of polar groups to sustain second-sphere hydration via hydrogen-bond interactions, thereby stabilizing the nine-coordinate ground state leading to slow water-exchange rates.[15] This trend in water-exchange rates is the opposite of what was reported for complexes **1.40** and **1.66–1.71** likely because both polarity and bulkiness of ligand side chains contribute to water-exchange rates and the difficulty of separating one from the other.

In general, water-exchange rates of $\mathrm{Eu^{III}}$-containing DOTA-tetraamide-based complexes tend to be slower when the polarity of ligand side chains is greater (primary amides<alkyl substituents<carboxylates<phosphonates).[64] An example of this trend can be observed in the differences in water-exchange rates among complexes **1.66**, **1.69**, **1.77**, and **1.78** [primary amide-containing complex **1.66** > alkyl substituent-containing complex **1.77** > carboxylate-ester-containing complex **1.69** > phosphonateester-containing complex **1.78**] (**Table 1.4**).[27,65,66] The slowing of water-exchange rates as a function of polarity can be attributed to the stabilization of the nine-coordinate ground state through hydrogen-bond interactions. Although polar ligand side chains are expected to result in slow water-exchange rates, it was observed that complexes bearing negatively charged side chains display faster water-exchange rates than their neutral analogs.[64] For example, a 2-fold difference in water-exchange rate was observed between negatively charged carboxylate-side-chain-containing analog **1.76** and neutral ethylester-side-chain-containing complex **1.79**.[15] In another example, a 52-fold difference in water-exchange rate was observed between neutral phosphate-ester-side-chain-containing complex **1.78** and negatively charged phosphonate-side-chain-containing analog **1.80**.[27,66] The slower water-exchange rates of neutral ester-containing complexes relative to their negatively charged analogs is likely due to the ability of ethyl groups to block incoming water molecules, subsequently lowering the number of water molecules available for exchange.[15] The observation of complexes with negatively charged side chains leading to fast water-exchange rates is consistent with the second section that relates negatively charged complexes to fast water-exchange rates.

Another instance of polar side chains leading to slow water-exchange rates can be observed with HOPO-based polyethylene glycol (PEG) conjugates **1.81**–**1.83**.[67,68] Moreover, a 4-fold difference in water-exchange rate was observed between parent HOPO complex **1.4** without

PEG and HOPO complex **1.83** with the PEG moiety with 123 monomer units (**Table 1.5**).[67,68] The observed difference in water-exchange rate is likely due to hydrogen-bonding and steric interactions brought about by PEG moieties.

Table 1.5. Water-exchange rates and water-coordination numbers of Gd^{III}-containing HOPO-based (**1.4** and **1.81**–**1.83**) PEG conjugates.

Complex	k_{ex} ($\times 10^6$ s^{-1})	q	Reference
1.4	130	2	30
1.81	77	1	67
1.82	53	1	68
1.83	32	1	68

Based on the studies described in this section, Ln^{III}-containing complexes with bulky, hydrophobic side chains are desirable in designing T_1-shortening agents, because they are expected to lead to fast water-exchange rates. On the other hand, Ln^{III}-containing complexes with neutral hydrophilic side chains are suitable for developing PARACEST agents because hydrophilic side chains tend to result in slow water-exchange rates.

Modification of TSAP/SAP Ratios for DOTA-Type Complexes

The water-exchange rates of DOTA-type Ln^{III}-containing complexes are also governed by the ratio of the twisted-square-antiprism (TSAP) to square-antiprism (SAP) isomers. In this section, the influence of the TSAP/SAP ratio on water-exchange rate will be discussed using complexes **1.18**–**1.20** and **1.84**–**1.93** (**Figures 1.4** and **1.8** and **Table 1.6**). DOTA-type complexes exist as two diasteriomers in aqueous solution, namely TSAP and SAP that differ in the arrangement of their carboxylate arms and macrocyclic rings. Specifically, these two isomers differ in the twist angle between macrocyclic nitrogen plane and carboxylate oxygen plane: the TSAP isomer has a narrow O–Gd^{III}–N twist angle (20°), and the SAP isomer has a wide O–Gd^{III}–N twist angle (40°) (**Figure 1.9**). These isomers have the ability to interconvert by ring inversion or arm rotation.[69]

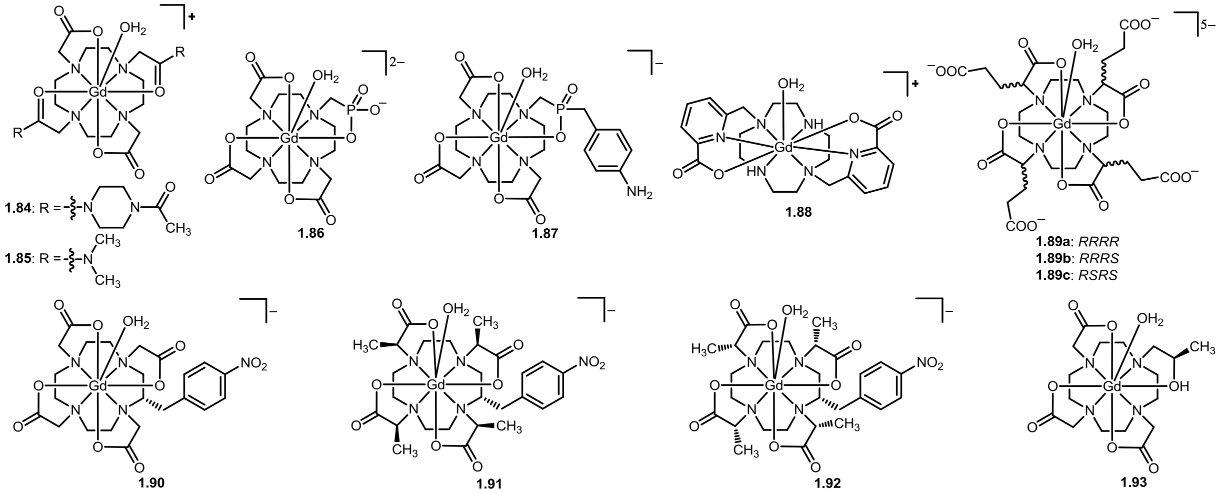

Figure 1.8. Representative complexes **1.88**–**1.93** that relate the influence of TSAP/SAP ratios with water-exchange rates of DOTA-type complexes.[41,70–77]

Table 1.6. Water-exchange rates and TSAP/SAP ratios of Gd^{III}-containing complexes (**1.18**–**1.20** and **1.88**–**1.93**).

Complex	k_{ex} ($\times 10^6$ s^{-1})	TSAP/SAP ratio	k_{ex} ($\times 10^6$ s^{-1}) for TSAP	k_{ex} ($\times 10^6$ s^{-1}) for SAP	Reference
1.18	80	1.3	Nr	nr	41
1.19	20	0.56	Nr	nr	41
1.20	4.4	0.39	Nr	nr	41
1.84	140 ^{a}	0.78^b	330	0.43	70
1.85	31 ^{a}	0.77^b	70	0.74	70
1.86	71	1.5	Nr	nr	71
1.87	61.7	1.5^b	Nr	nr	72
1.88	58	∞	Nr	nr	73
1.89a	15.4	2	Nr	nr	74
1.89b	9.0	0.75	Nr	nr	74
1.89c	3.45	0.20	Nr	nr	74
1.90	5	0.08	Nr	nr	75
1.91	67	∞	Nr	nr	76
1.92	8.3	0	Nr	nr	76
1.93	4.5 (37 °C)	0.4	110	1.6	77,78

nr = not reported, ^{a}calculated from weighted average, ^{b}TSAP/SAP ratios obtained from Eu^{III}-containing complexes

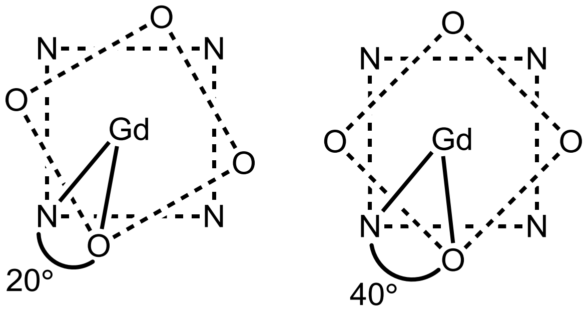

Figure 1.9. Top-down view of (left) TSAP and (right) SAP isomers with the O–Gd^{III}–N twist angles indicated. In these views, the oxygen plane is above the Gd^{III} ion and the nitrogen plane is below the Gd^{III} ion.

In general, the measured water-exchange rate of DOTA-type complexes is the weighted average of the water-exchange rates of the TSAP and SAP isomers. Between the two isomers, the TSAP isomer tends to display a water-exchange rate that is approximately 50–200 times faster than the SAP isomer in DOTA-tetraamide type complexes.[69,79] The faster water-exchange rate in the TSAP isomer relative to the SAP isomer is likely due to the higher amount of steric encumbrance at the site of water coordination, which facilitates the dissociation of coordinated water similar to fast water-exchange rates (discussed in the third section) due to the steric hindrance at the site of water-coordination. Because the TSAP and SAP isomers display different water-exchange rates, the water-exchange rates of DOTA-type complexes can be tuned by changing the relative abundance of the two isomers in solution using coordination-chemistry-based strategies. Complexes with sterically bulky substituents tend to favor the TSAP isomer, while complexes without bulky substituents favor the SAP isomer. However, it is important to note that relative abundance of the two isomers also depends on other factors including ionic radius, solvent, ionic strength of the solution, and salt composition.[80–82]

To study the influence of steric bulk on amide nitrogen atoms on the relative abundance of the TSAP and SAP isomers, complexes **1.84** and **1.85** were investigated. The TSAP/SAP ratios of 0.78 and 0.77 were measured for Eu^{III}-containing complexes **1.84** and **1.85**, respectively. These ratios are 2-times greater than Eu^{III}-containing complex **1.1** that has a TSAP/SAP ratio of 0.36.[70] The water-exchange rates obtained for the Gd^{III}-containing complexes **1.84** and **1.85** indicated that the TSAP isomers displayed 782- and 95-times faster water-exchange rates, respectively, than the SAP isomers.[70]

In addition to introducing steric bulk on amide nitrogen atoms, other bulky DOTA-type complexes increase the population of the TSAP isomer relative to the SAP isomer, leading to faster water-exchange rates. This idea can be exemplified using phosphonate-containing DOTA-type systems.[41,71,72] In one example, a TSAP/SAP ratio of approximately 1.5 was observed for phosphonate-containing complex **1.86** and resulted in a 17-fold faster water-exchange rate relative to that of complex **1.1**.[71] In another example, a TSAP/SAP ratio of 1.5 for phosphonate-containing complex **1.87**, which is 4-times greater than that of complex **1.1**, resulted in a water-exchange rate that is 15-times faster than complex **1.1**.[72] Interestingly, the series of phosphonate-containing complexes **1.18**–**1.20** were used to demonstrate that the TSAP/SAP ratios are larger with complexes of more negative charge. The TSAP/SAP ratios were 1.3 and 0.56 in negatively charged complexes **1.18** and **1.19**, respectively, and 0.39 in neutral complex **1.20** suggesting that the TSAP isomer dominates in complexes with more negative charge. The difference in the populations of the TSAP isomers was reflected in the water-exchange rates of complexes **1.18**–**1.20**: 18- and 4.5-fold differences in water-exchange rates were observed in complexes **1.18** and **1.19**, respectively, relative to complex **1.20**.[41]. The differences in water-exchange rates of complexes **1.18**–**1.20** are likely due to the difference in the TSAP isomer population, the difference in complex charge as described in the second section, or both factors. In addition to bulky phosphonate-containing complexes, complex **1.88** with a bulky bis-methylene picolinate platform was explored. Complex **1.88** displayed a water-exchange rate that is 14-times faster than that of complex **1.1**.[73] The faster water-exchange rate is likely because complex **1.88** exists exclusively as the distorted TSAP isomer.[73]

In addition to incorporating steric bulk on the ends of the arms farthest from the macrocycle, DOTA-type complexes with substituents at the α-positions of the pendent arms increase the abundance of the TSAP isomer. As an example, Parker and co-workers observed that a Gd^{III}-containing DOTA analog with propionate groups in the α-positions of the pendent arms contains the three isomers **1.89a**, **1.89b**, and **1.89c**. In this series, the water-exchange rate increases with increasing TSAP/SAP ratios.[74] Interconversion between TSAP and SAP isomers in complexes **1.89a** and **1.89b** was reported to occur only through ring inversion because the bulky propionate group in the α-position of the pendent arm hinders arm rotation affording TSAP/SAP ratios that are 10- and 3.8-times higher, respectively, than in complex **1.89c**. The low TSAP/SAP ratio in complex **1.89c** is likely due to interconversion between TSAP and SAP isomers through arm rotation as well as ring inversion. The differences in the TSAP/SAP ratios are likely responsible for the 4.5- and 2.6-fold faster water-exchange rates of complexes **1.89a** and **1.89b**, respectively, relative to complex **1.89c**.[74] In addition to blocking arm rotation, complexes containing bulky substituents on the macrocycle were synthesized with the objective of blocking ring inversion in DOTA-type complexes. A study of complex **1.90** with a *p*-nitrobenzyl group on the macrocycle demonstrated that TSAP to SAP interconversion through ring inversion can be blocked. However, arm rotation persisted affording a TSAP/SAP ratio of 0.08 resulting in a water-exchange rate that is only 1.2-times faster than that of complex **1.1**.[75] Based on the observations that arm rotation and ring inversion can be blocked by arm and ring substitutions, respectively, complexes with both arm and ring substitutions were reported to control isomer type. Furthermore, controlling the chirality at five carbons led to preference for a single isomer. For example, complexes **1.91** (*S*-*SSSS*) and **1.92** (*S*-*RRRR*) with substituents on the macrocycle as well as the pendant arms were reported to exist exclusively as TSAP and SAP isomers, respectively.[76] The water-exchange rate of **1.91** (*S*-*SSSS*) in the TSAP form was 8-times faster than the water-exchange rate of **1.92** (*S*-*RRRR*) in the SAP form.[76] These examples substantiate that complexes existing exclusively in the TSAP form have faster water-exchange rates relative to complexes existing in the SAP form.

In addition to experimental studies carried out to tune TSAP/SAP ratios in DOTA-type complexes, a computational study was carried out on complex **1.93** to understand the rationale behind the TSAP isomer leading to fast water-exchange rates.[77] This computational study suggested that the TSAP isomer displays hydrogen-bond interactions between pendant arms and second-sphere water, enabling the coordinated water to exchange readily with bulk water, leading to fast water-exchange rates. On the other hand, the SAP isomer is expected to form hydrogen-bond interactions between second-sphere and inner-sphere water, stabilizing the ground state in dissociative exchange processes and leading to slow water-exchange rates. Based on this study, increasing the ability of pendant arms to form hydrogen bonds without lengthening side chains is likely to result in large proportions of the TSAP isomer with DOTA-type complexes. Although the predictions of this study at first glance appear to be in contrast with the studies discussed in the previous section that relates ligand side chains to water-exchange rates, the difference is likely because the side chains of complexes **1.81**–**1.83** are long compared to the side chain of complex **1.93**. The length of the side chain influences how far from the Ln^{III} ion hydrogen bonding occurs, and this distance is an important difference between the complexes described in the previous section and this section.

Complexes with large TSAP/SAP ratios are expected to lead to fast water-exchange rates necessary for conventional T_1-shortening agents because the TSAP isomers display fast water-exchange rates. Large TSAP/SAP ratios are likely to form with complexes that contain bulky substituents on the α-position of pendant arms, on the macrocycle, and on amide nitrogen atoms as well as from complexes with side chains that facilitate hydrogen-bonding interactions near the inner-sphere water. On the other hand, for the design of PARACEST agents, low TSAP/SAP ratios are desirable because the SAP isomers display water-exchange rates that are 1–2 orders of magnitude slower than the TSAP isomers. Complexes with low TSAP/SAP ratios are likely with low steric strain on pendant arms and the macrocycle as well as on amide nitrogen atoms. Also, side chains that hinder hydrogen-bond interactions close to the inner-sphere water might favor the SAP isomer leading to slow water-exchange rates useful for PARACEST agents.

Summary

Water-exchange rate is an important molecular parameter in $\mathrm{Ln^{III}}$-containing complexes that governs the efficiency of T_1-shortening and PARACEST contrast agents for MRI. Consequently, tuning water-exchange rates of $\mathrm{Ln^{III}}$-containing complexes to achieve maximum efficiencies for both types of agents has led to a great deal of research. As discussed in this chapter, several coordination-chemistry-based strategies have been employed to tune water-exchange rates of $\mathrm{Ln^{III}}$-containing complexes toward the optimum values desirable for both types of agents. It is important to re-emphasize that there is overlap among the strategies discussed in this chapter. Based on the influence of different coordination-chemistry-based strategies on water-exchange rate, complexes with the following properties are expected to lead to fast water-exchange rates that are desirable for the design of T_1-shortening agents: that undergo associative water exchange; that are negatively charged; with steric hindrance at the site of water coordination; with side chains containing non-polar substituents; and with large TSAP/SAP ratios for DOTA-type complexes. On the other hand, complexes that undergo dissociative exchange; that are positively charged; without bulky substituents at the site of water coordination; with polar substituents on side chains; and with predominantly SAP isomers for DOTA-type complexes are expected to lead to slow water-exchange rates that are desirable for the design of PARACEST agents. Careful consideration and application of the coordination-chemistry-based strategies described in this chapter have the potential to enable fine-tuning of water-exchange rates towards optimal fast or slow rates. Consequently, these strategies are expected to aid the design of both T_1-shortening and PARACEST contrast agents for MRI.

Research Approach

As discussed in this chapter, a great deal of research efforts have been employed to tune the water-exchange rates of $\mathrm{Ln^{III}}$-containing complexes towards fast (10^8 $\mathrm{s^{-1}}$) and slow (10^3 $\mathrm{s^{-1}}$) rates that are useful for T_1-shortening and PARACEST agents, respectively. Literature examples discussed in this chapter demonstrate that even minor modifications to ligand structure lead to considerable changes in the water-exchange rates of $\mathrm{Ln^{III}}$-containing complexes. Consequently, it was envisioned that the water-exchange rates of $\mathrm{Ln^{III}}$-containing DOTA-type complexes could be tuned by introducing a modular and tunable system of modifications, based on the biocompatible and hydrophilic polymer polyethylene glycol (PEG). Moreover, this modular and tunable PEG-based system was expected to enable investigation of the influence of both length and density of PEG on water-exchange rates of these complexes. The goal of this work was to use PEG to tune water-exchange rates of $\mathrm{Ln^{III}}$-containing complexes to slow water-exchange rates. To accomplish this goal, it was hypothesized that PEG is able to tune water-exchange rates of Ln^{III}-containing complexes towards slower rates. The experimental design that was used to test this hypothesis and the data obtained are explained in the subsequent chapters.

Chapter 2 describes key features of the PEG-based Ln^{III}-containing DOTA-type systems that lead to modular systems with the potential to tune water-exchange rates of Ln^{III}-containing complexes as a function of length and density of PEG. This chapter also illustrates the coordination-chemistry-based strategies employed in the design of PEG-based Ln^{III}-containing DOTA-type systems. Furthermore, a discussion is included in Chapter 2 on how Ln^{III} ions were chosen for the PEG-based DOTA-type systems based on the expected properties of the designed complexes. In Chapter 3, the ability of PEG to influence water-exchange rates is described for Ln^{III}-containing complexes in a systematic fashion as a function of length of PEG. Moreover, Chapter 3 includes contrast-agent-relevant properties of PEG-based Ln^{III}-containing complexes and a plausible explanation for the ability of PEG to influence water-exchange rates as a function of length of PEG. Chapter 4 describes the synthetic attempts performed for the synthesis of PEG-based Ln^{III}-containing complexes designed to study the influence of density of PEG on water-exchange rates of Ln^{III}-containing complexes. Chapter 5 concludes the thesis by discussing the potential of PEG-based Ln^{III}-containing DOTA-type systems to tune water-exchange rates as a function of length of PEG. Moreover, the implications of PEG-based systems for the design of T_1-shortening and PARACEST contrast agents for MRI with tunable water-exchange rates is illustrated. In addition, a few suggestions for future work to further tune water-exchange rates of PEG-based systems is described with specific focus on factors to be considered in designing contrast agents with optimum water-exchange rates.

CHAPTER 2: Ligand Design and Synthetic Approach

Ligand Design

The modular systems of lanthanide(III) (Ln^{III})-containing polyethylene glycol (PEG) conjugates were designed considering several factors including (1) the ability to form thermodynamically stable and kinetically inert complexes with Ln^{III} ions; (2) the capacity to incorporate one or more functional groups capable of reacting with commercially available PEG moieties; and (3) the modularity necessary to enable the investigation of the molecular parameters including water-exchange rates of Ln^{III}-containing complexes as a function of length and density of PEG in a systematic fashion. Careful consideration and combination of all three factors led to the design of modular systems based on 1,4,7,10-tetraazacyclododecane-1,4,7-tris(acetic acid) (DO3A) and 1,4,7,10-tetraazacyclododecane-1,7-bis(acetic acid) (DO2A). Moreover, the DO3A-based system (**Figure 2.1**) and the DO3A- and DO2A-based systems (**Figure 2.2**) were designed to investigate the influence of length and density of PEG, respectively, on the water-exchange rates of Ln^{III}-containing complexes. Details of the design consideration choices are described in this chapter.

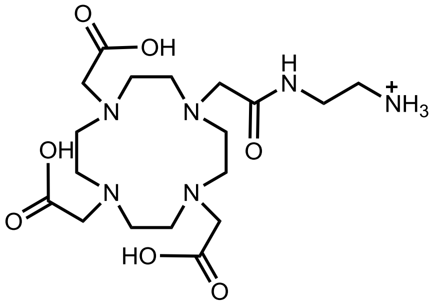

2.1

Figure 2.1. The DO3A-based ligand (**2.1**) designed to investigate the influence of length of PEG on water-exchange rates of Ln^{III}-containing complexes. This ligand system incorporates one amine-terminated arm that can be conjugated to one PEG moiety. The counteranion of ligand **2.1** is not shown for clarity.

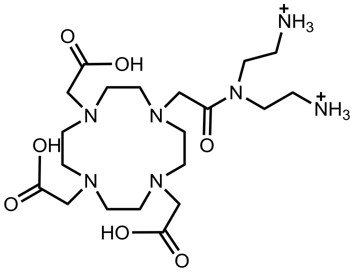

2.2

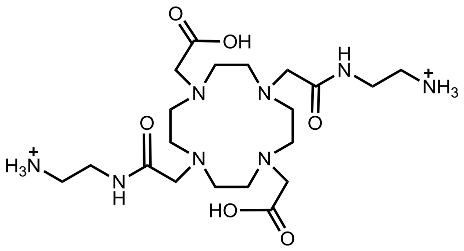

2.3

Figure 2.2. The DO3A- (**2.2**) and DO2A-based (**2.3**) systems designed to investigate the influence of density of PEG on water-exchange rates of Ln^{III}-containing complexes. Ligand **2.2** incorporates one arm that branches into two terminal amines and ligand **2.3** incorporates two amine-terminated arms. The terminal amines on ligands **2.2** and **2.3** can be conjugated to two PEG moieties. The counteranions of ligands **2.2** and **2.3** are not shown for clarity.

Each ligand system is composed of two parts: a DO3A or DO2A macrocycle and one or more linear or branched amine arms. Polyaminopolycarboxylate-type macrocycles based on 1,4,7,10-tetraazacyclododecane (cyclen) tend to form thermodynamically stable and kinetically inert Ln^{III}-containing complexes through the chelate and macrocyclic effects.[2,8,9] Also, the carboxylate arms in DO3A and DO2A are known to form stronger interactions with Ln^{III} ions relative to other coordinating functional groups including amides, esters, and ketones.[83–86] The non-carboxylate arms in the ligand systems included amide functional groups to bind with the Ln^{III} ion and linear or branched terminal amines that can be conjugated to succinimidyl ester-derivatives of PEG. The amide groups were chosen over ester and ketone groups because amides tend to form stronger interactions with Ln^{III} ions.[49] In addition, the amide groups were placed so that they coordinate the Ln^{III} ion through the formation of five-membered rings because Ln^{III} ions prefer coordination through five-membered rings relative to larger or smaller rings.[87] Moreover, ligand system **2.1** consists of one linear terminal amine that can be conjugated to one PEG moiety to investigate the influence of the length of PEG on the properties of the molecules. Ligand systems **2.2** and **2.3** consist of branched and linear terminal amines, respectively, that can be conjugated to two PEG moieties to investigate the influence of the density of PEG on the properties of the molecules.

Gd^{III} was chosen as the Ln^{III} ion for ligand systems **2.1–2.3** to enable determination of contrast agent relevant parameters including water-exchange rate, k_{ex}; relaxivity, r_1; and longitudinal and transverse electron spin relaxation times, T_{1e} and T_{2e}, respectively. In addition, Eu^{III}-containing complexes of ligand systems **2.1–2.3** were synthesized to obtain water-coordination number (q) data. Also, Y^{III}-containing complexes of ligand systems **2.1–2.3** were synthesized as diamagnetic controls for the determination of water-exchange rates. The structures of metal complexes of ligand systems **2.1–2.3** are shown in **Figure 2.3**.

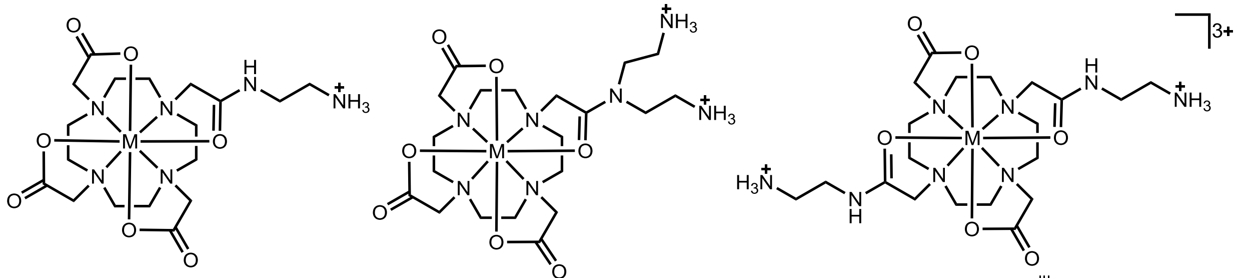

2.4, M = Gd^{III}
2.5, M = Eu^{III}
2.6, M = Y^{III}

2.7, M = Gd^{III}
2.8, M = Eu^{III}
2.9, M = Y^{III}

2.10, M = Gd^{III}
2.11, M = Eu^{III}
2.12, M = Y^{III}

Figure 2.3. Structures of metal complexes **2.4–2.12** formed using ligands **2.1–2.3**. The counteranions of the complexes are not shown for clarity.

PEG was chosen to tune water-exchange rates of Ln^{III}-containing DOTA-type complexes through steric and hydrogen bonding interactions. Hydrogen bond formation with bound and bulk water is expected through oxygen-based hydrogen bond acceptors present in PEG. Based on the coordination-chemistry-based strategies described in Chapter 1, the hydrogen bond forming ability of ligand side chains and steric blocking of the water-coordination sites tend to influence water-exchange rates of Ln^{III}-containing complexes. In addition, conjugation to PEG is not detrimental to the biocompatibility of Ln^{III}-containing contrast agents.[88–90] Commercially available PEG moieties were selected to enable investigation of influence of length and density of PEG on water-exchange rates of Ln^{III}-containing complexes. The structures of M^{III}-containing PEG conjugates and PEG moieties explored are illustrated in **Figure 2.4**. Conjugation between M^{III}-containing complexes and PEG moieties was carried out using different combinations as described below to enable variation of length and density of PEG. Moreover, to enable variation of length of PEG, metal complexes **2.4–2.6** were conjugated to succinimidyl ester derivatives of **a**–**d**. To enable variation of density, metal complexes **2.4–2.6** were conjugated to succinimidyl ester derivative of **e** and metal complexes **2.7–2.9** and **2.10–2.12** were conjugated to succinimidyl ester derivatives of **a** and **c**. Conjugates **2.16–2.18** and **2.19–2.21** that were designed to study the influence of density of PEG, also enable comparison between the influence of cis and trans conjugation of PEG, respectively, on water-exchange rates. However, it is important to note that the difference in charge between systems **2.16–2.18** (neutral) and **2.19–2.21** (+1) can lead to differences in water-exchange rates as described in Chapter 1.

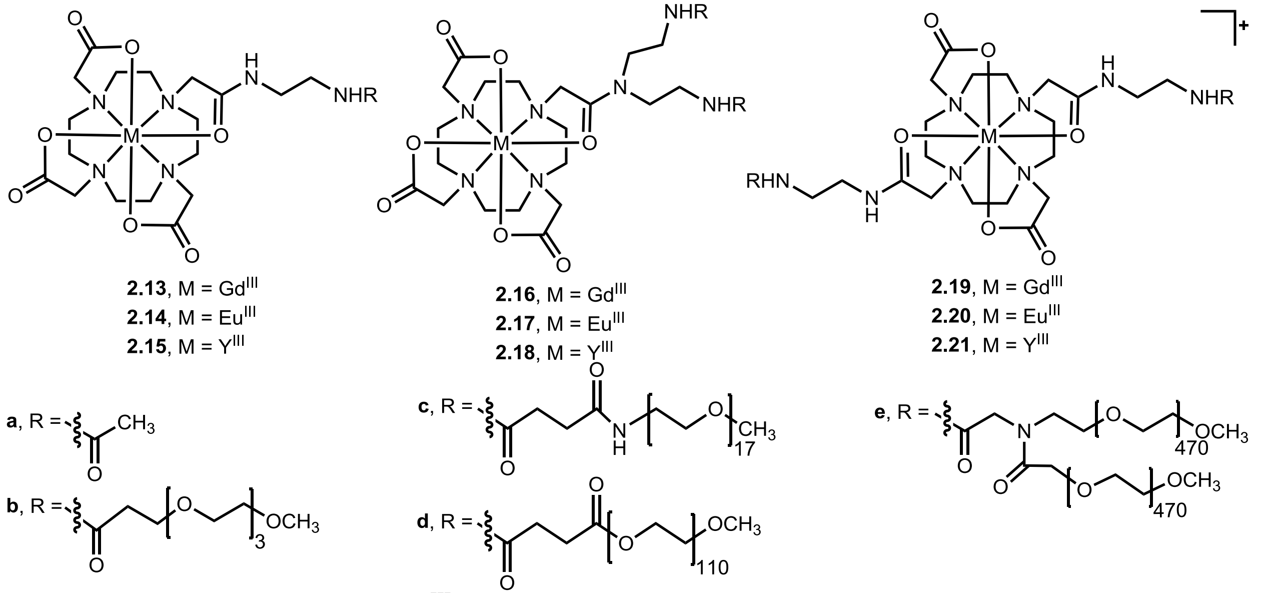

Figure 2.4. The structures of M^{III}-containing PEG conjugates, **2.13–2.21**, acetate, **a**, used as a control, and PEG moieties **b**–**e** used to investigate the influence of length and density of PEG on water-exchange rates of Ln^{III}-containing complexes. The counteranions of complexes **2.19–2.21** and are not shown for clarity.

Synthetic Approach

It was proposed that a four step synthetic approach could afford the desired M^{III}-containing PEG conjugates based on the retrosynthetic analysis of conjugates **2.13–2.15**, **2.16–2.18**, and **2.19–2.21** illustrated in **Schemes 2.1–2.3**, respectively.

In general, the first step involves nucleophilic substitution of the protected arms (**2.24** or **2.26**) with DO3A-*tert*-butyl ester (**2.23**) or DO2A-*tert*-butyl ester (**2.28**) to yield protected ligands **2.22**, **2.25**, and **2.27**. The *tert*-butyl esters, *tert*-butoxycarbamates, and carboxybenzyl protecting groups could be cleaved upon treatment with concentrated hydrochloric acid to afford deprotected ligands **2.1**, **2.2**, and **2.3**. Metallation of the deprotected ligands could be accomplished using metal chlorides to obtain Gd^{III}-, Eu^{III}-, or Y^{III}-containing complexes **2.4–2.12**. Conjugation of PEG to terminal amines of M^{III}-containing complexes could be achieved using succinimidyl ester derivatives of acetate, **a**, and PEG, **b–e**, to yield conjugates **2.13–2.21**.

Scheme 2.1. Four step retrosynthetic analysis of **2.13–2.15**. The counteranions of complexes **2.4–2.6** and ligand **2.1** are not shown for clarity.

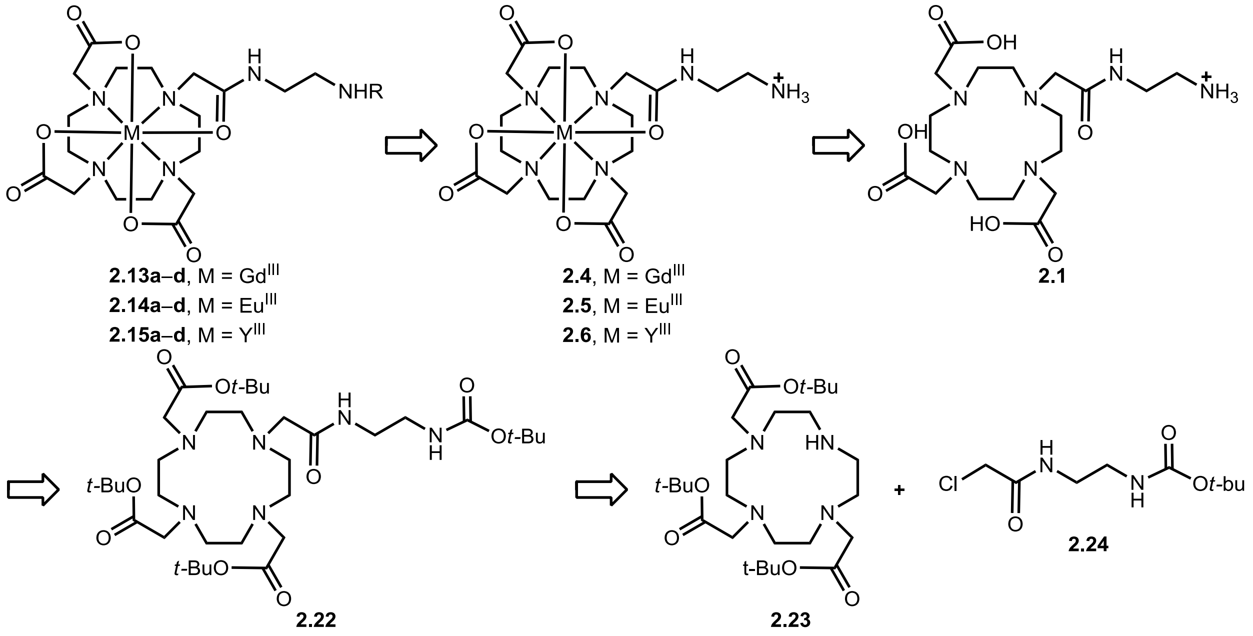

Scheme 2.2. Four step retrosynthetic analysis of **2.16–2.18**. The counteranions of complexes **2.7–2.9** and ligand **2.2** are not shown for clarity.

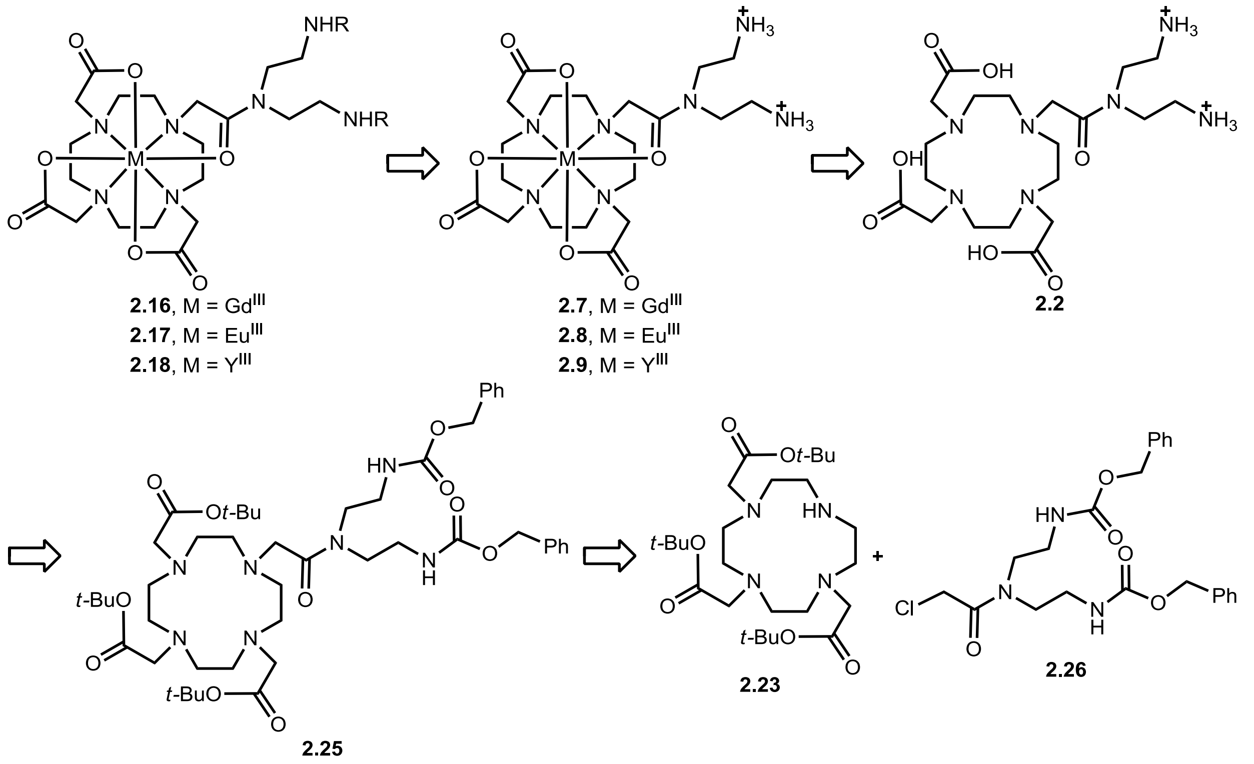
2.16, M = Gd^{III}
2.17, M = Eu^{III}
2.18, M = Y^{III}
2.7, M = Gd^{III}
2.8, M = Eu^{III}
2.9, M = Y^{III}
2.2
2.25
2.23
2.26

Scheme 2.3. Four step retrosynthetic analysis of **2.19–2.21**. The counter anions of complexes **2.10–2.12** and ligand **2.3** are not shown for clarity.

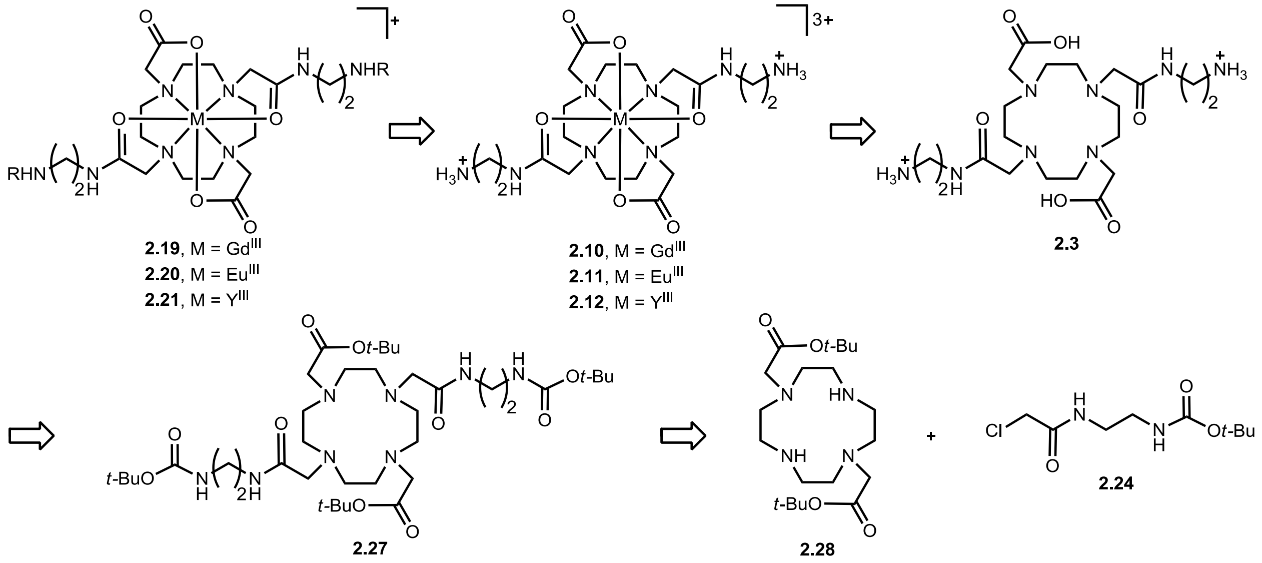
2.19, M = Gd^{III}
2.20, M = Eu^{III}
2.21, M = Y^{III}
2.10, M = Gd^{III}
2.11, M = Eu^{III}
2.12, M = Y^{III}
2.3
2.27
2.28
2.24

Experimental Procedures

Commercially available chemicals were of reagent-grade purity and were used without further purification unless otherwise noted. Water was purified using a PURELAB Ultra Mk2 (ELGA) water purification system. Flash chromatography was carried out with silica gel 60, 230−400 mesh (EMD chemicals).[91] Thin-layer chromatography (TLC) was performed on ASTM TLC plates with a silica gel 60 F254 coating (250 μm layer thickness). Visualization of TLC was carried out with a UV lamp followed by staining with potassium permanganate (2 g $KMnO_4$, 20 g K_2CO_3, 5 mL 5% w/v aqueous NaOH, and 300 mL H_2O). Spectra/Por Biotech cellulose ester dialysis membranes of 100−500, 500−1,000, and 8,000−10,000 Da molecular weight cut off (MWCO) were used for dialysis. Freeze drying was carried out using a LABCONCO FreeZone 2.5 freeze dryer. Resin reactions were performed in Poly-Prep chromatography columns on a Barnstead/Thermolyne LABQUAKE rotator. Centrifugation was carried out using a Fisher Scientific Centrific centrifuge. High-performance liquid chromatography (HPLC) was carried out on a Shimadzu HPLC system equipped with a C4 column (RESTEK Ultra C4, 5.0 μm × 250 mm) and fluorescence (λ_{ex} = 273 nm, λ_{em} = 622 nm for Gd^{III} complexes and λ_{ex} = 396 nm and λ_{em} = 593 nm Eu^{III} complexes, photodiode array (absorbance at 210 nm), and refractive index detectors. Aqueous size-exclusion chromatography (SEC) was performed on the same HPLC system using three aquagel-OH columns in series (VARIAN PLaquagel-OH-mixed, 8 μm × 300 mm). A binary gradient method (pump A: H_2O, pump B: CH_3CN; 95−5% B over 20 min; flow rate: 1 mL/min) was used with the C4 column, and an isocratic method (100% H_2O; flow rate: 1 mL/min) was used with the aquagel-OH columns.

^{1}H NMR spectra were acquired using Varian Unity 400 (400 MHz) or Varian-500S (500 MHz) spectrometers, and ^{13}C NMR spectra were acquired using Varian Unity 400 (101 MHz) or

Varian-500S (125 MHz) spectrometers. Chemical shifts (ppm) for ^{1}H NMR spectra are reported relative to residual $CHCl_3$ in $CDCl_3$ (7.27 ppm) or CH_3OH in CD_3OD (3.30 ppm). Multiplicities are reported as “s” = singlet, “m” = multiplet, and “brs” = broad singlet. The elements responsible for particular shifts are noted with italicized font. Chemical shifts for ^{13}C NMR spectra are reported relative to $CDCl_3$ (77.23 ppm) in $CDCl_3$ or CD_3CN (118.26 ppm) as an internal standard in D_2O. High-resolution electrospray ionization mass spectra (HRESIMS) were obtained on an electrospray time-of-flight high-resolution Waters Micromass LCT Premier XE mass spectrometer. Matrix-assisted laser desorption ionization (MALDI) mass spectrometry was performed on a Waters SYNAPT G2 mass spectrometer (Manchester, UK) equipped with a commercial MALDI source and a Nd:YAG laser (355 nm, 200 Hz) or a Bruker Ultraflex MALDI-TOF mass spectrometer. α-Cyano-4-hydroxycinnamic acid (5 mg in 50:50 CH_3CN/H_2O with 0.1% formic acid) was used as the matrix. Prior to plating, samples (~1 μg/mL in water with 0.1% formic acid or ~1 mg/mL in water) and matrix were mixed in 1:1 or 1:100 v/v ratios. *N*-(*tert*-Butoxycarbonyl)-*N'*-aminoacetylchloride, **2.24**,[92] and DO2A-*tert*-butyl ester, **2.28**,[93,94] were synthesized according to previously published procedures. The synthetic route to PEG conjugates designed to explore the influence of length (**2.13a–d**, **2.14a–d**, and **2.15a–d**) and density (**2.13e**, **2.14e**, and **2.15e**) of PEG on water-exchange rates is shown in **Scheme 2.4**.

Scheme 2.4. Synthetic route to M^{III}-containing PEG conjugates **2.13a–e**, **2.14a–e**, and **2.15a–e**.

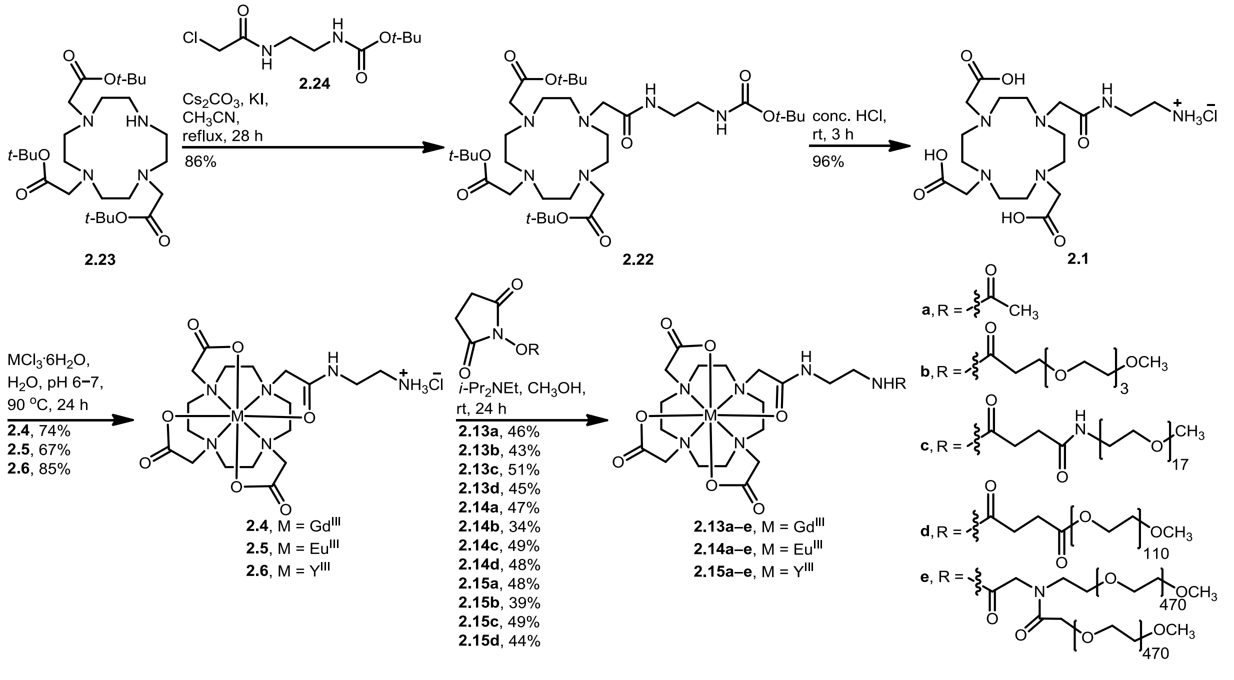
2.24
Cs2CO3, KI,
CH3CN,
reflux, 28 h
86%
2.23
2.22
conc. HCl,
rt, 3 h
96%
2.1
MCl3·6H2O,
H2O, pH 6–7,
90 °C, 24 h
2.4, 74%
2.5, 67%
2.6, 85%
2.4, M = Gd^III
2.5, M = Eu^III
2.6, M = Y^III
i-Pr2NEt, CH3OH,
rt, 24 h
2.13a, 46%
2.13b, 43%
2.13c, 51%
2.13d, 45%
2.14a, 47%
2.14b, 34%
2.14c, 49%
2.14d, 48%
2.15a, 48%
2.15b, 39%
2.15c, 49%
2.15d, 44%
2.13a–e, M = Gd^III
2.14a–e, M = Eu^III
2.15a–e, M = Y^III
a, R =
b, R =
c, R =
d, R =
e, R =
3
17
110
470
470

Attempted synthesis of **2.13e**, **2.14e**, and **2.15e** is discussed in Chapter 4.

1,4,7-Tris(*tert*-butyloxycarbonylmethyl)-1,4,7,10-tetraazacyclododecane (**2.23**): The synthesis of this molecule is based on a previous report with modifications as noted in the following text.[95] To a mixture of cyclen (1.00 g, 5.80 mmol, 1 equiv) and $NaHCO_3$ (1.61 g, 19.2 mmol, 3.3 equiv) in anhydrous CH_3CN (15 mL) at 0 °C under Ar was added a solution of *tert*-butyl bromoactetate (2.90 mL, 19.4 mmol, 3.3 equiv) in anhydrous CH_3CN (20 mL) over a period of 18 h (instead of 30 min as described in the previous report). The reaction mixture was allowed to warm to ambient temperature during the addition of *tert*-butyl bromoactetate (instead of after the addition as previously reported). The reaction mixture was stirred under Ar for 48 h after the addition of *tert*-butyl bromoactetate. The reaction mixture was filtered through celite, and the filtrate was concentrated to dryness under reduced pressure to yield a pale yellow solid that was purified using silica gel column chromatography (9:1 $CHCl_3/CH_3OH$) (not described in the previous report). Fractions with R_f values (9:1 $CHCl_3/CH_3OH$) between 0.39 and 0.63 were combined, and the solvent was removed under reduced pressure. The resulting solid was recrystallized from hot toluene, dissolved in saturated $NaHCO_3$ (50 mL), extracted with $CHCl_3$ (3 × 50 mL), and dried over anhydrous $MgSO_4$. Solvent was removed under reduced pressure to obtain 1.46 g (49%) of **2.23** as an off-white solid. ^{1}H NMR (500 MHz, $CDCl_3$, δ): 1.34−1.52 (m, C*H*$_3$, 27H), 2.70−2.91 (m, C*H*$_2$C*H*$_2$, 12H), 3.00 (brs, C*H*$_2$C*H*$_2$, 4H), 3.30 (s, C*H*$_2$C=O, 2H), 3.35 (s, C*H*$_2$C=O, 4H); ^{13}C NMR (125 MHz, $CDCl_3$, δ): 28.20 (*C*H$_3$), 28.24 (*C*H$_3$), 47.8 (*C*H$_2$*C*H$_2$), 50.4 (*C*H$_2$C=O), 51.3 (*C*H$_2$*C*H$_2$), 51.7 (*C*H$_2$*C*H$_2$), 58.1 (*C*H$_2$C=O), 81.5 (*C*(CH$_3$)$_3$), 81.6 (*C*(CH$_3$)$_3$), 170.4, 171.1; R_f = 0.47 (9:1 CH_3Cl/CH_3OH); HRESIMS (*m*/*z*): $[M + H]^+$ calcd for $C_{26}H_{51}N_4O_6$, 515.3809; found 515.3817.

1,4,7-Tris(*tert*-butyloxycarbonylmethyl)-10-(*N*-(2-*tert*-butoxycarbonylaminoethyl) acetamide-1,4,7,10-tetraazacyclododecane (**2.22**): To a mixture of **2.23** (0.394 g, 0.765 mmol, 1 equiv), Cs_2CO_3 (0.584 g, 1.79 mmol, 2.3 equiv), and KI (0.278 g, 1.67 mmol, 2.2 equiv) in anhydrous CH_3CN (16 mL) was added a solution of **2.24** (0.219 g, 0.925 mmol, 1.2 equiv) in anhydrous CH_3CN (16 mL) under Ar. The reaction mixture was heated at reflux under Ar for 28 h. The reaction mixture was cooled to ambient temperature and filtered through celite, and the solvent was removed under reduced pressure. The resulting residue was dissolved in $CHCl_3$ (40 mL) and washed sequentially with H_2O (40 mL) and saturated aqueous KCl (3 × 40 mL). The organic layer was dried over anhydrous K_2CO_3 and concentrated under reduced pressure to obtain 0.470 g (86%) of **2.22** as a light brown solid. ^{1}H NMR (400 MHz, $CDCl_3$, δ): 1.32−1.52 (m, C*H*$_3$, 36H), 2.51 (brs, C*H*$_2$C*H*$_2$, 4H), 2.68 (brs, C*H*$_2$C*H*$_2$, 4H), 2.89 (brs, C*H*$_2$C=O, 6H), 3.07 (s, C*H*$_2$C=O, 2H), 3.16−3.58 (m, C*H*$_2$C*H*$_2$, 12H), 5.99 (brs, N*H*, 1H), 8.79 (brs, N*H*, 1H); ^{13}C NMR (101 MHz, $CDCl_3$, δ): 27.9 (*C*H$_3$), 28.0 (*C*H$_3$), 28.2 (*C*H$_3$), 28.6 (*C*H$_3$), 39.6 (*C*H$_2$*C*H$_2$), 41.1 (*C*H$_2$*C*H$_2$), 51.7 (*C*H$_2$*C*H$_2$), 52.3 (*C*H$_2$C=O), 53.7 (*C*H$_2$C=O), 55.1 (*C*H$_2$*C*H$_2$), 56.2

(CH_2CH_2), 57.1 (CH_2CH_2), 57.8 (CH_2C=O), 79.1 ($C(CH_3)_3$), 80.9 ($C(CH_3)_3$), 81.0 ($C(CH_3)_3$), 81.9 ($C(CH_3)_3$), 155.9, 156.5, 170.6, 171.8, 172.7; HRESIMS (*m*/*z*): $[M + H]^+$ calcd for $C_{35}H_{67}N_6O_9$, 715.4970; found 715.4976.

1,4,7-Tris(carbonylmethyl)-10-(aminoethyl-*N′*)-acetyl)-1,4,7,10-tetraazacyclododecane (**2.1**): To *tert*-butylester **2.22** (0.248 g, 0.347 mmol) was added concentrated HCl (25 mL), and the resulting mixture was stirred at ambient temperature for 3 h. The reaction mixture was concentrated under reduced pressure, and the resulting residue was dissolved in H_2O and freeze dried to obtain 0.161 g (96%) of **2.1** as a yellow–brown solid. ^1H NMR (400 MHz, CD_3OD, δ at 55 °C): 3.02−3.24 (m, CH_2CH_2, 10H), 3.36−3.58 (m, CH_2CH_2, and CH_2C=O, 12H), 3.70 (s, CH_2C=O, 2H), 3.94 (s, CH_2C=O, 4H); ^{13}C NMR (125 MHz, D_2O, δ at 65 °C): 35.4 (CH_2CH_2), 38.3 (CH_2CH_2), 48.2 (CH_2CH_2), 48.3 (CH_2CH_2), 48.9 (CH_2CH_2), 49.0 (CH_2CH_2), 52.1 (CH_2C=O), 52.3 (CH_2C=O), 52.9 (CH_2C=O), 169. 0, 169.3, 170.0; HRESIMS (*m*/*z*): $[M + H]^+$ calcd for $C_{18}H_{35}N_6O_7$, 447.2567; found 447.2562.

General procedure for the synthesis of M^{III}-containing complexes (**2.4**, **2.5**, and **2.6**): Ligand **2.1** (0.100 g, 0.207 mmol, 1 equiv) was dissolved in H_2O (20 mL) and the pH of the solution was adjusted to between 6 and 7 using 1 M NH_4OH. To the resulting solution was added $MCl_3\cdot6H_2O$ (0.311 mmol, 1.5 equiv), and the pH of the solution was adjusted to between 6 and 7 using 1 M NH_4OH. The reaction mixture was heated at 90 °C for 24 h and then cooled to ambient temperature. The pH of the solution was increased to 11 by adding 1 M NH_4OH followed by centrifugation, and the supernatant was filtered through a 0.2 µm hydrophilic syringe filter (Millipore, IC MILLEX-LG). The filtrate was dialyzed in a 500 Da molecular weight cut off (MWCO) dialysis membrane against H_2O (4 L). The dialysis reservoir was changed at 2–4, 6–8, and 10–14 h. After the last change, dialysis was continued for 7 h. Contents within the dialysis membrane were freeze dried to obtain 0.0948 g (74%) of **2.4**, 0.0851 g (67%) of **2.5**, or 0.0981 g (85%) of **2.6** as off-white solids. Purity of the complexes was verified by SEC, and the chromatograms are included in appendix B.

Gd^{III} complex (**2.4**): HRESIMS (*m*/*z*): $[M + H]^+$ calcd for $GdC_{18}H_{32}N_6O_7$, 599.1559; found 599.1579.

Eu^{III} complex (**2.5**): HRESIMS (*m*/*z*): $[M + H]^+$ calcd for $EuC_{18}H_{32}N_6O_7$, 595.1531; found 595.1523.

Y^{III} complex (**2.6**): HRESIMS (*m*/*z*): $[M + H]^+$ calcd for $YC_{18}H_{32}N_6O_7$, 533.1391; found 533.1396.

General procedure for the synthesis of M^{III}-containing conjugates (**2.13a–c**, **2.14a–c**, and **2.15a–c**): To a flask containing *N*-acetoxysuccinimide, **a**, or succinimidyl ester derivatives of PEG, **b** or **c** (5 equiv), was added dropwise a mixture of the M^{III} complex, **2.4**, **2.5**, or **2.6** (1 equiv), and diisopropylethylamine (5 equiv) in anhydrous CH_3OH (5 mL). The resulting mixture was allowed to stir at ambient temperature under Ar for 24 h. The resulting reaction mixture was added to aminomethylated polystyrene HL (100–200 mesh) resin (5 equiv, pre-swollen in C_2H_5OH for 0.5–1 h), and the resulting mixture was allowed to rotate for 15 to 18 h. The liquid portion of the reaction mixture was separated from the resin via filtration, and the resin was washed with C_2H_5OH (3 × 7 mL). The washings were combined with the liquid portion of the reaction mixture, and the solvents were removed under reduced pressure to obtain an oil that was dissolved in H_2O (10 mL) and washed with hexanes (4 × 10 mL). The H_2O layer was dialyzed in either a 500 (**2.13a**, **2.14a**, **2.15a**, **2.13b**, **2.14b**, and **2.15b**) or a 1,000 Da (**2.13c**, **2.14c**, and **2.15c**) MWCO dialysis membrane against H_2O (4 L). The dialysis reservoir was changed at 2–4, 6–8, and 10–14 h. After the last change, dialysis was continued for 7 h. Contents within the dialysis membrane were freeze dried and the resulting solids were washed with CH_3CN (3 × 5 mL) to yield M^{III}-containing conjugates **2.13a–c** and **2.14a–c**, and **2.15a–c** as white solids. The purity of the conjugates **2.13a–c**, **2.14a–c**, and **2.15a–c** was verified by reversed-phase HPLC, and the chromatograms are in appendix B.

Conjugate **2.13a**: 18.6 mg (46%), HRESIMS (*m*/*z*): $[M + H]^+$ calcd for $GdC_{20}H_{34}N_6O_8$, 641.1664; found 641.1640.

Conjugate **2.13b**: 29.1 mg (43%), HRESIMS (*m*/*z*): $[M + H]^+$ calcd for $GdC_{28}H_{50}N_6O_{12}$, 817.2713; found 817.2708.

Conjugate **2.13c**: 18.8 mg (51%), MALDI-MS: median peak $[M + H]^+$ calcd for $GdC_{57}H_{107}N_7O_{26}$, 1463.65; found 1463.19.

Conjugate **2.14a**: 18.9 mg (47%), HRESIMS (*m*/*z*): $[M + H]^+$ calcd for $EuC_{20}H_{34}N_6O_8$, 637.1637; found 637.1634.

Conjugate **2.14b**: 22.5 mg (34%), HRESIMS (*m*/*z*): $[M + H]^+$ calcd for $EuC_{28}H_{50}N_6O_{12}$, 813.2685; found 813.2682.

Conjugate **2.14c**: 12.87 mg (49%), MALDI-MS: median peak $[M + H]^+$ calcd for $EuC_{57}H_{107}N_7O_{26}$, 1458.65; found 1458.19.

Conjugate **2.15a**: 16.0 mg (48%), HRESIMS (*m*/*z*): $[M + H]^+$ calcd for $YC_{20}H_{34}N_6O_8$, 575.1497; found 575.1498.

Conjugate **2.15b**: 27.2 mg (39%), HRESIMS (*m*/*z*): $[M + H]^+$ calcd for $YC_{28}H_{50}N_6O_{12}$, 751.2545; found 751.2543.

Conjugate **2.15c**: 16.1 mg (49%), MALDI-MS: median peak $[M + H]^+$ calcd for $YC_{57}H_{107}N_7O_{26}$, 1394.63; found 1394.19.

General procedure for the synthesis of M^{III}-containing conjugates (**2.13d**, **2.14d**, and **2.15d**): To a flask containing succinimidylester derivative of PEG **d** (1 equiv) was added dropwise a mixture of the M^{III}-containing complex, **2.4**, **2.5**, or **2.6** (3 equiv), and diisopropylethylamine (3 equiv) in anhydrous CH_3OH (5 mL). The resulting mixture was allowed to stir at ambient temperature under Ar for 24 h. The resulting reaction mixture was concentrated under reduced pressure to obtain a white solid that was dissolved in H_2O (10 mL) and washed with hexanes (4 × 10 mL). The H_2O layer was dialyzed using a 1,000 Da MWCO dialysis membrane against H_2O (4 L). The dialysis reservoir was changed at 2–4, 6–8, and 10–14 h. After the last change, dialysis was continued for 7 h. Contents within the dialysis membrane were freeze dried, and the resulting solids were washed with CH_3CN (3 × 5 mL) to yield M^{III}-containing conjugates **2.13d** and **2.14d**, and **2.15d** as white solids. The purity of **2.13d**, **2.14d**, and **2.15d** was verified by aqueous SEC, and the chromatograms are in appendix B.

Conjugate **2.13d**: 42.6 mg (45%), MALDI-MS: median peak $[M + H]^+$ calcd for $GdC_{228}H_{448}N_6O_{112}$, 5222.87; found 5222.03.

Conjugate **2.14d**: 44.6 mg (48%), MALDI-MS: median peak $[M + H]^+$ calcd for $EuC_{228}H_{448}N_6O_{112}$, 5217. 87; found 5217.01.

Conjugate **2.15d**: 41.9 mg (44%), MALDI-MS: median peak $[M + Na]^+$ calcd for $YC_{228}H_{447}N_6O_{112}Na$, 5175.84; found 5175.88.

The attempted synthesis of M^{III}-containing conjugates **2.13e**, **2.14e**, and **2.15e** is discussed in Chapter 4.

The synthetic route to DO3A-based conjugates, **2.16a–2.18a** and **2.16c–2.18c**, is illustrated in **Scheme 2.5**. These conjugates were designed to investigate the influence of density of PEG on water-exchange rates.

Scheme 2.5. Synthetic route to M^{III}-containing PEG conjugates **2.16a–2.18a** and **2.16c–2.18c**.

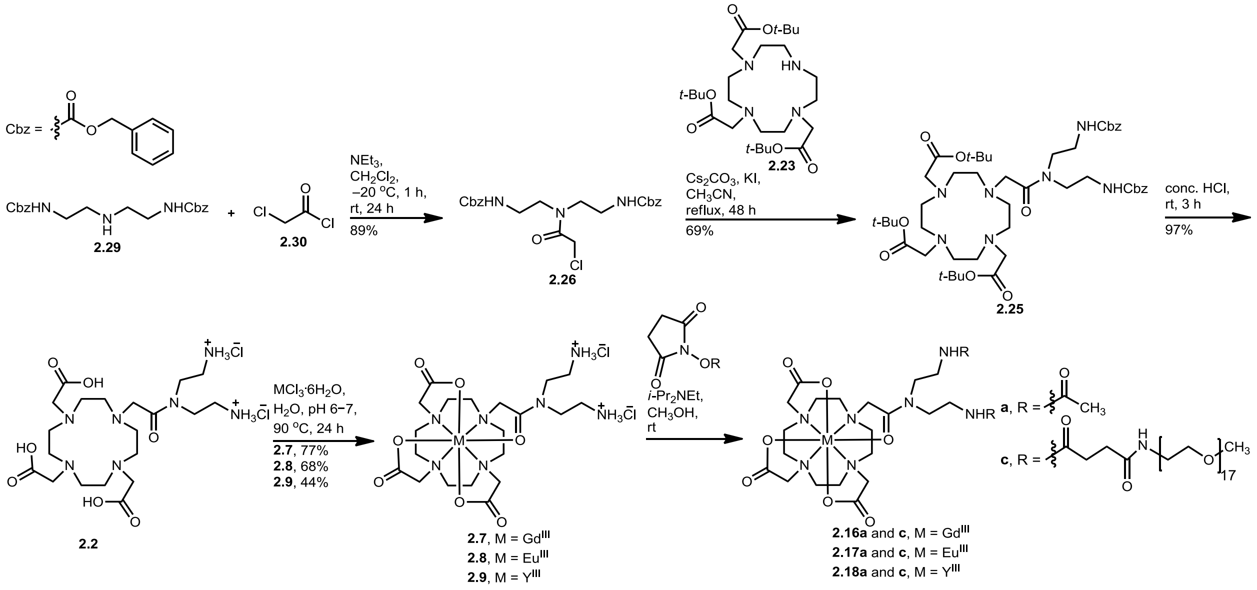
Cbz =
2.29
2.30
NEt3, CH2Cl2, –20 °C, 1 h, rt, 24 h
89%
2.26
2.23
Cs2CO3, KI, CH3CN, reflux, 48 h
69%
2.25
conc. HCl, rt, 3 h
97%
2.2
MCl3·6H2O, H2O, pH 6–7, 90 °C, 24 h
2.7, 77%
2.8, 68%
2.9, 44%
2.7, M = Gd(III)
2.8, M = Eu(III)
2.9, M = Y(III)
i-Pr2NEt, CH3OH, rt
2.16a and c, M = Gd(III)
2.17a and c, M = Eu(III)
2.18a and c, M = Y(III)
a, R =
c, R =

Attempted synthesis of conjugates **2.16a–2.18a** and **2.16c–2.18c** is discussed in Chapter 4.

N,N''-(Dicarboxybenzyl)diethylenetriamine-*N'*-acetylchloride (**2.26**): To a mixture of *N,N''*-(dicarboxybenzyl)diethylenetriamine **2.29** (0.999 g, 2.69 mmol, 1.0 equiv) and triethylamine (2.20 mL, 15.9 mmol, 5.9 equiv) in anhydrous CH_2Cl_2 (20 mL) was added dropwise a solution of chloroacetyl chloride **2.30** (0.65 mL, 8.06 mmol, 3.0 equiv) in CH_2Cl_2 (20 mL) over 1 h at –20 °C under Ar. The reaction mixture was stirred at ambient temperature under Ar for 24 h, then filtered through celite. The filtrate was washed with aqueous citric acid (40 mL) followed by H_2O (3 × 40 mL). The organic layer was dried over anhydrous K_2CO_3 and concentrated under reduced pressure to obtain a dark brown solid that was purified using silica gel column chromatography (100% $CH_3COOC_2H_5$). Fractions with an R_f value (100% $CH_3COOC_2H_5$) of 0.69 were combined and concentrated under reduced pressure to obtain 1.070 g (89%) of **2.26** as a light yellow oil. ^1H NMR (400 MHz, $CDCl_3$, δ): 2.15–3.65 (m, CH_2CH_2, 8H), 4.02 (s, $COCH_2Cl$, 2H), 5.07 (s, $CO_2CH_2C_6H_5$, 2H), 5.11 (s, $CO_2CH_2C_6H_5$, 2H), 5.38 (brs, N*H*, 1H), 5.56 (brs, N*H*, 1H), 7.28–7.43 (m, C_6H_5, 10H); ^{13}C NMR (101 MHz, $CDCl_3$, δ): 39.4

(CH_2CH_2), 39.7 (CH_2CH_2), 41.0 ($COCH_2Cl$), 46.4 (CH_2CH_2), 48.6 (CH_2CH_2), 66.9 ($CO_2CH_2C_6H_5$), 67.1 ($CO_2CH_2C_6H_5$), 128.1 (C_6H_5), 128.2 (C_6H_5), 128.3 (C_6H_5), 128.5 (C_6H_5), 128.6 (C_6H_5), 136.2, 136.4, 156.7, 156.9, 168.2; HRESIMS (*m/z*): $[M + H]^+$ calcd for $C_{22}H_{27}N_3O_5Cl$, 448.1639; found 448.1639.

1,4,7-Tris(*tert*-butyloxycarbonylmethyl)-10-*N,N''*-(dicarboxybenzyl)diethylenetriamine-*N'*-acetamide-1,4,7,10-tetraazacyclododecane (**2.25**): To a mixture of **2.23** (0.431 g, 0.837 mmol, 1.0 equiv), Cs_2CO_3 (0.632 g, 1.94 mmol, 2.3 equiv), and KI (0.294 g, 1.77 mmol, 2.1 equiv) in anhydrous CH_3CN (35 mL) was added a solution of **2.26** (0.448 g, 1.00 mmol, 1.2 equiv) in CH_3CN (35 mL). The resulting mixture was stirred under Ar at reflux for 48 h. The reaction mixture was allowed to cool to ambient temperature and filtered through celite. The filtrate was concentrated under reduced pressure. The resulting residue was dissolved in $CHCl_3$ (40 mL) and sequentially washed with H_2O (40 mL) and saturated aqueous KCl (3 × 40 mL). The organic layer was dried over anhydrous K_2CO_3 and concentrated under reduced pressure. The resulting yellow solid was purified by silica gel column chromatography (10:1 $CH_3COOC_2H_5/CHCl_3$). Fractions with an R_f value of 0.2 (10:1 $CH_3COOC_2H_5/CHCl_3$) were combined and concentrated under reduced pressure to obtain 0.535 g (69%) of **2.25** as a light yellow solid. ^1H NMR (400 MHz, $CDCl_3$, δ): 1.28–1.50 (m, CH_3, 27H), 1.66–3.00 (m, CH_2CH_2 ring, and NCH_2CO, 24H), 3.08–3.60 (m, CH_2CH_2 arm, 8H), 4.95–5.07 (m, $CH_2OC{=}O$, 4H), 6.12 (brs, N*H*), 6.97 (brs, N*H*), 7.17–7.35 (m, $CH_2C_6H_5$, 10H); ^{13}C NMR (101 MHz, $CDCl_3$, δ): 27.9 (CH_3), 39.3 (CH_2CH_2 arm), 39.9 (CH_2CH_2 arm), 47.0 (CH_2CH_2 ring), 47.8 (CH_2CH_2 ring), 49.0 (CH_2CH_2 ring), 52.5 (CH_2CH_2 ring), 55.0 ($CH_2C{=}O$), 55.6 ($CH_2C{=}O$), 66.2 ($CH_2OC{=}O$), 81.8 ($C(CH_3)_3$), 127.7 (C_6H_5), 127.9 (C_6H_5), 128.1 (C_6H_5), 128.4 (C_6H_5), 136.9, 156.7, 157.1, 172.5, 172.8; HRESIMS (*m/z*): $[M + H]^+$ calcd for $C_{48}H_{76}N_7O_{11}$, 926.5603; found 926.5609.

1,4,7-Tris(carbonylmethyl)-10-*N,N''*-(dicarboxybenzyl)diethylenetriamine-*N'*-acetyl)-1,4,7,10-tetraazacyclododecane (**2.2**): To protected ligand **2.25** (0.499 g, 0.539 mmol) was added concentrated HCl (50 mL) and the resulting mixture was stirred at ambient temperature for 3 h. The reaction mixture was concentrated under reduced pressure. The resulting residue was dissolved in water and freeze dried to obtain 0.294 g (97%) of **2.2** as a light brown solid. ^{1}H NMR (400 MHz, D_2O, δ at 80 °C): 3.50−3.70 (m, CH_2CH_2 ring, and CH_2CH_2 arm, 12H), 3.79 (brs, CH_2CH_2 ring, 8H), 4.04–4.12 (m, CH_2CH_2 arm, 4H), 4.19 (brs, CH_2C=O, 2H), 4.30–4.44 (m, CH_2C=O, 6H); ^{13}C NMR (125 MHz, D_2O, δ at 70 °C): 36.2 (*C*H$_2$*C*H$_2$ arm), 38.4 (*C*H$_2$*C*H$_2$ arm), 43.6 (*C*H$_2$*C*H$_2$ ring), 48.7 (*C*H$_2$*C*H$_2$ ring), 50.1 (*C*H$_2$C=O), 53.0 (*C*H$_2$C=O), 53.7 (*C*H$_2$C=O), 169.8, 171.4; HRESIMS (*m/z*): calcd for $C_{20}H_{40}N_7O_7$, 490.2989; found 490.2982.

General procedure for the synthesis of M^{III}-containing complexes (**2.7**, **2.8**, and **2.9**): Ligand **2.2** (0.100 g, 0.179 mmol, 1.0 equiv) was dissolved in H_2O (20 mL) and the pH of the solution was adjusted to between 6 and 7 using 1 M NH_4OH. To the resulting solution was added $MCl_3 \cdot 6H_2O$ (0.267 mmol, 1.5 equiv), and the pH of the solution was adjusted to between 6 and 7 using 1 M NH_4OH. The reaction mixture was heated at 90 °C for 24 h and then allowed to cool to ambient temperature. The pH of the solution was increased to 11 by adding 1 M NH_4OH followed by centrifugation, and the supernatant was filtered through a 0.2 μm hydrophilic syringe filter (Millipore, IC MILLEX-LG). The filtrate was dialyzed in a 500 Da MWCO dialysis membrane against H_2O (4 L). The dialysis reservoir was changed at 2–4, 6–8, and 10–14 h. After the last change, dialysis was continued for 3 h. Contents within the dialysis membrane were freeze dried to obtain 0.0912 g (77%) of **2.7**, 0.0799 g (68%) of **2.8**, or 0.0467 g (44%) of **2.9** as off-white solids. The purity of complexes was verified using SEC, and the chromatograms are in appendix B.

Gd^{III} complex (**2.7**): HRESIMS (*m*/*z*): $[M + H]^+$ calcd for $GdC_{20}H_{37}N_7O_7$, 642.1981; found 642.1973.

Eu^{III} complex (**2.8**): HRESIMS (*m*/*z*): $[M + H]^+$ calcd for $EuC_{20}H_{37}N_7O_7$, 638.1953; found 638.1927.

Y^{III} complex (**2.9**): HRESIMS (*m*/*z*): $[M + H]^+$ calcd for $YC_{20}H_{37}N_7O_7$, 576.1813; found 576.1812.

Attempted synthesis of M^{III}-containing conjugates **2.16a–2.18a** and **2.16c–2.18c** is discussed in Chapter 4.

The synthetic routes to DO2A-based conjugates, **2.19a–2.21a** and **2.19c–2.21c**, designed to investigate the influence of density of PEG on water-exchange rates is illustrated in **Scheme 2.6**.

Scheme 2.6. Synthetic route to M^{III}-containing PEG conjugates **2.19a–2.21a** and **2.19c–2.21c**.

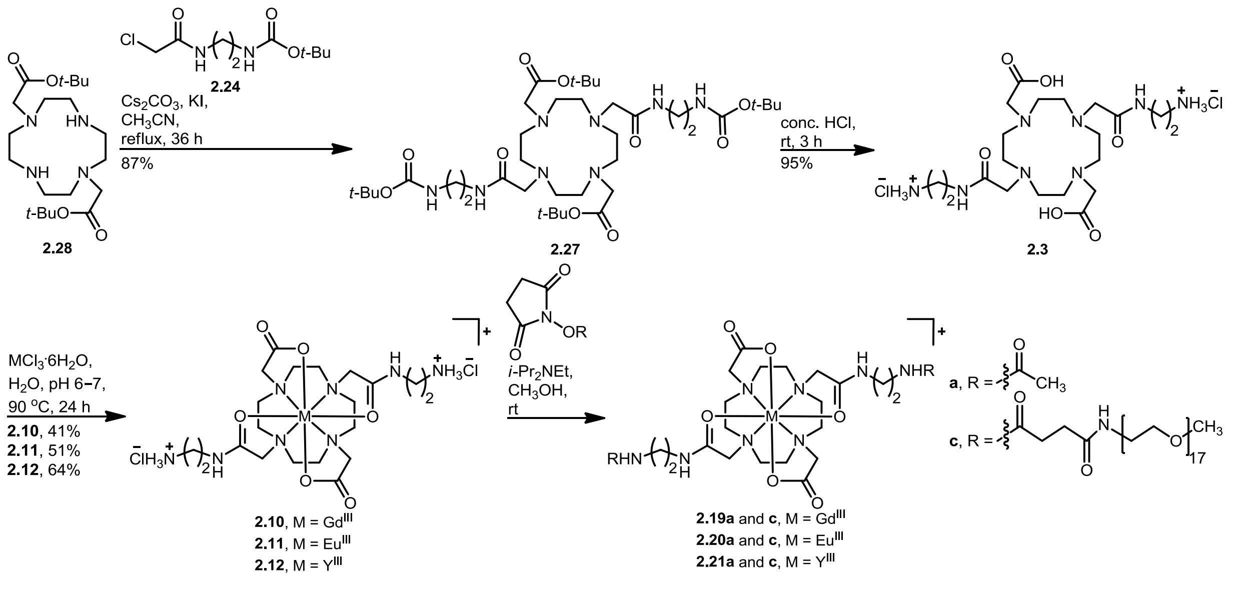
2.24
Cs2CO3, KI, CH3CN, reflux, 36 h
87%
2.28
2.27
conc. HCl, rt, 3 h
95%
2.3
MCl3·6H2O, H2O, pH 6–7, 90 °C, 24 h
2.10, 41%
2.11, 51%
2.12, 64%
2.10, M = Gd^III
2.11, M = Eu^III
2.12, M = Y^III
i-Pr2NEt, CH3OH, rt
2.19a and c, M = Gd^III
2.20a and c, M = Eu^III
2.21a and c, M = Y^III
a, R =
c, R =
17

Attempted synthesis of conjugates **2.19a–2.21a and 2.19c–2.21c** is discussed in Chapter 4.

1,7-Bis(*tert*-butyloxycarbonylmethyl)-7,10-bis(*N*-(2-*tert*-butoxycarbonylaminoethyl) acetamide-1,4,7,10-tetraazacyclododecane (**2.27**): To a mixture of **2.28** (0.250 g, 0.624 mmol, 1.0 equiv), Cs_2CO_3 (0.854 g, 2.62 mmol, 4.2 equiv), and KI (0.477 g, 2.87 mmol, 4.6 equiv) in anhydrous CH_3CN (20 mL) was added a solution of **2.24** (0.325 g, 1.37 mmol, 2.2 equiv) in CH_3CN (20 mL). The resulting mixture was stirred under Ar at reflux for 36 h. The reaction mixture was allowed to cool to ambient temperature and filtered through celite. The filtrate was concentrated under reduced pressure. The resulting residue was dissolved in $CHCl_3$ (40 mL) and sequentially washed with H_2O (40 mL) and saturated aqueous KCl (3 × 40 mL). The organic layer was dried over anhydrous K_2CO_3 and concentrated under reduced pressure to obtain 0.435 g (87%) of **2.27** as a yellow solid. ^1H NMR (400 MHz, $CDCl_3$, δ): 1.35–1.52 (m, CH_3, 36 H), 2.62 (brs, CH_2CH_2 ring, 8H), 2.75 (brs, CH_2CH_2 ring, 8H), 3.02 (s, NCH_2CO, 4H), 3.13–3.46 (m, NCH_2CO and CH_2CH_2 arm, 12 H), 5.39 (brs, *H*N, 2H), 8.26 (brs, *H*N, 2H); ^{13}C NMR (101 MHz, $CDCl_3$, δ): 28.3 (CH_3), 28.6 (CH_3), 39.4 (CH_2CH_2 arm), 41.2 (CH_2CH_2 arm), 53.0 (CH_2CH_2 ring), 54.8 (CH_2CH_2 ring), 56.6 ($CH_2C{=}O$), 59.4 ($CH_2C{=}O$), 79.2 ($C(CH_3)_3$), 81.5 ($C(CH_3)_3$), 156.3, 170.5, 172.4; HRESIMS (*m/z*): $[M + H]^+$ calcd for $C_{38}H_{73}N_8O_{10}$, 801.5450; found 801.5411.

1,7-Bis(carbonylmethyl)-7,10-bis(*N*-(2-*tert*-butoxycarbonylaminoethyl)acetamide-1,4,7,10-tetraazacyclododecane (**2.3**): To protected ligand **2.27** (0.465 g, 0.581 mmol) was added concentrated HCl (50 mL), and the resulting mixture was stirred at ambient temperature for 3 h. The reaction mixture was concentrated under reduced pressure. The resulting residue was dissolved in water and freeze dried to obtain 0.316 g (97%) of **2.3** as a light brown solid. ^1H NMR (400 MHz, $CDCl_3$, δ at 70 °C): 3.64−3.74 (m, CH_2CH_2 arm, and CH_2CH_2 ring, 12H), 3.86 (brs, CH_2CH_2 ring, 8H), 3.96−4.08 (m, CH_2CH_2 arm, 4H), 4.17 (s, $CH_2C{=}O$, 4H), 4.47 (s, $CH_2C{=}O$, 4H); ^{13}C NMR (125 MHz, D_2O, δ at 70 °C): 36.4 (CH_2CH_2 arm), 38.8 (CH_2CH_2 arm), 48.4 (CH_2CH_2 ring), 50.5 (CH_2CH_2 ring), 53.0 ($CH_2C{=}O$), 54.4 ($CH_2C{=}O$), 167.5, 172.1; HRESIMS (*m/z*): $[M + H]^+$ calcd for $C_{20}H_{41}N_8O_6$, 489.3149; found 489.3170.

General procedure for the synthesis of M^{III}-containing complexes (**2.10**, **2.11**, and **2.12**): Ligand **2.3** (0.150 g, 0.267 mmol, 1.0 equiv) was dissolved in H_2O (20 mL), and the pH of the solution was adjusted to between 6 and 7 using 1 M NH_4OH. To the resulting solution was added $MCl_3 \cdot 6H_2O$ (0.401 mmol, 1.5 equiv), and the pH of the solution was adjusted to between 6 and 7 using 1 M NH_4OH. The reaction mixture was heated at 90 °C for 24 h and then allowed cooled to ambient temperature. The pH of the solution was increased to 11 by adding 1 M NH_4OH followed by centrifugation, and the supernatant was filtered through a 0.2 μm hydrophilic syringe filter (Millipore, IC MILLEX-LG). The filtrate was dialyzed using a 500 Da MWCO dialysis membrane against H_2O (4 L). The dialysis reservoir was changed at 2–4, 6–8, and 10–14 h. After the last change, dialysis was continued for 3 h. Contents within the dialysis membrane were freeze dried to obtain 0.0705 g (41%) of **2.10**, 0.103 g (51%) of **2.11**, or 0.0993 g (64%) of **2.12** as off-white solids. The purity of complexes was verified using SEC, and the chromatograms are in appendix B.

Gd^{III} complex (**2.10**): HRESIMS (*m*/*z*): $[M]^+$ calcd for $GdC_{20}H_{38}N_8O_6$, 641.2141; found 641.2125.

Eu^{III} complex (**2.11**): HRESIMS (*m*/*z*): $[M]^+$ calcd for $EuC_{20}H_{38}N_8O_6$, 637.2113; found 637.2081.

Y^{III} complex (**2.12**): HRESIMS (*m*/*z*): $[M]^+$ calcd for $YC_{20}H_{38}N_8O_6$, 575.1973; found 575.1976.

Attempted synthesis of conjugates **2.19a–2.21a** and **2.19c–2.21c** is discussed in Chapter 4.

Applications

Properties of the synthesized Ln^{III}-containing polyaminopolycaboxylate-type PEG conjugates are discussed in Chapter 3. Moreover, Chapter 3 illustrates studies performed to investigate the influence of length of PEG on contrast-agent-relevant properties including water-exchange rates of Ln^{III}-containing complexes. In addition, interpretation of the data obtained, followed by the implications of these findings to the design of contrast agents for magnetic resonance imaging is discussed.

CHAPTER 3: Modulating Water-Exchange Rates of Lanthanide(III)-Containing Polyaminopolycarboxylate-Type Complexes Using Polyethylene Glycol

Adapted with permission from Siriwardena-Mahanama, B.N.; Allen, M.J. *Dalton Trans.* **2013,** *42*, 6724–6727. Reproduced by permission of The Royal Society of Chemistry.

http://pubs.rsc.org/en/results?artrefjournalname=dalton%20trans.&artrefstartpage=6724&artrefvolumeyear=2013&fcategory=journal

Introduction

The efficiency of Ln^{III}-containing complexes as conventional (T_1-reducing) and paramagnetic chemical exchange saturation transfer (PARACEST) contrast agents for magnetic resonance imaging (MRI) is governed by the interactions among the structural and electronic properties of these complexes and by the interactions of these complexes with the environment.[4,54,96–101] The optimal value for a specific parameter is a moving target that varies as a function of magnetic field strength and the other parameters.[8,15,80,102] Of these parameters, the exchange rate between coordinated and bulk water, k_{ex}, plays a critical role in establishing contrast-enhancing efficiency.[15,49,96–101] Hence, the ability to precisely control the water-exchange rates of Ln^{III}-containing complexes is imperative to achieving optimal efficiencies of contrast agents for both conventional and PARACEST imaging.

For example, conventional, Gd^{III}-containing, small molecular-weight agents require a fast water-exchange rate ($\sim 10^8$ s^{-1}) to achieve optimal efficiency at the clinically relevant field strength of 1.5 T,[8,103] and macromolecular Gd^{III}-based agents require a faster water-exchange rate ($\sim 10^{10}$ s^{-1}).[102] However, these target values change with changes in field strength. Different from conventional agents, Ln^{III}-based PARACEST agents require slow-to-intermediate water-exchange rates on the NMR time scale, and the optimal value for the water-exchange rate depends on the frequency of the pulse used to presaturate the exchangeable protons.[17] The estimated optimal water-exchange rate for PARACEST agents is between 0.3×10^3 and 1×10^3 s^{-1} at clinically relevant pulse frequencies (50–100 Hz).[17]

The water-exchange rates of clinically approved Gd^{III}-containing small molecular-weight contrast agents are slower (1×10^6 to 4×10^6 s^{-1}) than the optimal value (10^8 s^{-1} at 1.4 T),[50] and the water-exchange rates of most Ln^{III}-based complexes developed as potential PARACEST agents are faster (0.3×10^4 to 1×10^4 s^{-1}) than the optimal value.[17] Consequently, there is a need to tune the water-exchange rates of Ln^{III}-containing complexes to achieve optimum efficiencies for conventional and PARACEST agents. This need has been the focus of a great deal of research. Tuning water-exchange rates of Ln^{III}-containing complexes has been achieved by several coordination-chemistry-based modifications as described in Chapter 1 including modifying (1) the charge of the Ln^{III}-based complex;[39] (2) the accessibility of the metal center to bulk water;[10,15,55,63,67,68,104–106] (3) the mechanism of water exchange;[28] and (4) the ratio between twisted square anti-prism and square anti-prism isomers for Ln^{III}-based complexes with 1,4,7,10-tetraazacyclododecane-1,4,7,10-tetraacetic acid (DOTA)-type ligands.[69,79] These studies demonstrate that small modifications in ligand structure can have large impacts on the water-exchange rates of Ln^{III}-containing complexes, but most of these studies are specific to the system being studied.

It was envisioned that a modular and tunable system of modifications could be incorporated into Ln^{III}-based DOTA-type systems to tune water-exchange rates. Consequently, it was hypothesized that bio-compatible, hydrophilic oligomers of polyethylene glycol (PEG) could be used to modulate water-exchange rates by altering the accessibility of bulk water to the Ln^{III}-center through both steric and hydrogen bonding interactions in a systematic fashion based on oligomer length. In this chapter, the influence of length of PEG on the molecular parameters, including water-exchange rates, of Ln^{III}-containing DOTA-type complexes is described.

To investigate the influence of PEG oligomers on the water-exchange rates of Ln^{III}-containing complexes, a PEG-containing model system, **2.13a–d** and **2.14a–d** in **Figure 3.1** was designed and synthesized to modulate the water-exchange rates of Ln^{III}-DOTA-type complexes. It was expected that PEG would hydrogen bond to water through the large number of oxygen-based hydrogen bond acceptors, thereby changing the extent of the hydrogen bonding network as PEG length is varied. This hypothesis is consistent with reports of changes in water-exchange rates being observed as the length of PEG was varied with PEG-conjugates of Gd^{III}-containing hydroxypyridonate (HOPO)-based complexes.[67,68,105,106] The HOPO-based systems have a water-coordination number of two and display fast water-exchange rates (~10^8 s^{-1}). The PEG moiety in those systems led to slower water-exchange rates and a decrease in water-coordination number from two to one. It was expected that PEG could be used to fine-tune the water-exchange rates of other systems including Ln^{III}-containing DOTA-type complexes with water-coordination numbers of one and relatively slow water-exchange rates (~10^6 s^{-1}).

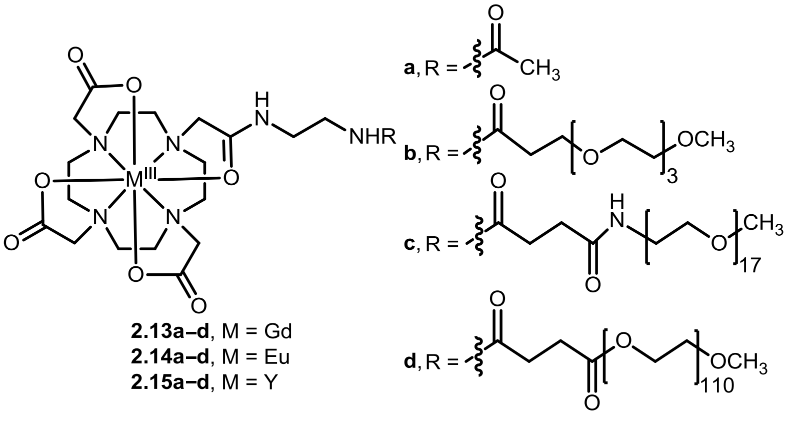

2.13a–d, M = Gd
2.14a–d, M = Eu
2.15a–d, M = Y

Figure 3.1. Structures of M^{III}-containing PEG conjugates **2.13a–d**, **2.14a–d**, and **2.15a–d**.

The model system that was designed includes M^{III}-containing complexes without PEG (**2.13a**, **2.14a**, and **2.15a**) as well as six complexes with different length oligomers of PEG (**2.13b–d**, **2.14b–d**, and **2.15b–d**). The synthetic route to M^{III}-containing complexes **2.13a–d**, **2.14a–d**, and **2.15a–d** is shown in **Scheme 2.4** in Chapter 2.

Experimental Procedures

Synthesis, purification, and characterization of compounds **2.13a–d** discussed in this chapter were carried out as described in Chapter 2.

Inductively coupled plasma optical emission spectroscopy (ICP-OES) measurements were performed on a HORIBA Jobin Yvon *ULTIMA* spectrometer or by Columbia Analytical Services Inc., Tucson, Arizona, USA. Samples measured with the *ULTIMA* spectrometer were diluted with nitric acid (2% v/v, aqueous), and standards were prepared by serial dilution of Gd, Eu, and Y standards (High-Purity Standards).

Water proton relaxation rate data were obtained using a Bruker mq 60 NMR Analyzer (1.4 T) at 37 °C for Gd^{III}-containing conjugates **2.13a–d** in phosphate-buffered saline (pH 7.4). The relaxivities of Gd^{III}-containing conjugates were obtained from the slopes of the linear plots of $1/T_1$ versus Gd^{III} concentration. Measurements were repeated three times with independently prepared solutions for each Gd^{III}-containing conjugate. The Gd^{III} concentration was verified by ICP–OES. The water proton relaxation rate data obtained for complexes **2.13a–d** are illustrated in **Tables C.1–C.4** (Appendix C).

Variable-temperature ^{17}O-NMR measurements of Gd^{III}-containing conjugates **2.13a** (6 mM), **2.13b** (6 mM), **2.13c** (4 mM), and **2.13d** (17 mM) and their diamagnetic Y^{III} analogues (**2.15a–d**) in H_2O were carried out on a Varian-500S spectrometer. Enrichment in ^{17}O (1%) was achieved using ^{17}O-enriched water (10% $H_2{}^{17}O$, Cambridge Isotope Laboratories, Inc.). Line widths at half height were measured at 20 (or 25), 30, 40, 50, 60, and 70 °C. A/ħ and ΔE were fixed to -3.8×10^{-6} rad/s and 2.5×10^{-11} J/mol, respectively, for Gd^{III}-containing conjugates, **2.13a–d**. The water-coordination number, *q*, was set to the value obtained from luminescence-decay measurements for Eu^{III}-containing conjugates **2.14a–d**. The least-squares fits of the ^{17}O-NMR relaxation data were calculated using origin software (8.0951 B951) following a previously published procedure[107] to obtain the water-exchange rates of Gd^{III}-containing conjugates, **2.13a–d**. Gd^{III} and Y^{III} concentrations were verified by ICP–OES. The data obtained from variable temperature ^{17}O-NMR measurements and corresponding least-squares fits of ^{17}O-NMR data are shown in **Tables C.5–C.8** (Appendix C).

Luminescence-decay measurements of Eu^{III}-containing conjugates **2.14a–d**, in H_2O and D_2O were acquired using a HORIBA Jobin Yvon Fluoromax-4 spectrofluorometer in decay by delay scan mode using the phosphorescence lifetime setting. Excitation and emission wavelengths of 393 and 596 nm were used, respectively, while the other parameters were kept constant: excitation and emission slit widths (5 nm), flash count (100), initial delay (0.01 ms), maximum delay (2 ms for solutions in H_2O and 8 ms for solutions in D_2O), and delay increment (0.01 ms). The decay rates obtained from luminescence-decay measurements for conjugates **2.14a–d** are included in **Table C.9** (Appendix C). The number of coordinated water molecules, *q*, was determined using the method developed by Horrocks and coworkers.[108]

Electron paramagnetic resonance (EPR) measurements of **2.13a–d** in water were performed on a Bruker EMX X-band spectrometer. From the EPR spectra, the electronic Landé *g* factors, g_L, peak-to-peak line widths, ΔH_{pp}, and transverse electronic relaxation rates, $1/T_{2e}$, were obtained according to a previously reported method.[31] The EPR spectra and the parameters obtained from EPR spectra for conjugates **2.13a–d** (**Table C.10**) are illustrated in Appendix C.

Results and Discussion

Analysis of Water-Coordination Number Data

The water-coordination number, q, was obtained for Eu^{III}-containing complexes **2.14a–d** using luminescence-decay measurements (**Table 3.1**).[108] Values of q were close to 1, and these values agree with what is expected for Ln^{III}-complexes coordinated to octadentate ligands. Water-coordination number data for **2.14a–d** suggest that steric blocking has little if any influence on the properties of the complexes.

Table 3.1. Molecular parameters of complexes **2.13a–d**.

Parameter	**2.13a**	**2.13b**	**2.13c**	**2.13d**
$q^{a,b,c}$	0.90 ± 0.01	0.89 ± 0.01	0.96 ± 0.01	0.76 ± 0.01
$\tau_m{}^{298} \times 10^{-6}$ (s)^a	0.37 ± 0.01	0.66 ± 0.01	1.2 ± 0.1	1.5 ± 0.07
$k_{ex}{}^{298} \times 10^{6}$ (s^{-1})^d	2.7 ± 0.03	1.5 ± 0.02	0.83 ± 0.08	0.67 ± 0.05
$T_{1e}{}^{298} \times 10^{-9}$ (s)^a	440 ± 30	61 ± 1	12 ± 0.3	4.0 ± 0.04
ΔH (kJ mol^{-1})^a	36 ± 1	50 ± 1	71 ± 4	90 ± 2
r_1 (mM^{-1} s^{-1})^a	2.5 ± 0.1	4.0 ± 0.1	5.3 ± 0.1	6.3 ± 0.1
MW (Da)	641	817	1463	5222
g_L	1.98	1.98	1.99	1.98
$1/T_{2e} \times 10^{6}$ (s^{-1})	17.8	8.11	6.51	5.03
$\tau_R \times 10^{-12}$ (s)	46	79	110	220

[a]Reported as mean ± standard error. [b]From complexes **2.14a–d**. [c]The error associated with q determination is ±0.1 water molecules.[107] [d]Error represents relative uncertainty.

Analysis of Variable-Temperature ^{17}O-NMR Data

To investigate the influence of PEG on tuning water-exchange rates, variable-temperature ^{17}O-NMR experiments for Gd^{III}-containing conjugates **2.13a–d** were performed, and the fitted molecular parameters are summarized in **Table 3.1**: the residence lifetime of coordinated water, $\tau_m{}^{298}$ (water-exchange rate, $k_{ex}{}^{298}$, is $1/\tau_m{}^{298}$); the longitudinal electronic relaxation time, $T_{1e}{}^{298}$; and the enthalpy change for the water-exchange process, ΔH. Based on the results of the variable temperature ^{17}O-NMR experiments, a gradual decrease in water-exchange rates was observed with increasing length of PEG from **2.13a** (control without PEG) to **2.13d** (long PEG). Moreover, 1.8-, 3.3-, and 4.0-fold decreases in water-exchange rates were observed from **2.13a** to **2.13b**, **2.13c**, and **2.13d**, respectively. The observed decrease in water-exchange rates with increasing length of PEG was supported by an increase in ΔH from **2.13a** to **2.13d**. This increase in enthalpy suggests that the exchange between coordinated and bulk water molecules becomes difficult as length of PEG is increased, possibly due to a larger hydrogen-bond network. The increase in ΔH and decrease in water-exchange rates from **2.13a** to **2.13d** support the hypothesis that PEG is able to modify the water-exchange properties of $\mathrm{Gd^{III}}$-containing DOTA-type complexes as a function of length.

Analysis of Relaxivity Data

To investigate the influence of length of PEG on the efficiency of complexes **2.13a–d** as conventional contrast agents, relaxivity, r_1, measurements of **2.13a–d** at 37 °C and 1.4 T in phosphate-buffered saline (pH = 7.4) were carried out. The r_1 values of **2.13a–d** were obtained from the slopes of the plots of $1/T_1$ versus $\mathrm{Gd^{III}}$ concentration (**Table 3.1**). A 2.5-fold increase in relaxivity was observed as the length of PEG was increased from **2.13a** to **2.13d**. This increase in relaxivity corresponds to the increase in molecular weight (MW, **Table 3.1**) from **2.13a** to **2.13d**. As the molecular weight increases, complexes tend to tumble more slowly in solution leading to higher relaxivity values.[109]

Analysis of Estimated Rotational Correlation Times (τ_R)

To more rigorously unite ^{17}O-NMR spectroscopy and relaxivity data, electron paramagnetic resonance spectroscopy measurements were performed to obtain the electronic Landé g factor, g_L, and the transverse electronic relaxation rate, $1/T_{2e}$, of **2.13a–d**. These parameters together with r_1, k_{ex}, T_{1e}, and q were used with the Solomon–Bloembergen–Morgan equations, which describe the factors affecting the efficiency of contrast agents for MRI,[8] to obtain estimated rotational correlation times, τ_R, for **2.13a–d** (**Table 3.1** and calculations in

Appendix C). The values of τ_R seem lower than expected likely due to the internal motion of the PEG moieties as suggested for the HOPO-based system,[67,68,105,106] due to the ineffective coupling between the motion of Gd-water vector and rotational motion of the entire molecule,[7] or a combination of the two. An increase in the τ_R values was observed from **2.13a** to **2.13d**, which is consistent with the increase in molecular weight as the length of PEG is increased. This increase in τ_R is likely the cause of the observed increase in relaxivity from **2.13a** to **2.13d**. However, the increase in relaxivity observed from **2.13a** to **2.13d** is lower-than-expected based solely on the variation in τ_R from **2.13a** to **2.13d** (calculations illustrated in Appendix C), and this observation is a likely result of the decrease in water-exchange rates as length of PEG increases from **2.13a** to **2.13d**.

Conclusions

This chapter describes the influence of PEG oligomer length on the water-exchange rates and other molecular parameters that contribute to the efficiency of Ln^{III}-containing DOTA-type contrast agents. Based on the results obtained, PEG can be used to fine-tune, toward slower rates, the water-exchange rates of Ln^{III}-containing DOTA-type complexes. The findings discussed in this chapter demonstrate a similar magnitude of slowing of water-exchange rates as was reported with HOPO-based systems,[67,68,105,106] but without the associated change in water-coordination number. Consequently, PEG is able to slow the water-exchange rates of Ln^{III}-containing complexes regardless of water-coordination number, demonstrating that conjugation of PEG represents a modular and tunable strategy for slowing water-exchange rates that is general for Ln^{III}-containing complexes. It is expected that these findings will be useful in the design of Ln^{III}-based contrast agents that require slow water-exchange rates on the NMR time scale.

CHAPTER 4: Synthesis of Lanthanide(III)-Containing Polyethylene Glycol (PEG) Conjugates for the Investigation of the Influence of the Density of PEG on Water-Exchange Rates of Lanthanide(III)-Containing Complexes

Introduction

The prevalent use of magnetic resonance imaging (MRI) as an imaging tool in clinical medicine and biomedical research is a result of the non-invasive nature of the technique as well as excellent tissue penetration and capability to produce three-dimensional images with high spatial resolution (~1 mm^3).[1,2,8] The usefulness of MRI is enhanced with the use of paramagnetic substances known as contrast agents. Most clinically approved contrast agents are based on lanthanide(III) (Ln^{III})-containing complexes with polyaminopolycarboxylate-type ligand frameworks.[2,8] The efficiency of Ln^{III}-containing complexes as contrast agents for MRI is determined by interactions among the structural, dynamic, and electronic properties of these complexes.[4,54,96–101] The rate of exchange between coordinated and bulk water, k_{ex}, is an important parameter that contributes to the efficiency of Ln^{III}-containing complexes as T_1-shortening and paramagnetic chemical exchange saturation transfer (PARACEST) contrast agents for MRI.[15,49,96–101] Moreover, T_1-shortening and PARACEST agents rely on water-exchange rates to bring about optimum efficiencies. Consequently, tuning of water-exchange rates of Ln^{III}-containing complexes is critical for developing T_1-shortening and PARACEST contrast agents with improved efficiency. Because T_1-shortening and PARACEST agents differ in the mechanism of action that generates contrast enhancement in MRI, tuning of water-exchange rates in opposite directions is required for these two types of agents. Specifically, T_1-shortening agents need to be tuned toward fast rates (10^8 s^{-1})[8,103] and PARACEST agents need to be tuned toward slow rates (10^3 s^{-1}).[17] This need to tune water-exchange rates over a broad range from slow to fast (10^3–10^8 s^{-1}) has given rise to an extensive amount of research efforts to tune water-exchange rates of Ln^{III}-containing complexes through coordination-chemistry-based modifications.

Several different coordination-chemistry-based strategies have been employed to tune water-exchange rates of Ln^{III}-containing complexes. As described in Chapter 1, these strategies include modification of (1) the water-exchange mechanism;[28] (2) the charge of the Ln^{III}-containing complex;[39] (3) the steric hindrance at the water-coordination site;[10,55] (4) the ligand side chains;[15,63,67,68,104–106] and (5) the ratio of twisted square anti-prism to square anti-prism isomers for Ln^{III}-containing 1,4,7,10-tetraazacyclododecane-1,4,7,10-tetraacetate (DOTA)-type complexes.[69,79] Findings of studies that relate coordination-chemistry-based modifications to changes in water-exchange rates reveal that substantial differences in water-exchange rates can be achieved with minor alterations in the structure of the Ln^{III}-containing complexes.

Consequently, it was expected that a modular system of modifications based on hydrophilic polyethylene glycol (PEG) could be incorporated on to Ln^{III}-containing DOTA-type complexes to tune water-exchange rates. It was hypothesized that PEG could be used to tune water-exchange rates by stabilizing the coordinated water through hydrogen-bonding interactions and altering the accessibility of bulk water through steric and hydrogen-bonding interactions. Moreover, the results presented in Chapter 3 demonstrate that PEG is able tune water-exchange rates of Ln^{III}-containing DOTA-type complexes as a function of length of PEG. Because tuning of water-exchange rates was possible as a function of length of PEG, it was envisioned that varying the density of PEG could influence water-exchange rates of Ln^{III}-containing complexes. Consequently, M^{III}-containing DOTA-type PEG conjugates, **2.13–2.21**, illustrated in **Figure 4.1** were designed to investigate the influence of density of PEG on the water-exchange rates of Ln^{III}-containing complexes.

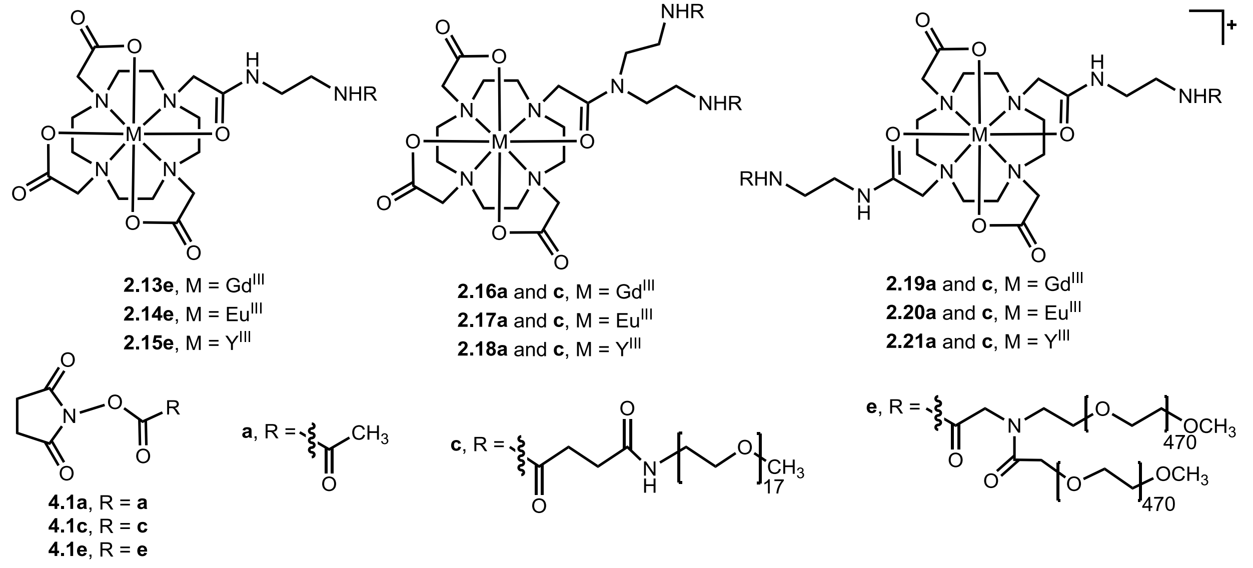
2.13e, M = Gd^III
2.14e, M = Eu^III
2.15e, M = Y^III
2.16a and c, M = Gd^III
2.17a and c, M = Eu^III
2.18a and c, M = Y^III
2.19a and c, M = Gd^III
2.20a and c, M = Eu^III
2.21a and c, M = Y^III
4.1a, R = a
4.1c, R = c
4.1e, R = e
a, R =
c, R =
e, R =
NHR
RHN
CH3
OCH3
470
17
+

Figure 4.1. The structures of M^{III}-containing PEG conjugates, **2.13–2.21**, *N*-acetoxysuccinimide, **4.1a**, used as a control, and PEG moieties **4.1c** and **4.1e** used to investigate the influence of density of PEG on water-exchange rates of Ln^{III}-containing complexes.

Incorporation of Gd^{III}, Eu^{III}, and Y^{III} as the M^{III} ion was envisioned to enable the determination of contrast-agent-relevant properties of the conjugates that are necessary to establish a relationship between density of PEG and the properties of the conjugates. Specifically, Gd^{III}-containing complexes **2.13**, **2.16**, and **2.19** were designed to enable the determination of water-exchange rate, k_{ex}; relaxivity, r_1; and longitudinal and transverse electron spin relaxation times, T_{1e} and T_{2e}, respectively. In addition, Eu^{III}-containing complexes **2.14**, **2.17**, and **2.20** were designed to obtain water-coordination number (q) data. Also, Y^{III}-containing complexes **2.15**, **2.18**, and **2.21** were designed to be used as diamagnetic controls in the determination of water-exchange rates. Conjugates **2.13–2.15** were designed to include a branched PEG moiety, and conjugates **2.16–2.18** and **2.19–2.21** were designed to include two identical units of a linear PEG moiety to enable investigation of the influence of the density of PEG on water-exchange rates of Ln^{III}-containing complexes. Also, conjugates that include acetate, were designed to be used as controls.

Synthesis of M^{III}-Containing PEG Conjugates

The synthetic routes to M^{III}-containing PEG conjugates **2.13–2.21** are illustrated in **Schemes 2.4**, **2.5**, and **2.6** (Chapter 2) and the synthesis of M^{III}-containing complexes **2.4–2.12** was carried out as described in Chapter 2. Conjugation of M^{III}-containing complexes **2.4–2.12** to succinimidyl ester derivatives of PEG, **4.1a**, **4.1c**, and **4.1e** (**Figure 4.1**) occurs through the reaction between one or more amine arms on the M^{III}-containing complexes and the succinimidyl ester group on the PEG moiety regardless of the identity of the M^{III} ion. Consequently, conjugation reactions were carried out using Eu^{III}-containing complexes as a starting point to establish reaction conditions for conjugation reactions between M^{III}-containing complexes and the succinimidyl ester derivatives of PEG, **4.1a**, **4.1c**, and **4.1e** (**Figure 4.1**). Synthesis of Eu^{III}-containing PEG conjugates was chosen as the starting point because these complexes enable the determination of water-coordination numbers, which in turn determine whether or not water-exchange rate and relaxivity measurements need to be performed. Attempted synthesis and purification of Eu^{III}-containing PEG conjugates **2.14e**, **2.17a**, **2.17c**, **2.20a**, and **2.20c** is described in the following text.

Experimental Procedures

Commercially available chemicals were of reagent-grade purity and were used without further purification unless otherwise noted. Water was purified using a PURELAB Ultra Mk2 (ELGA) water purification system. Spectra/Por Biotech cellulose ester dialysis membranes of 100−500; 500−1,000; and 8,000−10,000 Da molecular weight cut off (MWCO) were used for dialysis. Freeze drying was carried out using a LABCONCO FreeZone 2.5 freeze dryer. Resin reactions were performed in Poly-Prep chromatography columns on a Barnstead/Thermolyne LABQUAKE rotator. Thin-layer chromatography (TLC) was performed on ASTM TLC plates with a silica gel 60 F254 coating (250 μm layer thickness). Visualization of TLC was carried out with a UV lamp followed by staining with potassium permanganate (2 g $KMnO_4$, 20 g K_2CO_3, 5 mL 5% w/v aqueous NaOH, and 300 mL H_2O). Aqueous size-exclusion chromatography (SEC) was carried out on a Shimadzu high-performance liquid chromatography (HPLC) system equipped with three aquagel-OH columns in series (VARIAN PLaquagel-OH-mixed, 8 μm × 300 mm) or a Bio-Sil SEC 250 column (BIO-RAD gel filtration HPLC column, 5 μm × 300 mm), and fluorescence (λ_{ex} = 396 nm and λ_{em} = 593 nm for Eu^{III}-containing complexes), photodiode array (absorbance at 210 nm), and refractive index detectors. An isocratic method (100% H_2O) with a flow rate of 1 mL/min was used with the aquagel-OH columns, and flow rates of 0.7 or 0.5 mL/min were used with the Bio-Sil SEC 250 column. SEC was performed using commercially available Sephadex G-25 and Sephadex G-10 with H_2O as the mobile phase and under gravity flow.

*Synthesis of Eu^{III}-Containing PEG Conjugate **2.14e***

The synthetic route to Eu^{III}-containing PEG conjugate **2.14e** is shown in **Scheme 4.1**. In general, the synthesis of Eu^{III}-containing conjugate, **2.14e**, was carried out by adding a mixture of the Eu^{III}-containing complex, **2.5**, and diisopropylethylamine (DIEA) in anhydrous CH_3OH to a flask containing succinimidyl ester derivative of branched PEG, **4.1e** (1 equiv, **Figure 4.1**). The resulting mixture was allowed to stir at ambient temperature under Ar for 24 h, followed by concentration of the reaction mixture under reduced pressure to obtain a white solid that was dissolved in H_2O (10 mL) and washed with hexanes (4 × 10 mL) to remove excess DIEA. The H_2O layer was dialyzed using a 10,000 Da MWCO dialysis membrane against H_2O (4 L) to remove unreacted excess Eu^{III}-containing complex, **2.5**. The dialysis reservoir was changed at 2–

4, 6–8, and 10–14 h. After the last change, dialysis was continued for 3 h. Contents within the dialysis membrane were freeze dried to obtain a white solid.

Scheme 4.1. Synthesis of Eu^{III}-containing PEG conjugate **2.14e** from Eu^{III}-containing complex **2.5**.

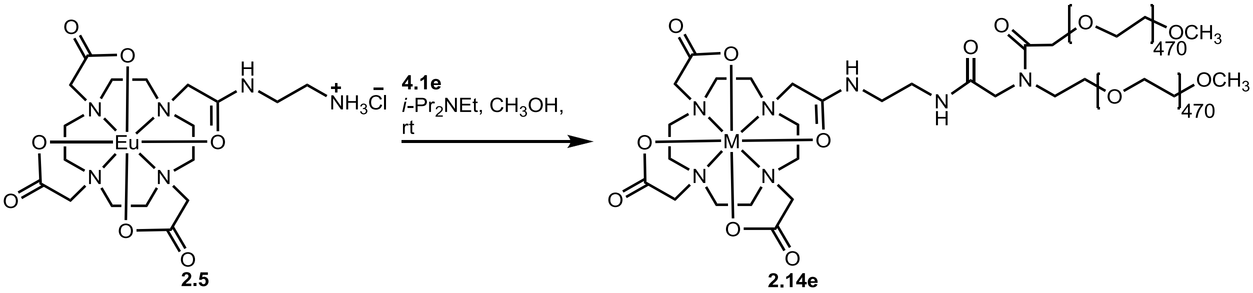

Several different reaction conditions were explored to test if a pure product can be obtained by driving the reaction to completion with increased ratios of Eu^{III}-containing complex **2.5** to succinimidyl ester derivative of PEG **4.1e** (**Table 4.1**). An excess of the Eu^{III}-containing complex was used with the expectation of achieving complete consumption of the PEG moiety resulting in a reaction mixture containing unreacted excess Eu^{III}-containing complex, **2.5**, and the conjugate, **2.14e**. The large difference in size between Eu^{III}-containing complex, **2.5**, (656 Da) and conjugate, **2.14e**, (42,000 Da) was expected to enable easy purification of the conjugate using dialysis. Four different ratios of Eu^{III}-containing complex, **2.5**, to succcinimidyl ester derivative of PEG **4.1e** (2 to 1, 5 to 1, 10 to 1, or 20 to 1 in **Table 4.1**) were explored to test if any of the tested ratios would result in a pure product at the end of dialysis. However, all four reaction conditions resulted in multiple peaks in the chromatograms acquired from SEC using HPLC equipped with a PL-aquagel OH column even after purification using dialysis. This observation indicated that none of the reaction conditions resulted in pure conjugate, **2.14e**, likely due to the steric hindrance caused by the large size of the succinimidyl ester derivative of PEG **4.1e**, leading to incomplete consumption of **4.1e** during the reaction.

Table 4.1. Different reaction conditions explored in the synthesis of Eu^{III}-containing PEG conjugate **2.14e**.

	condition 1	condition 2	condition 3	condition 4
equiv of **2.5**	2	5	10	20
equiv of **4.1e**	1	1	1	1
equiv of DIEA	2	5	10	20

Because varying the reaction conditions did not result in a pure conjugate at the end of dialysis, purification was attempted with SEC using the PL-aqaugel column. However, fractions that were collected did not yield any solid material upon removal of solvent by freeze drying and produced SEC chromatograms that were similar to that obtained for the blank indicating the absence of any Eu^{III}-containing material. This observation is likely a result of the dilution of the injected samples due to the presence of three columns in series in the PL-aquagel OH column, making the collection of fractions using this column ineffective. Consequently, SEC purification was attempted with the use of a Bio-Sil SEC 250 column. A flow rate of 0.7 mL/min was used initially, followed by a decrease in flow rate to 0.5 mL/min to improve the separation. Purification of **2.14e** was attempted by collecting fractions using the Bio-Sil SEC 250 column with a flow rate of 0.5 mL/min for the reaction mixture obtained from condition 4 (**Table 4.1**). Two fractions were collected within the elution time interval given in **Table 4.2**, and the fractions were freeze dried to remove water. However, when the two dried fractions were tested for purity with SEC using Bio-Sil SEC 250 column and the same method, both fractions displayed similar chromatograms with peak tailing and overlap (**Figure 4.2**). The peak tailing and overlap observed for fractions 1 and 2 are likely because the elution time interval included the middle portion of the two peaks that corresponds to portions of both peaks.

Table 4.2. Elution time range of the two fractions collected during the purification of **2.14e** (reaction condition 4, **Table 4.1**).

fraction number	elution time interval (min)
1	8.5–10.0
2	10.5–12.5

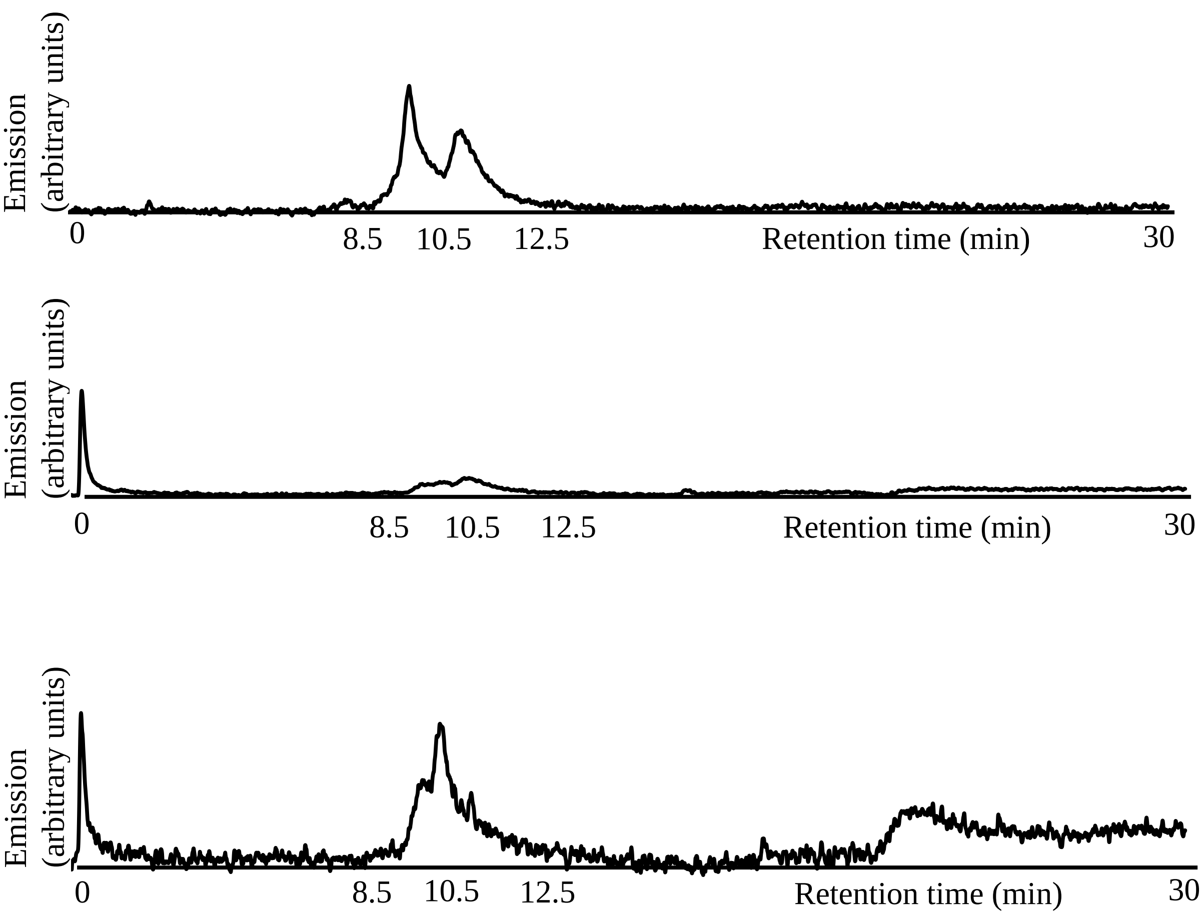

Figure 4.2. SEC chromatograms (fluorescence response) of **2.14e** (reaction condition 4 in **Table 4.1**, top) and fractions 1 (middle) and 2 (bottom) collected using a Bio-Sil SEC 250 column (0.5 mL/min flow rate).

Therefore, fraction collection was attempted once more using the same sample obtained from condition 4 (**Table 4.1**) with the Bio-Sil SEC 250 column and the same method but with different elution time intervals as listed in **Table 4.3** to facilitate collection of material corresponding to one peak rather than collecting material under overlapped peaks. Fractions 1 and 2 were freeze dried and tested to verify purity by SEC using the same conditions used for fraction collection. The chromatograms of fractions 1 and 2 are shown in **Figure 4.3**. Based on the chromatograms in **Figure 4.3**, fractions 1 and 2 display peak broadening possibly due to the presence of more than one species of similar size.

Table 4.3. Elution time range of the three fractions collected during the purification of **2.14e** (reaction condition 4, **Table 4.1**).

fraction number	elution time interval (min)
1	8.5–9.0
2	9.0–11.0
3	11.0–13.0

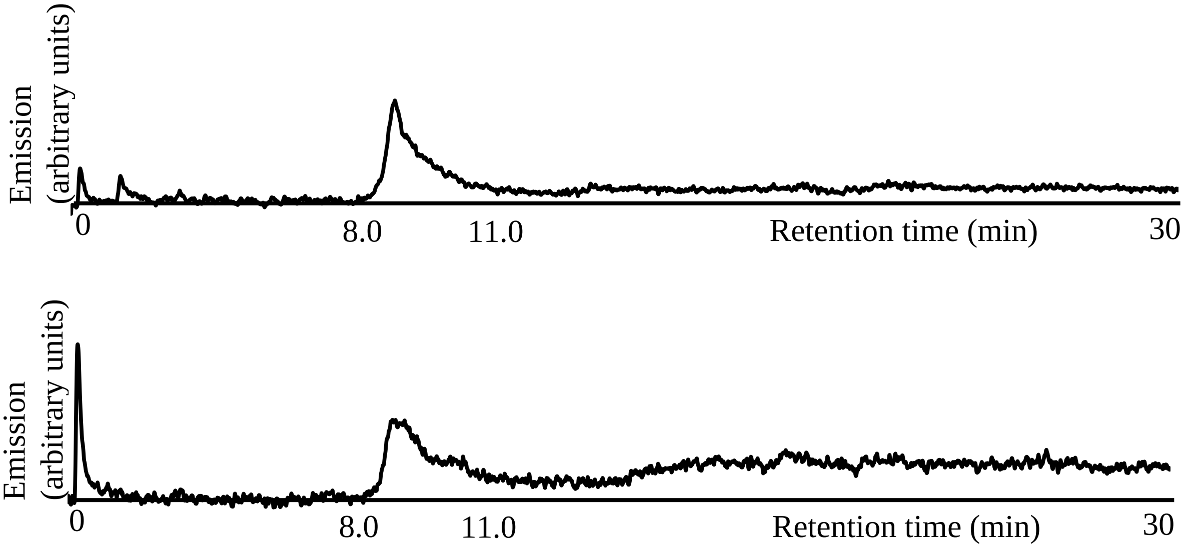

Figure 4.3. SEC chromatograms (fluorescence response) of fractions 1 (top) and 2 (bottom) collected using a Bio-Sil SEC 250 column (0.5 mL/min flow rate) from reaction condition 4 (**Table 4.1**) of **2.14e**.

Because the Bio-Sil SEC 250 column did not result in pure fractions, purification of **2.14e** from reaction 4 was attempted using a column packed with Sephadex G-25, using H_2O as the mobile phase and run under gravity flow. Only two of the fractions indicated the presence of material by means of spotting on a TLC place and visualization with UV and $KMnO_4$. However, both fractions indicated the presence of two peaks when tested by SEC with HPLC using the Bio-Sil Sec 250 column (**Figure 4.4**). This observation is likely due to the MW range (1,000–5,000 Da) of Sephadex G-25 being narrow and very different from the large MW (42,000 Da) of the conjugate.

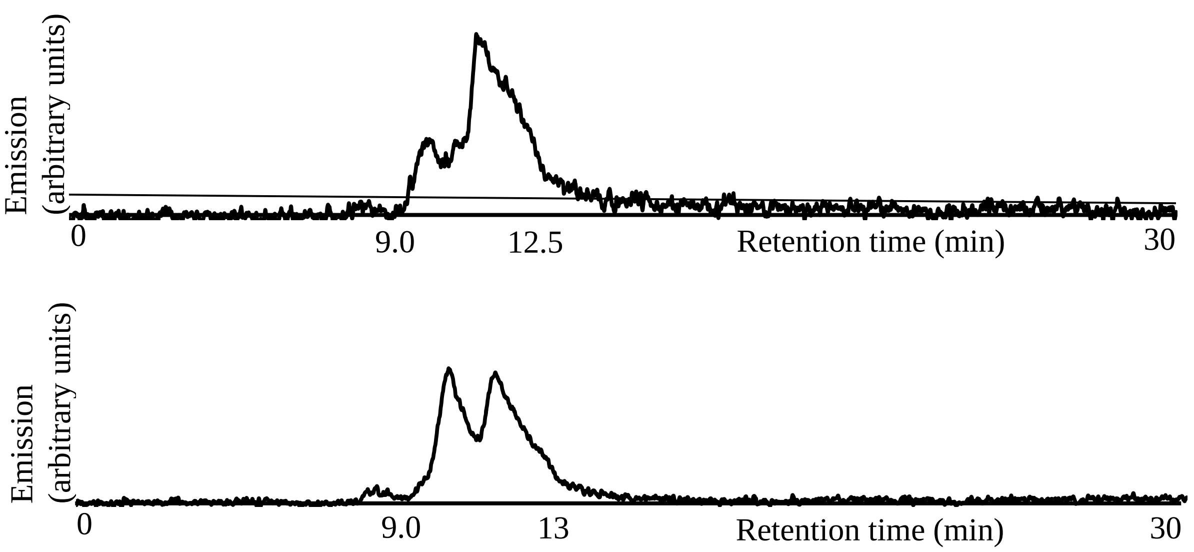

Figure 4.4. SEC chromatograms (fluorescence response) of fractions 1 (top) and 2 (bottom) collected from Sephadex G-25 chromatography from reaction condition 4 (**Table 4.1**).

*Synthesis of Eu^{III}-Containing PEG Conjugates **2.17c** and **2.20c***

The synthetic route to Eu^{III}-containing PEG conjugates **2.17c** and **2.20c** is shown in **Scheme 4.2**. In general, the synthesis of Eu^{III}-containing conjugates, **2.17c** and **2.20c**, was carried out by adding a mixture of Eu^{III}-containing complex **2.8** or **2.11** (1 equiv) and DIEA in anhydrous CH_3OH to a flask containing succinimidyl ester derivative of PEG, **4.1c**. The resulting mixture was allowed to stir at ambient temperature under Ar for 24–72 h, and the resulting reaction mixture was added to amine-terminated aminomethylated polystyrene HL (100–200 mesh) resin (25 equiv, pre-swollen in C_2H_5OH for 2–3 h) allowing to rotate for 15–18 h to remove unreacted excess succinimidyl ester derivative of PEG, **4.1c**. The liquid portion of the reaction mixture was separated from the resin via filtration, and the resin was washed with C_2H_5OH (3 × 7 mL). The washings were combined with the liquid portion of the reaction mixture, and the solvents were removed under reduced pressure to obtain an oil that was dissolved in H_2O (10 mL) and washed with hexanes (4 × 10 mL) to remove excess DIEA into hexanes. The H_2O layer was dialyzed using a 1,000 Da MWCO dialysis membrane against H_2O

(4 L) to remove unreacted Eu^{III}-containing complex, **2.5** or **2.8** and any unreacted succinimidyl ester derivative of PEG, **4.1c** remaining after the resin reaction. The dialysis reservoir was changed at 2–4, 6–8, and 10–14 h. After the last change, dialysis was continued for 3 h. Contents within the dialysis membrane were freeze dried to yield white solids.

Scheme 4.2. Synthesis of Eu^{III}-containing PEG conjugates **2.17c** and **2.20c** from Eu^{III}-containing complexes **2.8** and **2.11**, respectively.

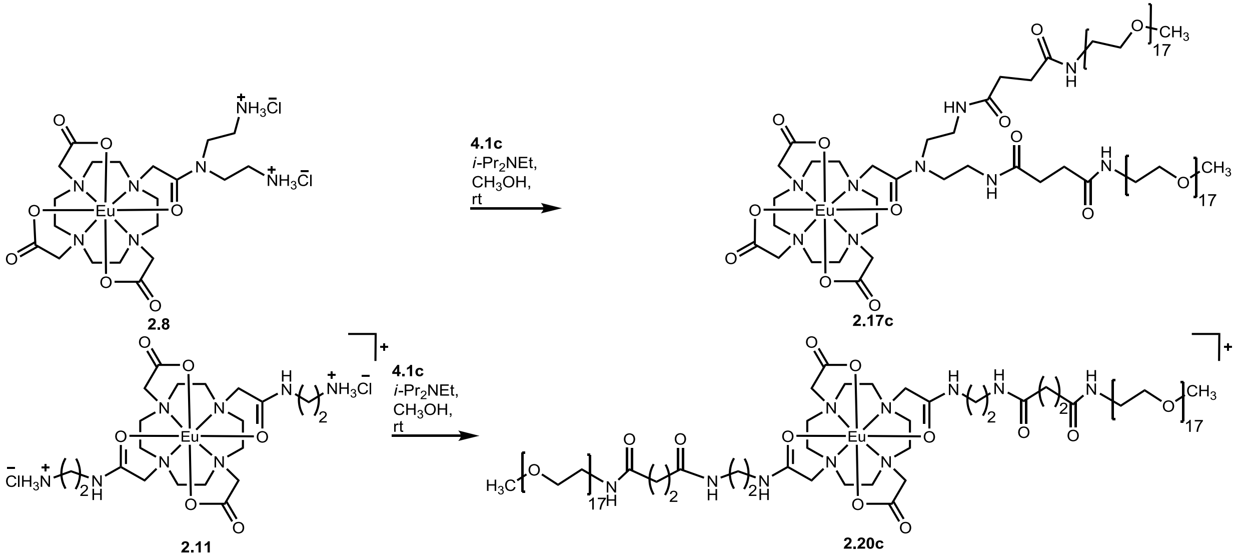

Several different reaction conditions were explored (**Table 4.4**) to test if the conjugation reaction could be driven to completion using the Eu^{III}-containing complexes, **2.8** or **2.11**, as limiting reactants and an excess of the succinimidyl ester derivative of PEG, **4.1c** to enable easy purification with the resin reaction to remove unreacted succinimidyl ester derivative of PEG, **4.1c** and dialysis to remove any unreacted Eu^{III}-containing complex **2.8** or **2.11**.

Reaction conditions 1–3 to obtain conjugate **2.17c** and reaction conditions 1 and 2 to obtain conjugate **2.20c** were carried out using the same number of equivalents of DIEA as the number of equivalents of PEG moiety, **4.1c**. Based on the peak intensities in SEC chromatograms obtained from HPLC using PL-aquagel OH column, the majority of the starting materials were present and the new peaks were insignificant. Because of the similar pK_a values

(~10–11) of protonated DIEA and protonated amine arms of the Eu^{III}-containing complexes, **2.8** and **2.11**, a large excess of DIEA (500 equiv) was added to increase the probability of deprotonating the amine arms of complexes **2.8** and **2.11** and thereby facilitate nucleophilic attack. Reaction conditions 4–5 to obtain conjugate **2.17c** and condition 3 to obtain conjugate **2.20c** resulted in higher intensities of the new peaks in the SEC chromatograms. SEC chromatograms obtained for conjugate **2.17c** with reaction conditions 1 and 4 are shown in **Figure 4.5** as representative chromatograms in the absence and presence of a large excess of DIEA, respectively.

Table 4.4. Different reaction conditions explored in the synthesis of Eu^{III}-containing PEG conjugates **2.17c** and **2.20c**.

2.17c	condition 1	condition 2	condition 3[a]	condition 4	condition 5
equiv of **2.8**	1	1	1	1	1
equiv of **4.1c**	10	10	40	20	10
equiv of DIEA	10	10	40	500	500
reaction time (h)	24	48	72	24	24
2.20c	condition 1	condition 2	condition 3		
equiv of **2.11**	1	1	1		
equiv of **4.1c**	10	20	10		
equiv of DIEA	10	20	500		
reaction time (h)	24	24	24		

[a] 20 equiv of succinimidyl ester derivative of PEG, **4.1c** and DIEA added at start, followed by subsequent addition of 10 equiv of **4.1c** and DIEA after 24 and 48 h

The reaction time was increased from 24 to 48 h to allow more time for the reaction between Eu^{III}-containing complex, **2.8**, and the PEG moiety, **4.1c**, to occur in case steric hindrance arising from the conjugation of one PEG moiety to Eu^{III}-containing complex, **2.8**, hindered the conjugation of a second PEG moiety to Eu^{III}-containing complex, **2.8**. However, increasing the reaction time from 24 to 48 h did not result in considerable changes in the amount of product formed based on the intensities of the new peaks in SEC chromatograms obtained with reaction conditions 1 and 2 in **Table 4.4** performed to obtain conjugate **2.17c** (**Figure 4.6**).

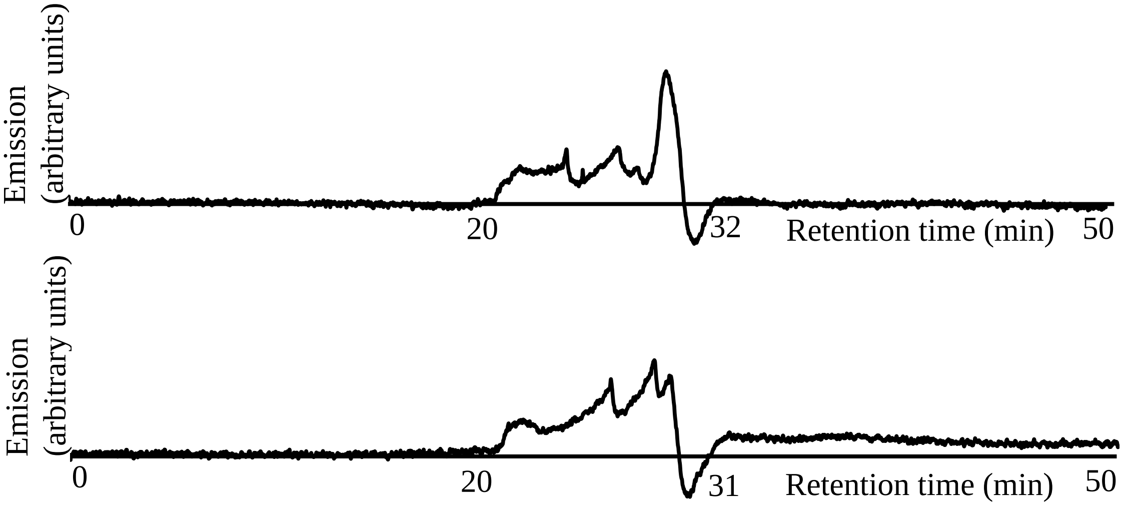

Figure 4.5. SEC chromatograms (fluorescence response) of **2.17c** obtained with a PL-aquagel OH column for reaction conditions 1 (top) and 4 (bottom) in **Table 4.4** in the absence and presence, respectively, of a large excess of DIEA.

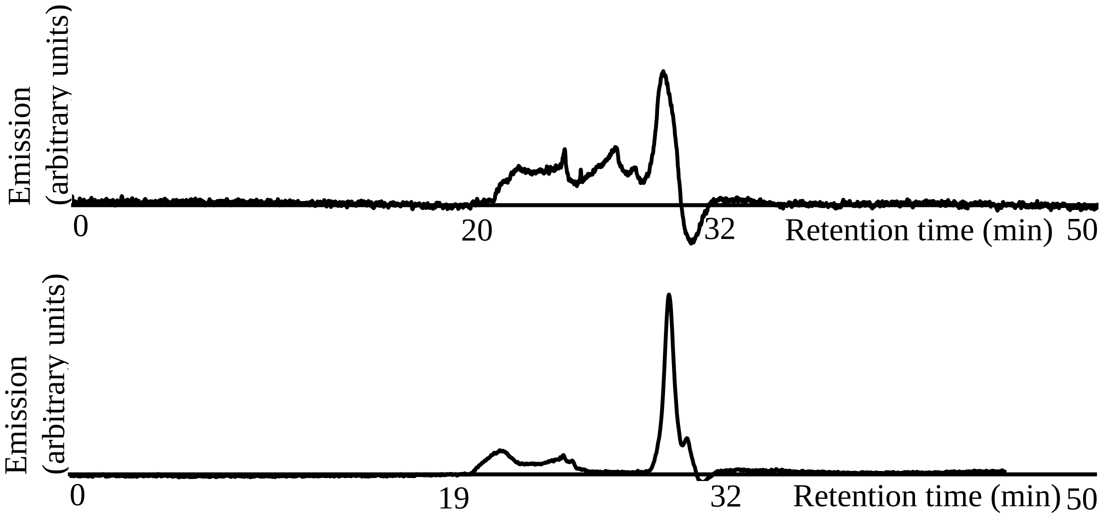

Figure 4.6. SEC chromatograms (fluorescence response) of **2.17c** obtained with a PL-aquagel OH column for reaction conditions 1 (top) and 2 (bottom) in **Table 4.4** with 24 and 48 h reaction times, respectively.

Also, increasing the number of equivalents of the succinimidyl ester derivative of PEG, **4.1c**, added did not increase the amount of product formed based on the new peak intensities in SEC chromatograms obtained with reaction conditions 4 and 5 (**Table 4.4**) carried out to synthesize conjugate **2.17c** (**Figure 4.7**). A similar observation was made from SEC chromatograms obtained for reaction conditions 1 and 2 (**Table 4.4**) carried out in the synthesis of conjugate **2.20c**.

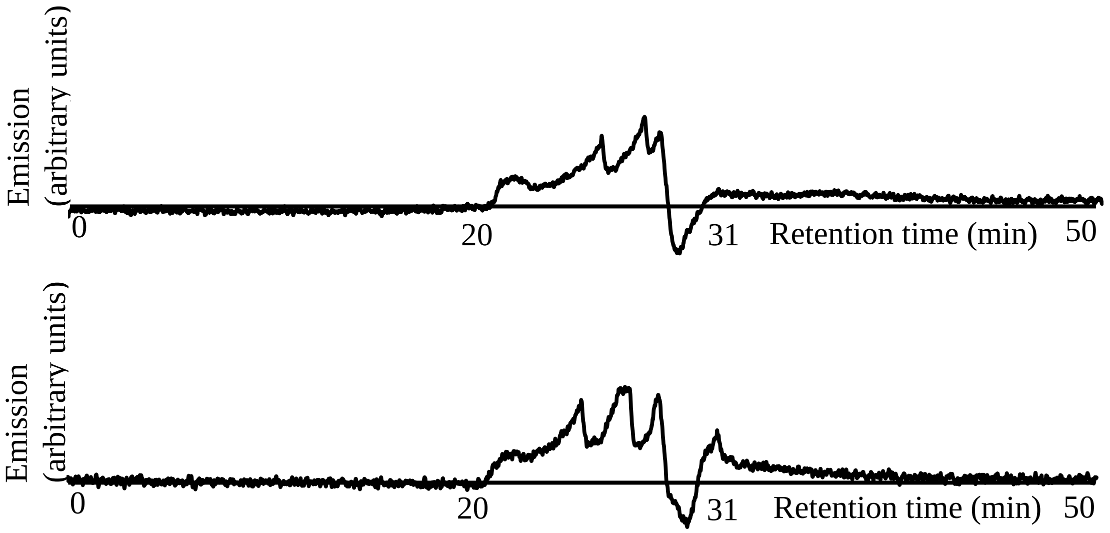

Figure 4.7. SEC chromatograms (fluorescence response) of **2.17c** obtained with a PL-aquagel OH column for reaction conditions 4 (top) and 5 (bottom) in **Table 4.4**.

In addition, sequential addition of the succinimidyl ester derivative of PEG, **4.1c**, at the start of reaction, 24 h, and 48 h was explored in reaction condition 3 (**Table 4.4**) in the synthesis of conjugate **2.17c**. Sequential addition was carried out with the expectation that the reaction between the Eu^{III}-containing complex, **2.8**, and **4.1c** will be facilitated by minimizing any side reactions between CH_3OH that was used as solvent and **4.1c**. However, similar SEC chromatograms were obtained at the end of 24, 48, and 72 h (**Figure 4.8**), indicating that any side reaction between CH_3OH and the PEG moiety is unlikely to hinder the reaction between Eu^{III}-containing complex, **2.8**, and the PEG moiety, **4.1c**.

Poor peak resolution was observed in SEC chromatograms obtained with all reaction conditions likely due to the similarity in size of the reactants and the possible products, including Eu^{III}-containing complexes (**2.8** or **2.11**) with one and two PEG moieties attached. Consequently, isolation of peaks by colleting fractions with HPLC was not possible. Therefore, purification of

2.17c and **2.20c** was attempted using a column packed with Sephadex G-25, using H_2O as the mobile phase and run under gravity flow. However, pure fractions were not observed upon testing each fraction by SEC with HPLC likely due to the similarity in MWs of unreacted reactants and products present in the reaction mixtures of **2.17c** and **2.20c** (**Table 4.5**).

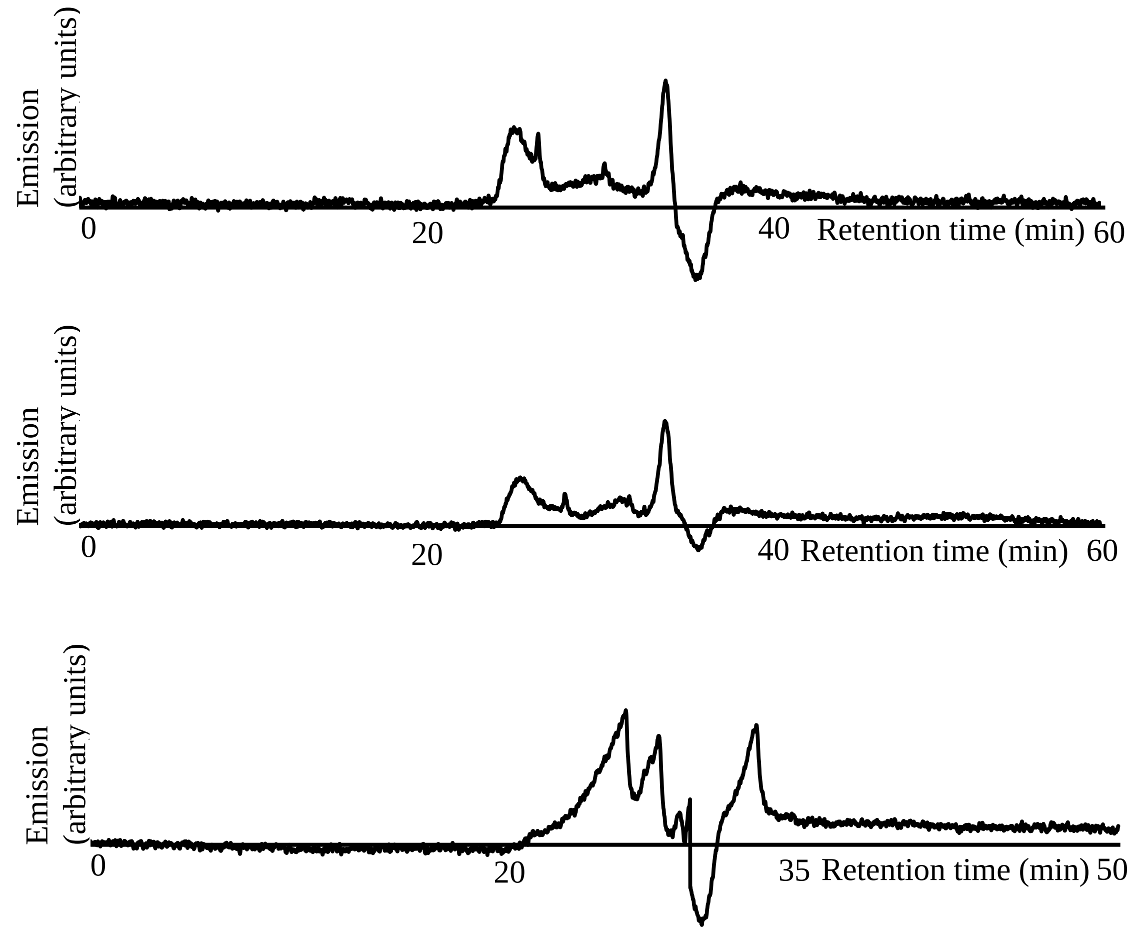

Figure 4.8. SEC chromatograms (fluorescence response) of **2.17c** obtained with a PL-aquagel OH column for reaction condition 3 at the end of 24 h (top), 48 h (middle), and 72 h (bottom).

Table 4.5. Calculated MWs of compounds present in reaction mixtures of **2.17c** or **2.20c**.

compounds present	MW (Da)
Eu^{III}-containing complex (**2.8** or **2.11**)	638
Eu^{III}-containing complex with one **c** moiety	1500
Eu^{III}-containing complex two **c** moieties	2362
Succinimidyl ester derivative of PEG (**4.1c**)	976

In addition, purification of **2.17c** and **2.20c** was attempted using a column packed with Sephadex G-10 (MW <700), using H_2O as the mobile phase and run under gravity flow. Similar to the observations from Sephadex-G25, pure fractions were not observed when each fraction was tested by SEC with HPLC. Inability to obtain pure fractions is likely due to the similarity in MWs of unreacted reactants and products present in the reaction mixtures of **2.17c** and **2.20c** (**Table 4.5**).

*Synthesis of Eu^{III}-Containing Acetamide Conjugates **2.17a** and **2.20a***

The synthetic route to Eu^{III}-containing PEG conjugates **2.17a** and **2.20a** is shown in **Scheme 4.3**. In general, the synthesis of Eu^{III}-containing conjugates, **2.17a** or **2.20a**, was carried out by adding a mixture of Eu^{III}-containing complex **2.8** or **2.11** (1 equiv) and DIEA in anhydrous CH_3OH to a flask containing *N*-acetoxysuccinimide, **4.1a**. The resulting mixture was allowed to stir at ambient temperature under Ar for 24–48 h, and the resulting reaction mixture was added to amine-terminated aminomethylated polystyrene HL (100–200 mesh) resin (25 equiv, pre-swollen in C_2H_5OH for 2–3 h) allowing to rotate for 15–18 h to remove unreacted excess *N*-acetoxysuccinimide, **4.1a**. The liquid portion of the reaction mixture was separated from the resin via filtration, and the resin was washed with C_2H_5OH (3 × 7 mL). The washings were combined with the liquid portion of the reaction mixture, and the solvents were removed under reduced pressure to obtain an oil that was dissolved in H_2O (10 mL) and washed with hexanes (4 × 10 mL) to remove excess DIEA. The H_2O layer was dialyzed in a 500 Da MWCO dialysis membrane against H_2O (4 L) to remove any unreacted *N*-acetoxysuccinimide, **4.1a**, and salts of DIEA. The dialysis reservoir was changed at 2–4, 6–8, and 10–14 h. After the last change, dialysis was continued for 3 h. Contents within the dialysis membrane were freeze dried to yield white solids.

Scheme 4.3. Synthesis of $\mathrm{Eu^{III}}$-containing acetamide conjugates **2.17a** and **2.20a** from $\mathrm{Eu^{III}}$-containing complexes **2.8** and **2.11**.

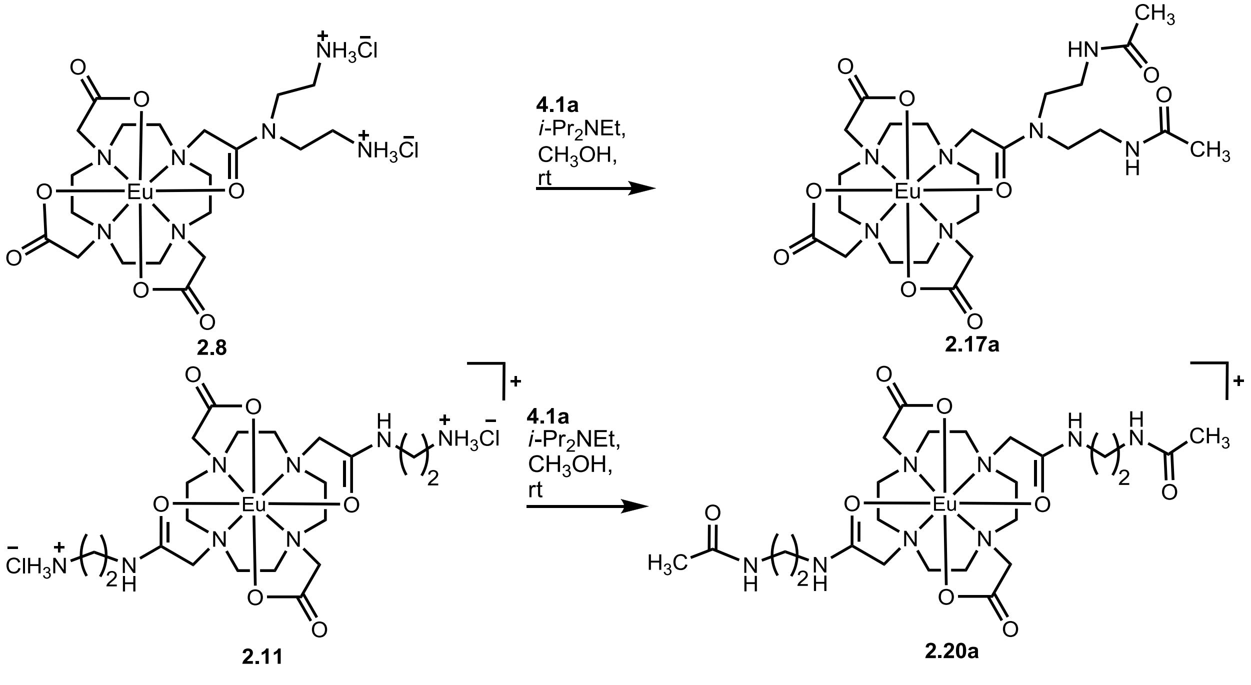

Although a few different reaction conditions were explored (**Table 4.6**) with the expectation of obtaining pure conjugates **2.17a** and **2.20a**, none of the reaction conditions yielded pure conjugates as observed by SEC. The reaction conditions were varied for the same reasons described in the previous section that describes the synthesis of conjugates **2.17c** and **2.20c**. Because purification of conjugates **2.17a** and **2.20a** was unlikely with HPLC, purification was attempted using a column packed with Sephadex G-10 (MW <700), using H_2O as the mobile phase and run under gravity flow. Similar to the observations from **2.17c** and **2.20c** discussed in the previous section, pure fractions were not observed when each fraction was tested by SEC with HPLC. Inability to obtain pure fractions is likely due to the similarity in MWs of unreacted reactants and products present in the reaction mixtures of **2.17c** and **2.20c** (**Table 4.7**).

Table 4.6. Different reaction conditions explored in the synthesis of Eu^{III}-containing PEG conjugates **2.17a** and **2.20a**

2.17a	condition 1	condition 2[b]	condition 3
equiv of **2.8**	1	1	1
equiv of **4.1a**	10	20	10
equiv of DIEA	10	20	500
reaction time (h)	24	48	24
2.20a	condition 1	condition 2	
equiv of **2.11**	1.0	1.0	
equiv of **4.1a**	10	20	
equiv of DIEA	500	500	
reaction time (h)	24	24	

[b] 10 equiv of *N*-acetoxysuccinimide, **4.1a**, and DIEA added at start, followed by subsequent addition of 10 equiv of **4.1a** and DIEA after 24 h

Table 4.7. Calculated MWs of compounds present in reaction mixtures of **2.17a** or **2.20a**.

compounds present	MW (Da)
Eu^{III}-containing complex (**2.8** or **2.11**)	638
Eu^{III}-containing complex with one **a** moiety	681
Eu^{III}-containing complex with two **a** moieties	723
N-acetoxysuccinimide (**4.1a**)	157

Future Directions

Although several attempts were made to purify the Eu^{III}-containing PEG, **2.14e**, **2.17a**, **2.17c**, **2.20a**, and **2.20c**, successful purification was not achieved likely due to the size similarity between the reactants and products formed during the conjugation reactions. However, use of other SEC media including Sephadex-LH 20 (100–10,000 Da) is likely to enable the isolation of **2.17a**, **2.17c**, **2.20a**, and **2.20c**. Also, the use of Sephadex G-50 (<30,000 Da) is likely to be useful in the isolation of **2.14e**. In addition, silica gel chromatography also can be tested with polar solvent conditions including H_2O/CH_3CN and $MeOH/NH_4OH$ mixtures. Once the conditions for purification of Eu^{III}-containing conjugates are established, the identities of the conjugates need to be confirmed by matrix assisted laser desorption ionization (MALDI) mass spectrometry. Next, Gd^{III}- and Y^{III}-containing conjugates need to be isolated and identified using the same purification and MALDI conditions established for the Eu^{III}-containing conjugates. If successful, these complexes would enable the determination of contrast agent relevant properties including water-exchange rates, k_{ex}, relaxivities, r_1, longitudinal and transverse electron spin relaxation times, T_{1e} and T_{2e}, respectively, and water-coordination numbers, q, which in turn could be used to establish a relationship between the density of PEG and water-exchange rates and other contrast agent relevant properties.

CHAPTER 5: Summary, Conclusions, and Future Directions

Summary

Water-exchange rates of lanthanide(III) (Ln^{III})-containing complexes are important determinants of the efficiency of these complexes as T_1-shortening and paramagnetic chemical exchange saturation transfer (PARACEST) contrast agents for magnetic resonance imaging (MRI). As a result of the differences in how these two types of MRI contrast agents operate, the water-exchange rates of Ln^{III}-containing complexes need to be tuned over a broad range: towards fast rates (10^8 s^{-1}) for T_1-shoretning agents and towards slow rates (10^3 s^{-1}) for PARACEST agents.

The need to tune water-exchange rates over a broad range has led to an enormous amount of research efforts to tune water-exchange rates of both types of contrast agents using modifications in the structure of the Ln^{III}-containing complexes. Examples of coordination-chemistry-based strategies explored include modification of (1) the mechanism of water exchange; (2) the charge of the Ln^{III}-containing complex; (3) the steric hindrance at the site of water coordination; (4) the ligand side chains; and (5) the ratio of twisted-square-antiprism (TSAP) to square-antiprism (SAP) isomers for 1,4,7,10-tetraazacyclododecane-1,4,7,10-tetraacetate (DOTA)-type complexes. Although the influence of each strategy was considered separately to allow structure-function comparisons to be made, there is considerable overlap among these strategies and they cannot be completely isolated from one another. Based on studies that relate different coordination-chemistry-based strategies to water-exchange rates, complexes with the following properties tend to lead to fast water-exchange rates desirable for T_1-shortening agents: complexes that undergo associative water exchange; that are negatively charged; with bulky groups at the site of water coordination; with side chains containing non-polar substituents; and with large TSAP/SAP ratios for DOTA-type complexes. In contrast, complexes that undergo dissociative water exchange; that are positively charged; without bulky groups at the site of water coordination; with side chains containing polar substituents; and with small TSAP/SAP ratios for DOTA-type complexes tend to lead to slow water-exchange rates desirable for PARACEST agents.

Studies describing the influence of coordination-chemistry-based modifications on water-exchange rates demonstrate that minor structural modifications give rise to substantial changes in the water-exchange rates. Consequently, a modular system of modifications based on a biocompatible and hydrophilic polymer, polyethylene glycol (PEG) was designed to enable tuning of water-exchange rates of Ln^{III}-containing DOTA-type complexes through steric and hydrogen-bonding interactions. Furthermore, the systems were designed to allow investigation of the influence of length and density of PEG on water-exchange rates of Ln^{III}-containing complexes and the designed systems are shown in **Figure 5.1**.

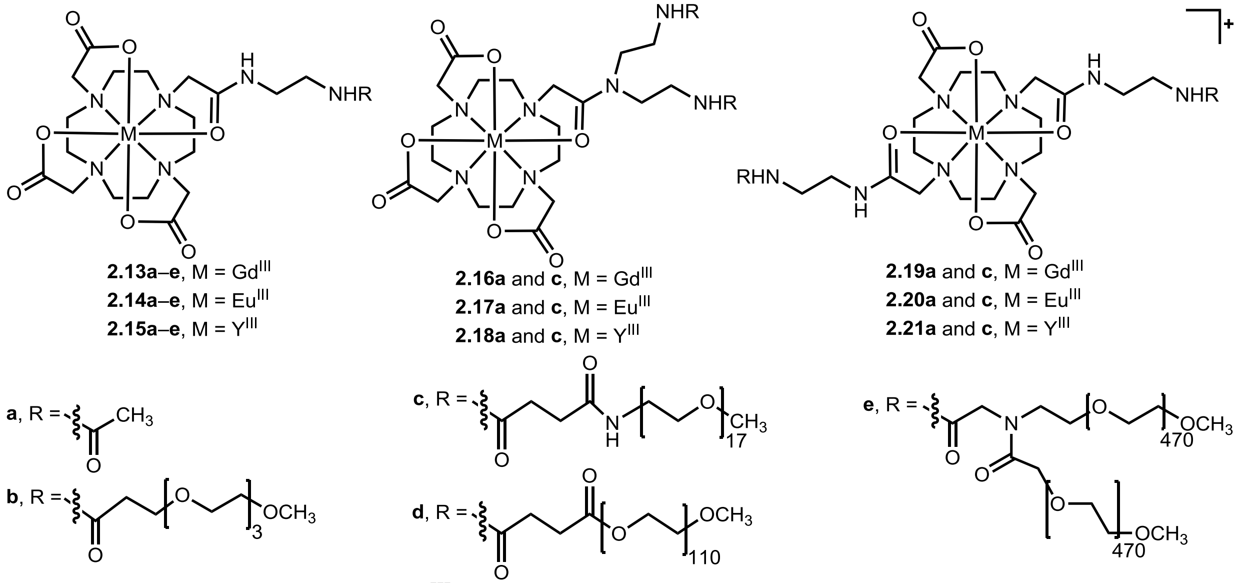
NHR
NHR
NHR
NHR
RHN
M
2.13a–e, M = Gd^{III}
2.14a–e, M = Eu^{III}
2.15a–e, M = Y^{III}
2.16a and **c**, M = Gd^{III}
2.17a and **c**, M = Eu^{III}
2.18a and **c**, M = Y^{III}
2.19a and **c**, M = Gd^{III}
2.20a and **c**, M = Eu^{III}
2.21a and **c**, M = Y^{III}
a, R =
b, R =
c, R =
d, R =
e, R =
CH$_3$
OCH$_3$
3
17
110
470

Figure 5.1. The structures of M^{III}-containing PEG conjugates, **2.13–2.21**, acetate, **a**, used as a control, and PEG moieties **b–e** used to investigate the influence of length and density of PEG on water-exchange rates of Ln^{III}-containing complexes.

PEG conjugates **2.13a–d**, **2.14a–d**, and **2.15a–d** were designed to study the influence of the length of PEG on water-exchange rates, and PEG conjugates **2.13–2.15e**, **2.16–2.21a**, and **2.16–2.21c** were designed to explore the influence of density of PEG on the water-exchange rates. M^{III}-containing PEG conjugates were synthesized starting from the reaction of tri-*tert*-butyl-1,4,7,10-tetraazacyclododecane-1,4,7-triacetate or di-*tert*-butyl-1,4,7,10-tetraazacyclo - dodecane-1,7-diacetate with protected linear or branched amine arms, followed by the deprotection of the protecting groups and *tert*-butyl esters to obtain the ligands. The deprotected ligands were metallated using metal chloride salts to obtain M^{III}-containing complexes, which were then reacted with succinimidyl ester derivatives of acetate **a**, or PEG moieties **b–d** to yield M^{III}-containing PEG conjugates **2.13a–d**, **2.14a–d**, and **2.15a–d**. The products of each synthetic step were purified by normal-phase, reversed-phase, or size-exclusion chromatography and characterized by mass spectrometry and NMR spectroscopy or high-performance liquid chromatography. However, M^{III}-containing PEG conjugates **2.13–2.15e**, **2.16–2.21a**, and **2.16–2.21c** that were designed to study the influence of density of PEG on water-exchange rates could not be isolated as a result of the challenges encountered in the purification of the conjugates. Although many different size-exclusion chromatography media including PL-aquagel OH, Bio-Sil SEC 250, Sephadex G-25, and Sephadex G-10 were used to purify the PEG conjugates, purification could not be achieved likely due to the similarity in size between the unreacted starting materials and products. Therefore, the studies on the investigation of density of PEG on water-exchange rates could not be performed.

Upon synthesis, purification, and characterization of M^{III}-containing PEG conjugates, **2.13a–d**, **2.14a–d**, and **2.15a–d**, properties relevant to MRI including water-coordination number, q; water-exchange rate, k_{ex}; relaxivity, r_1; and longitudinal and transverse electron spin relaxation times, T_{1e} and T_{2e}, respectively, were determined to evaluate the influence of length and density of PEG on water-exchange rates and contrast agent efficiency. Contrast-agent-relevant properties obtained for the system designed to explore the influence of length of PEG on the water-exchange rates are summarized in **Table 5.1**.

Luminescence-decay measurements that were performed to obtain water-coordination number data for Eu^{III}-containing complexes **2.14a–d** resulted in water-coordination numbers close to one for all four complexes. This observation suggests that there is little if any steric hindrance caused by PEG moieties to block the coordination of a water molecule at the ninth coordination site of Ln^{III}-containing octadentate DOTA-type complexes.

Table 5.1. Molecular parameters of complexes **2.13a–d**.

Parameter	**2.13a**	**2.13b**	**2.13c**	**2.13d**
$q^{a,b,c}$	0.90 ± 0.01	0.89 ± 0.01	0.96 ± 0.01	0.76 ± 0.01
$k_{ex}^{298} \times 10^6$ (s^{-1})^d	2.7 ± 0.03	1.5 ± 0.02	0.83 ± 0.08	0.67 ± 0.05
$T_{1e}^{298} \times 10^{-9}$ (s)^a	440 ± 30	61 ± 1	12 ± 0.3	4.0 ± 0.04
r_1 (mM^{-1} s^{-1})^a	2.5 ± 0.1	4.0 ± 0.1	5.3 ± 0.1	6.3 ± 0.1
MW (Da)	641	817	1463	5222
$1/T_{2e} \times 10^6$ (s^{-1})	17.8	8.11	6.51	5.03
$\tau_R \times 10^{-12}$ (s)	46	79	110	220

[a]Reported as mean ± standard error. [b]From complexes **2.14a–d**. [c]The error associated with q determination is ±0.1 water molecules.[107] [d]Error represents relative uncertainty.

To study the influence of length of PEG on water-exchange rates of Gd^{III}-containing complexes **2.13a–d**, variable-temperature ^{17}O NMR spectroscopy was performed. The water-exchange rates obtained demonstrated a 4-fold decrease in water-exchange rates from complex **2.13a** (used as a control without PEG) to **2.13d** (with the longest PEG moiety used in this study). The observed decrease in water-exchange rates as a function of length of PEG is likely due to the stabilization of the nine-coordinate ground state through hydrogen-bonding interactions, increase in extent of the hydrogen-bonding network between bulk and coordinated water as a function of length of PEG, or both factors. The ability of PEG to tune water-exchange rates as a function of length of PEG supports the hypothesis that PEG is able to tune water-exchange rates of Ln^{III}-containing DOTA-type complexes.

The efficiency of Gd^{III}-containing complexes **2.13a–d** as T_1-shortening contrast agents was obtained in terms of relaxivity from water-proton relaxation time measurements at 37 °C, pH 7.4 (in phosphate-buffered saline), and 1.4 T. The relaxivity values obtained for Gd^{III}-containing complexes **2.13a–d** indicated a 2.5-fold increase from **2.13a** to **2.13d** as length of PEG increased. This increase in relaxivity is possibly due to the molecular weight (MW) increase (**Table 5.1**) from **2.13a** to **2.13d**, because complexes with high molecular weights have a tendency to tumble slowly in solution leading to higher relaxivity values.

Rotational correlation times (τ_R) for Gd^{III}-containing complexes **2.13a–d** were estimated using the measured data in **Table 5.1** and the Solomon–Bloembergen–Morgan equations[8] to account for the increase in relaxivity from **2.13a** to **2.13d**. Based on the estimated rotational correlation times (**Table 5.1**), a 5-fold increase from **2.13a** to **2.13d** was observed suggesting that the increase in rotational correlation time is consistent with the increase in MW. Moreover, the observed increase in the estimated rotational correlation time is likely the cause of the observed increase in relaxivity from **2.13a** to **2.13d**.

Conclusions

This thesis describes the design, synthesis, and characterization of Ln^{III}-containing DOTA-type complexes conjugated to different lengths and densities of PEG. In addition, measurements performed to explore the influence of length and density of PEG on water-exchange rates and other molecular parameters that contribute to the efficiency of Ln^{III}-containing complexes as contrast agents for MRI are described, followed by the analysis and interpretation of data. The results suggest that PEG is able to tune the water-exchange rates of

Ln^{III}-containing DOTA-type complexes towards slower rates as a function of length of PEG. Moreover, the magnitude of slowing of water-exchange rates is comparable to that reported for Ln^{III}-containing hydroxypyridonate-based (HOPO) PEG conjugates.[67,68,104,105] However, the decrease in water-coordination number from two to one reported for the HOPO-based systems with long PEG moieties was not observed with the DOTA-type system. The results described in this thesis for DOTA-type complexes together with the results reported for the HOPO-based systems demonstrate that PEG can be used to slow water-exchange rates of Ln^{III}-containing complexes as a function of length of PEG, regardless of the differences in water-coordination numbers. Consequently, conjugation of PEG leads to a modular and tunable approach to slow water-exchange rates that can be generalized for Ln^{III}-containing complexes.

Because conjugation of PEG leads to slowing of water-exchange rates, the results described in this thesis are expected to be useful for the design of PARACEST agents for MRI, which require slow water-exchange rates. In addition, despite their relatively slow (~10^6 s^{-1}) water-exchange rates Gd^{III}-containing complexes, **2.13b–d**, have the potential to be used as T_1-shortening agents for MRI owing to the higher relaxivity values (4.0–6.3 mM^{-1} s^{-1}) observed relative to clinically approved Gd^{III}-DOTA (3.0 mM^{-1} s^{-1}) at 37 °C, pH 7.4, and 1.4 T.[106]

Future Directions

As described in this thesis, the conjugation of PEG enables tuning of water-exchange rates of Ln^{III}-containing complexes towards slower rates. However, the magnitude of slowing (×4) attained through conjugation of PEG alone is not sufficient to be used as PARACEST agents that require slower water-exchange rates (10^3 s^{-1}). To make conjugation of PEG a practical strategy for the design of PARACEST agents, conjugation of PEG can be combined with a few other strategies.

One approach to making the conjugation of PEG a useful strategy for the design of PARACEST agents is to begin with complexes that display slow water-exchange rates. Based on the coordination-chemistry-based strategies discussed in Chapter 1, positively charged complexes lead to substantial slowing of water-exchange rates of Ln^{III}-containing complexes.[40,43] Consequently, designing positively charged complexes that can be conjugated to PEG is likely to lead to water-exchange rates that are slow enough to perform as efficient PARACEST agents. Examples of positively charged complexes that can be conjugated to PEG are shown in **Figure 5.2**.

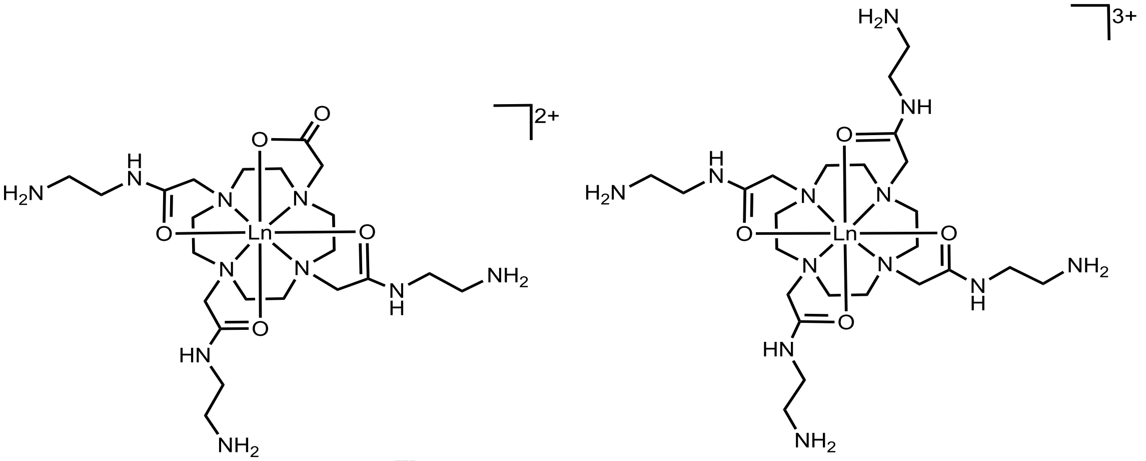

Figure 5.2. Positively charged Ln^{III}-containing complexes that can be conjugated to PEG with the potential to lead to slow water-exchange rates required for PARACEST agents.

Another approach to making the conjugation of PEG useful for the design of PARACEST agents is to incorporate other paramagnetic Ln^{III} ions including Ce^{III}, Pr^{III}, Nd^{III}, Sm^{III}, Tb^{III}, Dy^{III}, Ho^{III}, Er^{III}, Tm^{III}, and Yb^{III}. Incorporating other Ln^{III} ions is advantageous for the design of PARACEST agents because each Ln^{III} ion shifts the exchangeable protons peaks to different extents from that of bulk water. This difference in the extent of the shift of exchangeable protons alters the resonance frequency difference between the two exchanging pools of protons ($\Delta\omega$).[12] Ln^{III} ions that give rise to large values of $\Delta\omega$ are useful because they allow complexes with fast water exchange rates to be used as PARACEST agents.[12]

APPENDIX A

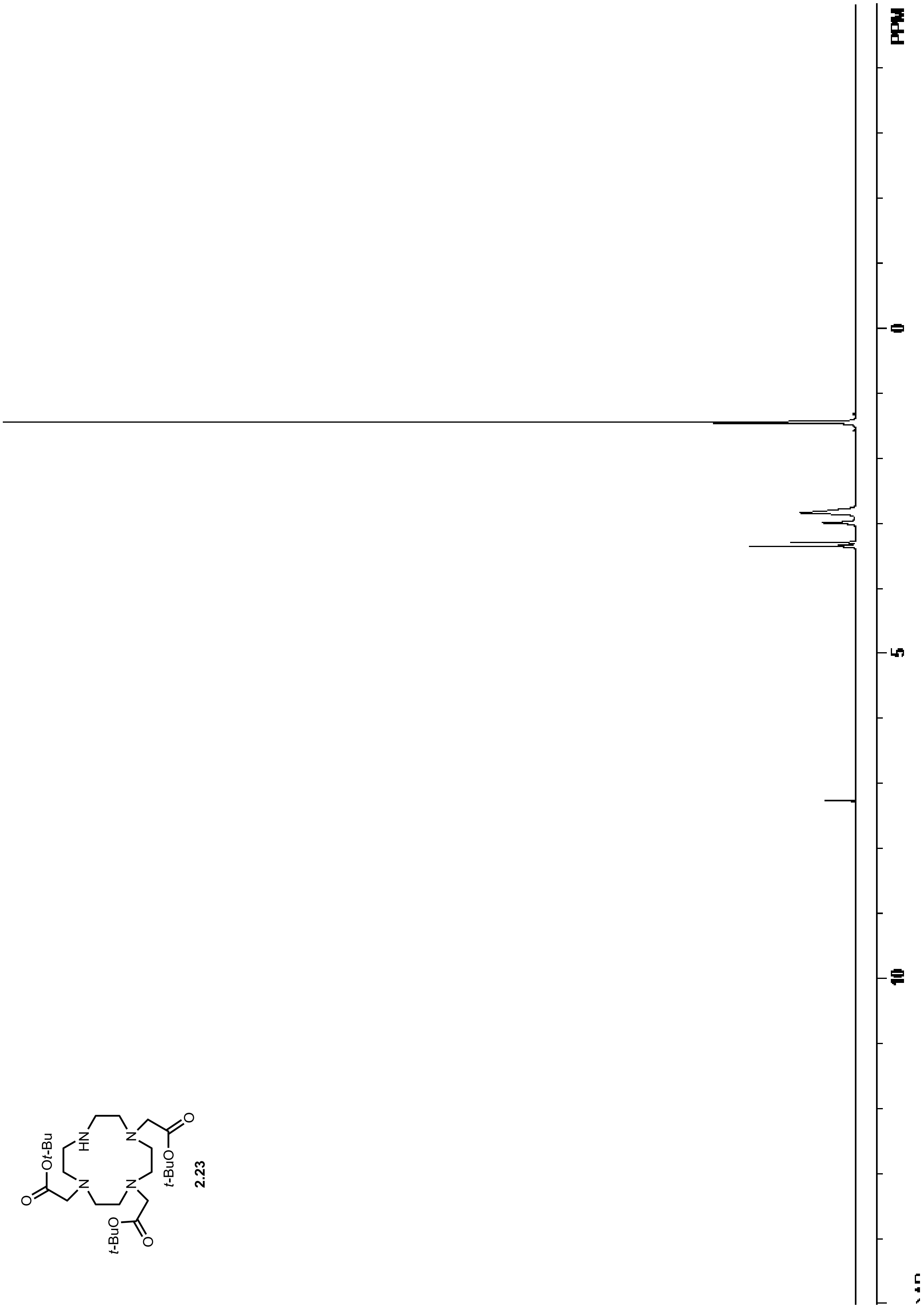

2.23

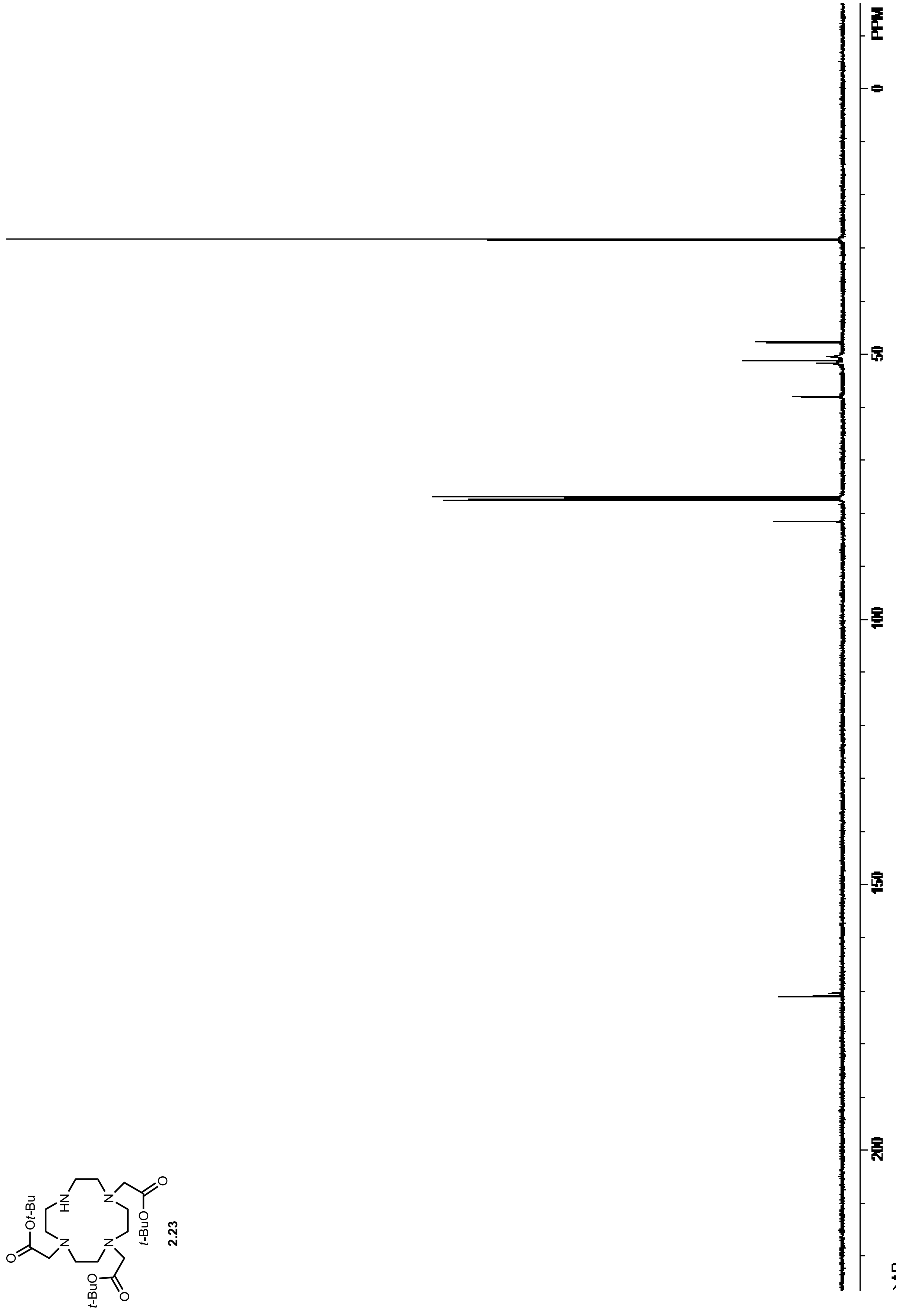

2.23

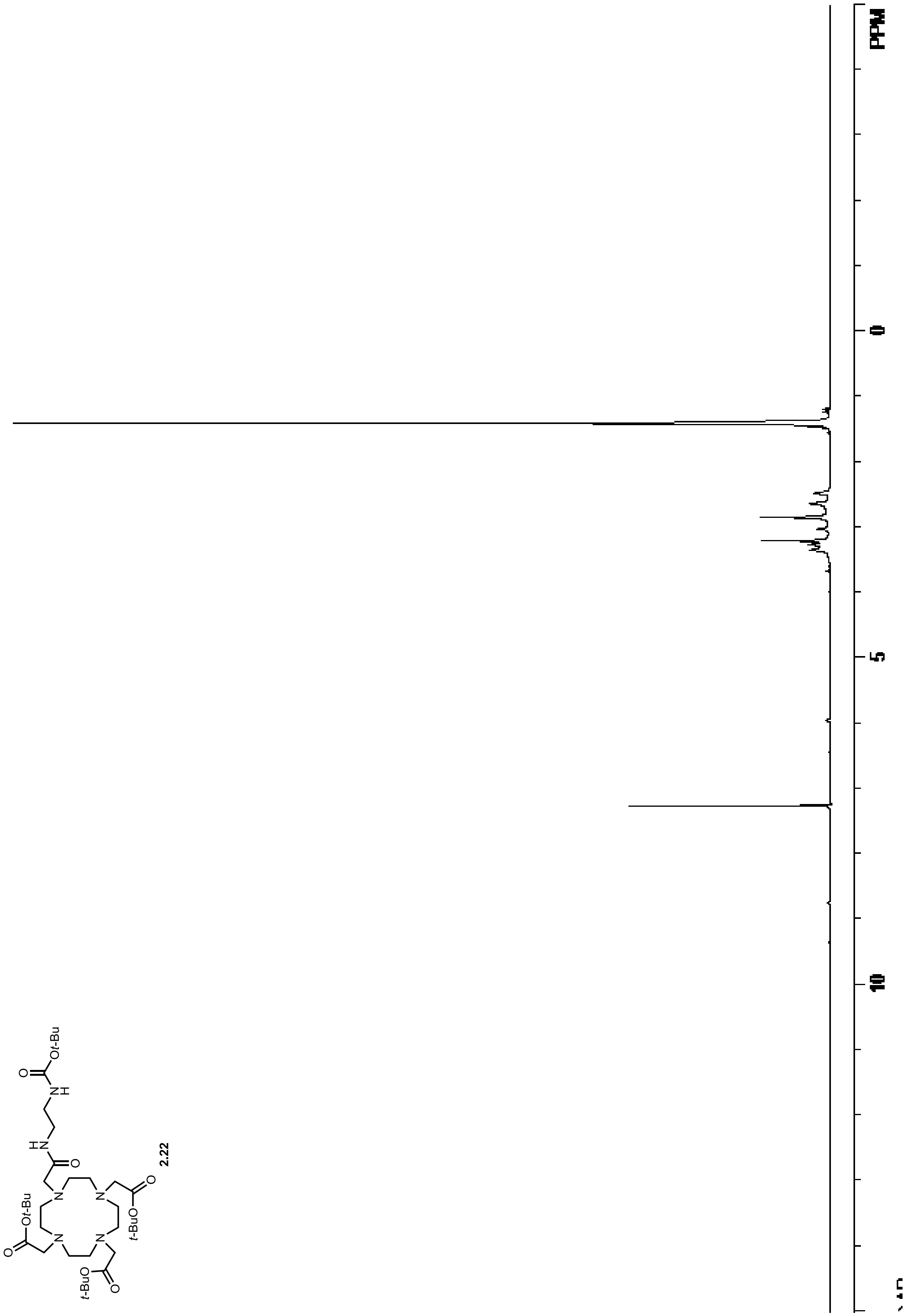

2.22

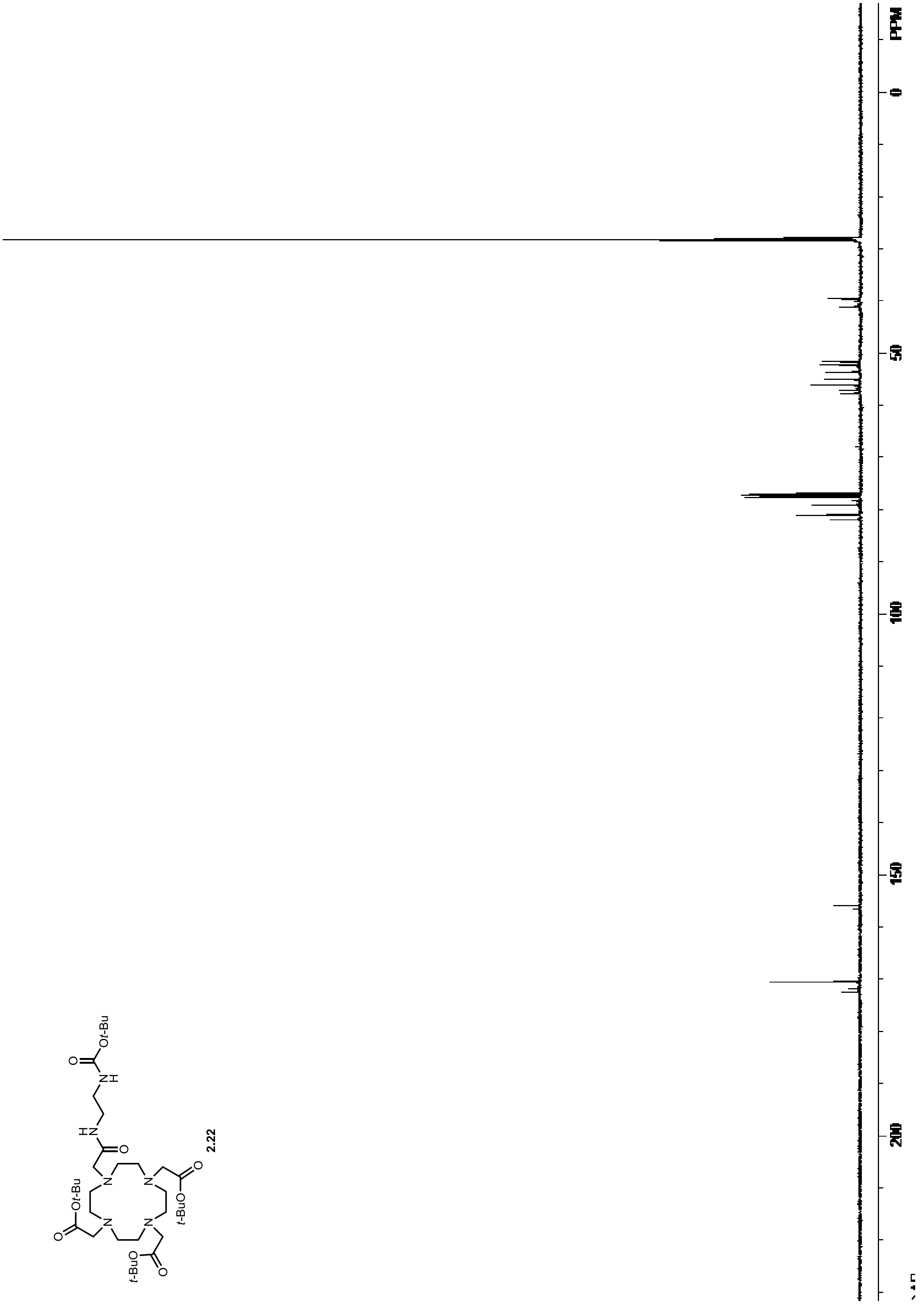

2.22

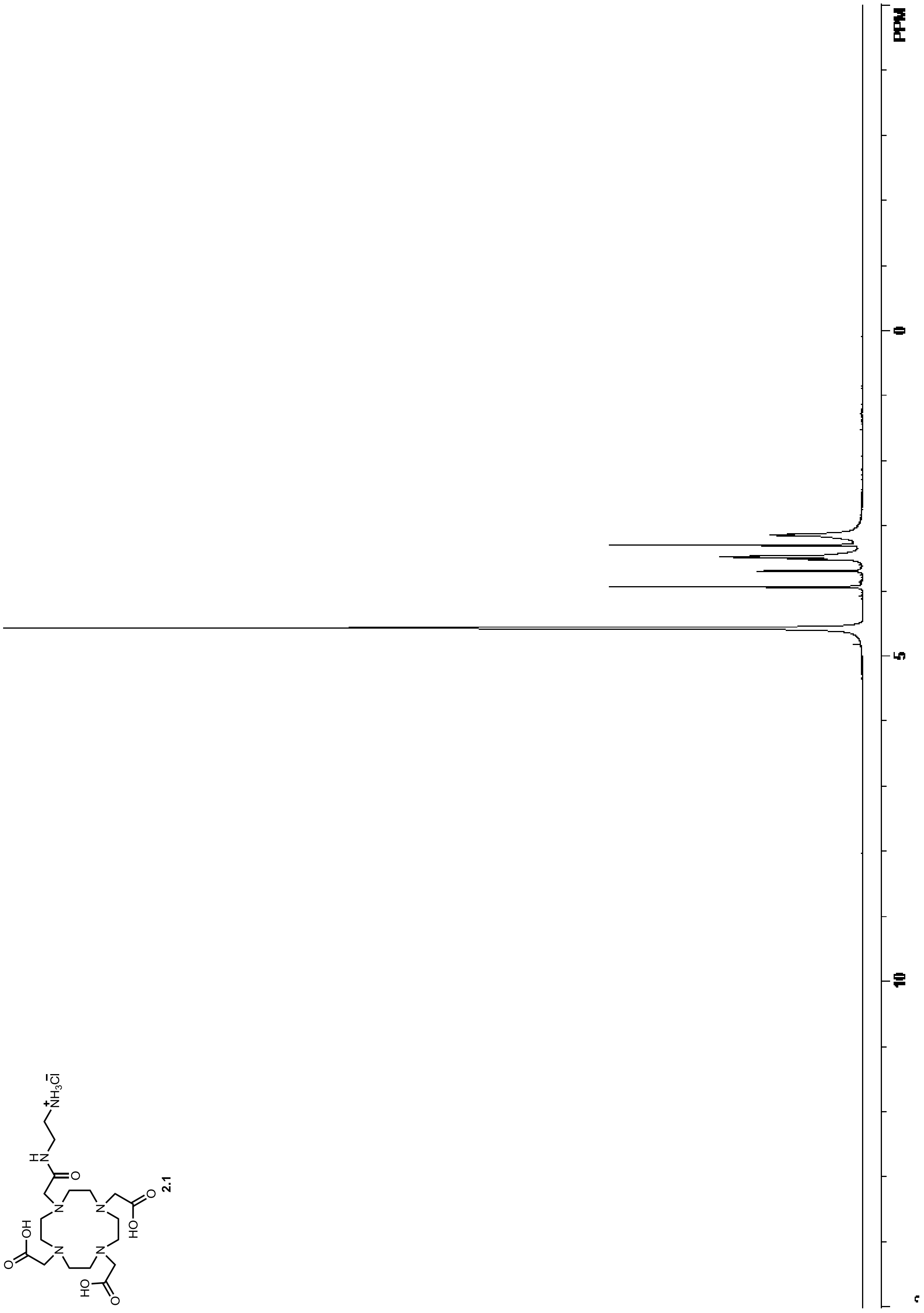
PPM
0
5
10
OH
HO
HO
O
N
N
N
N
H
N
O
$\overset{+}{N}H_3\bar{C}l$
2.1

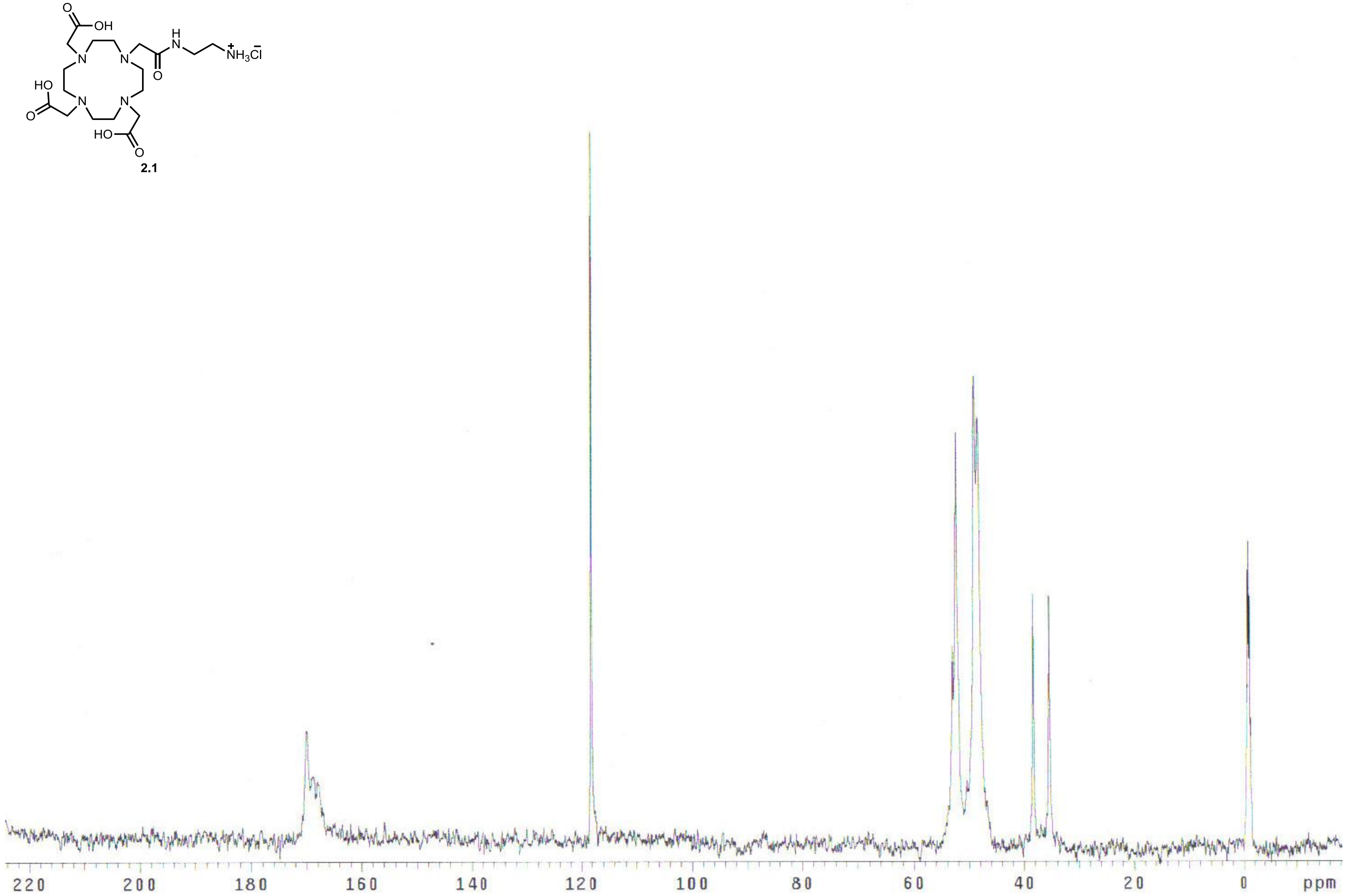

2.1

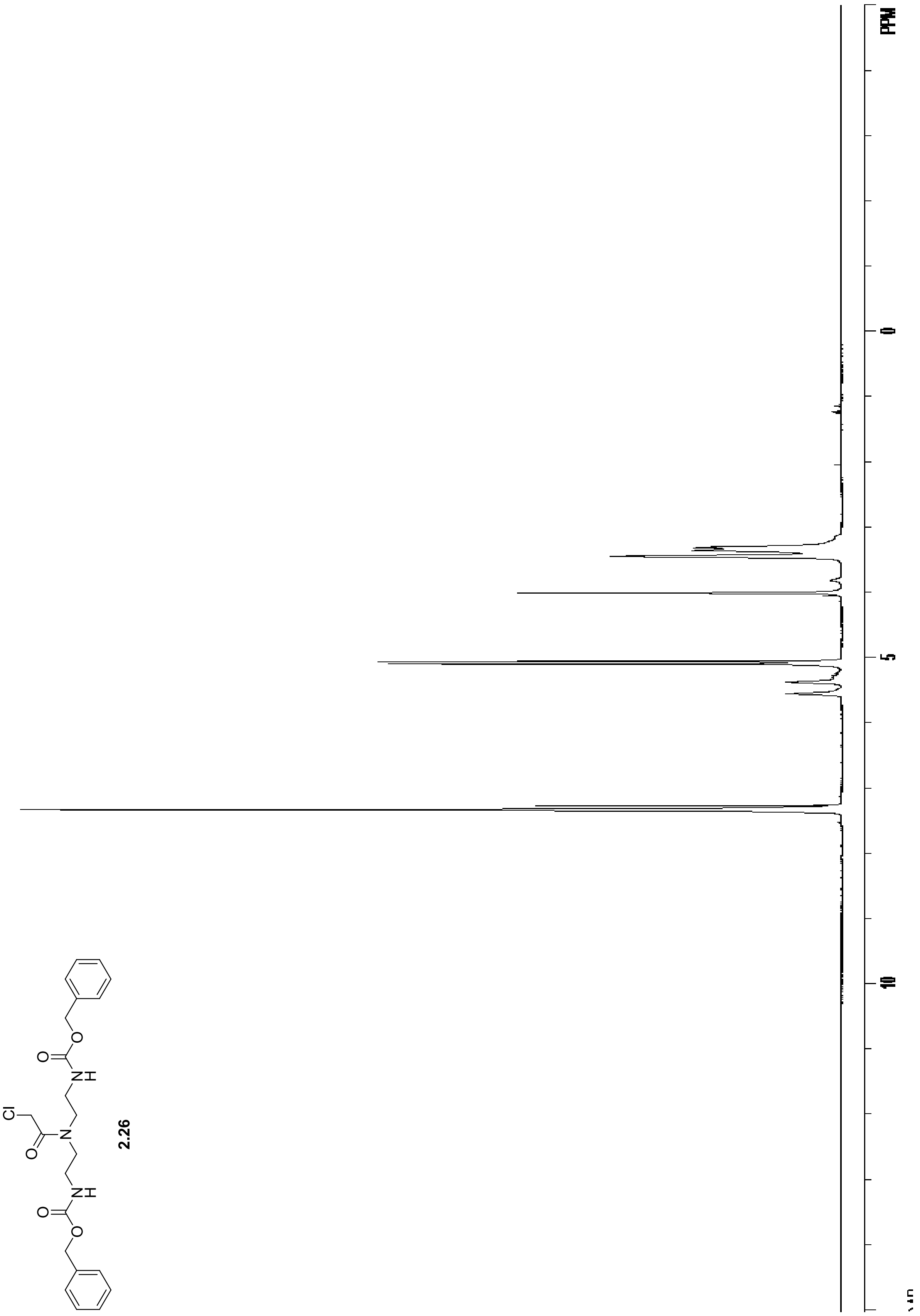

2.26

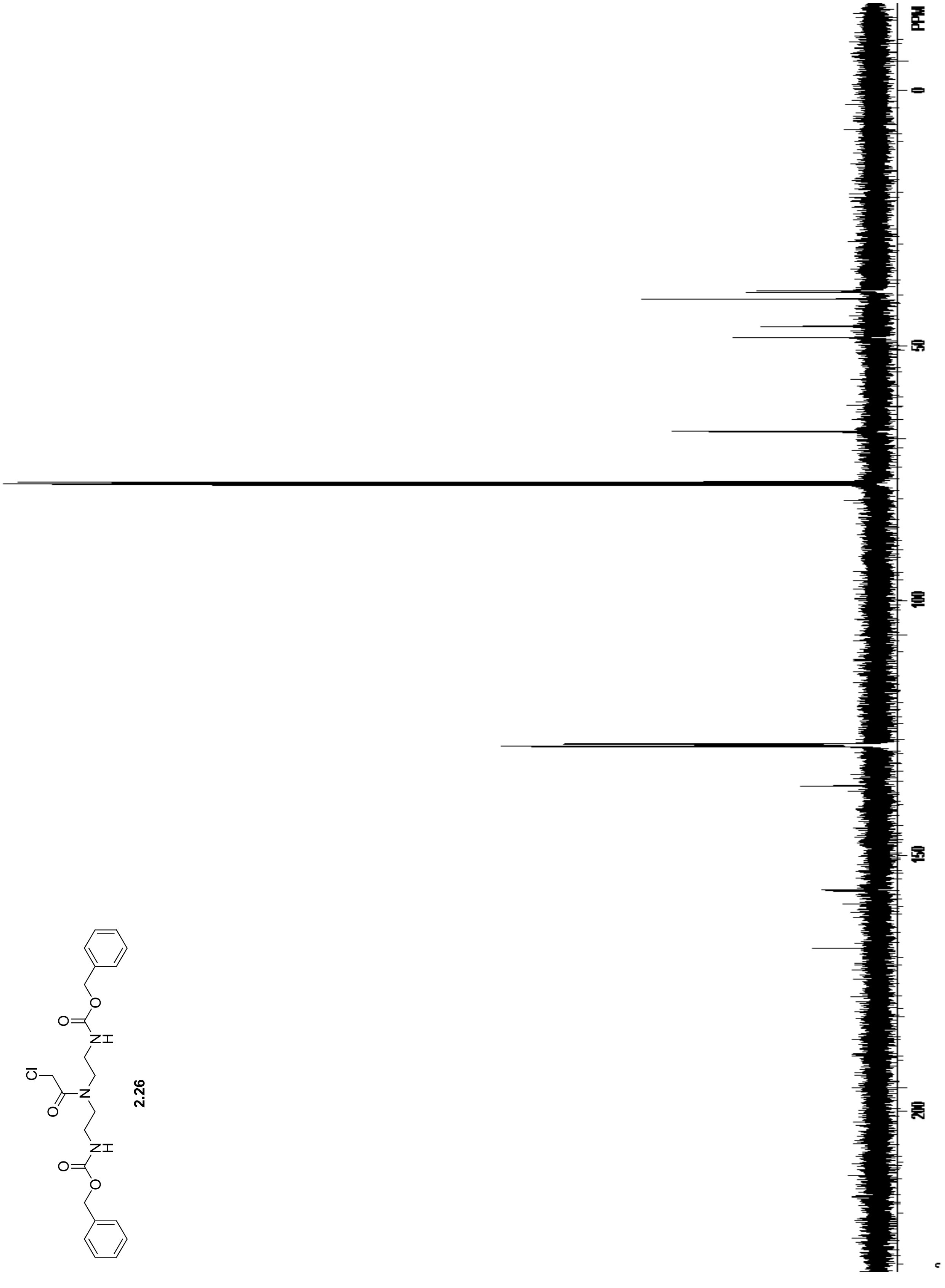

2.26

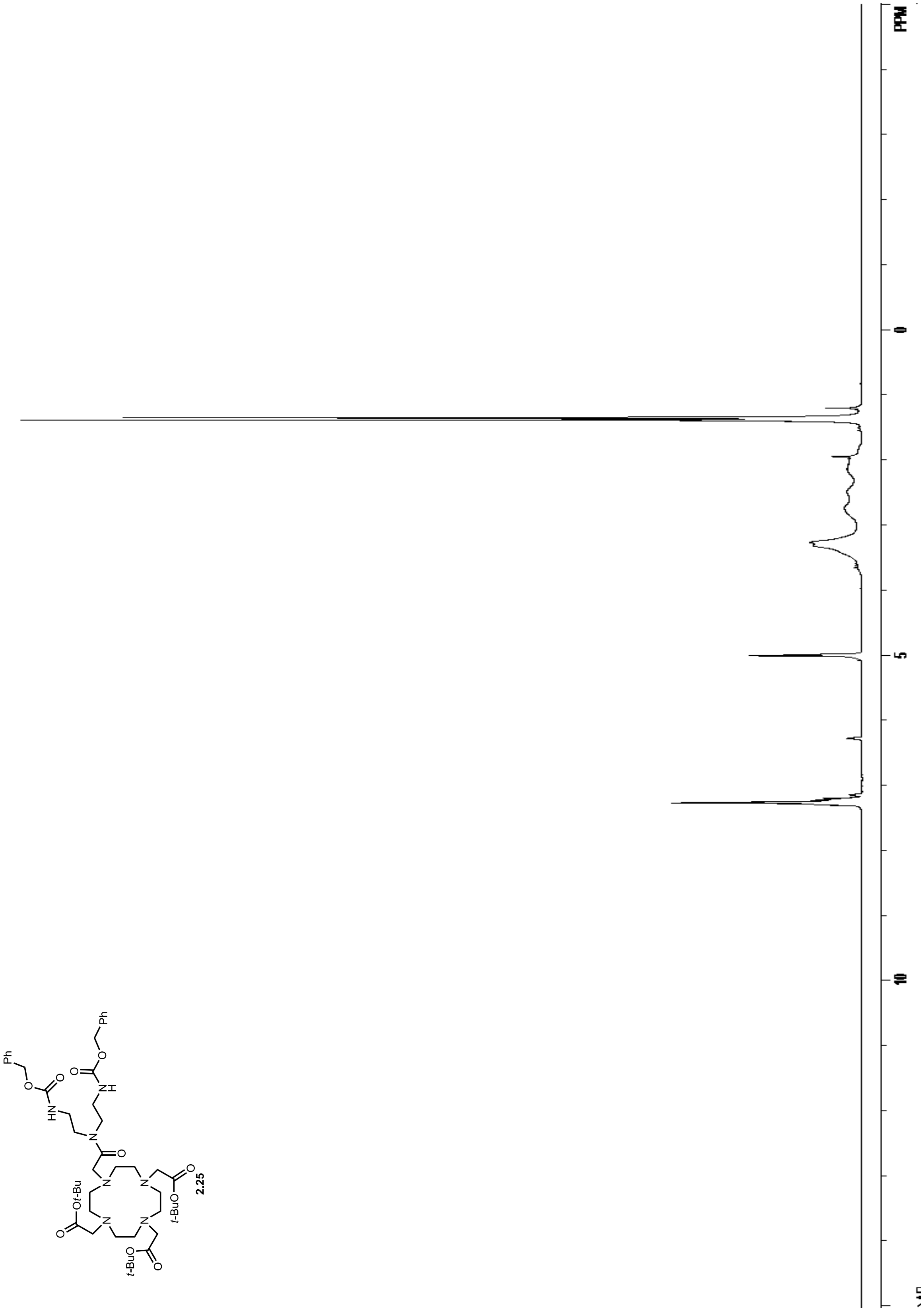

2.25

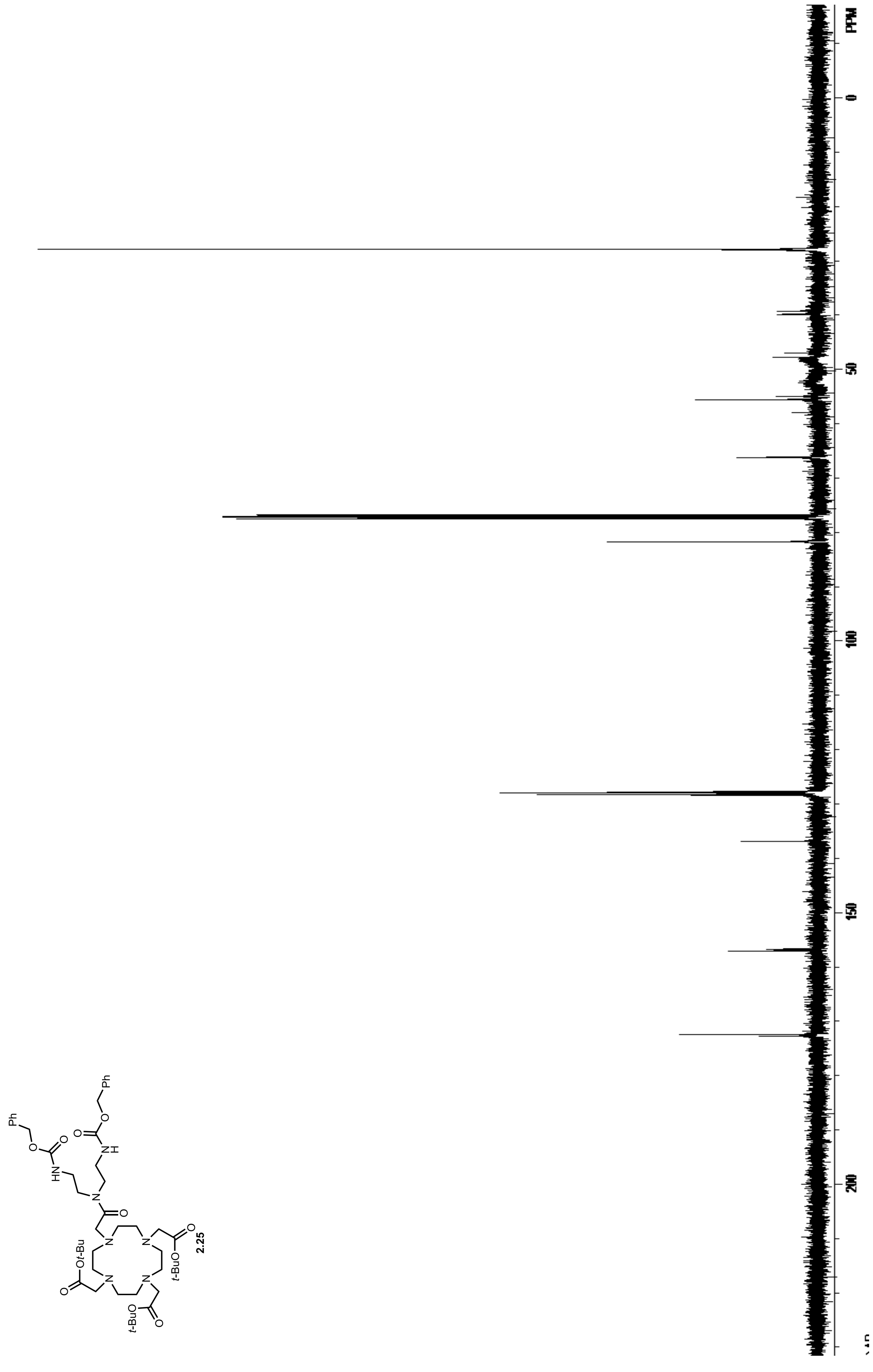

2.25

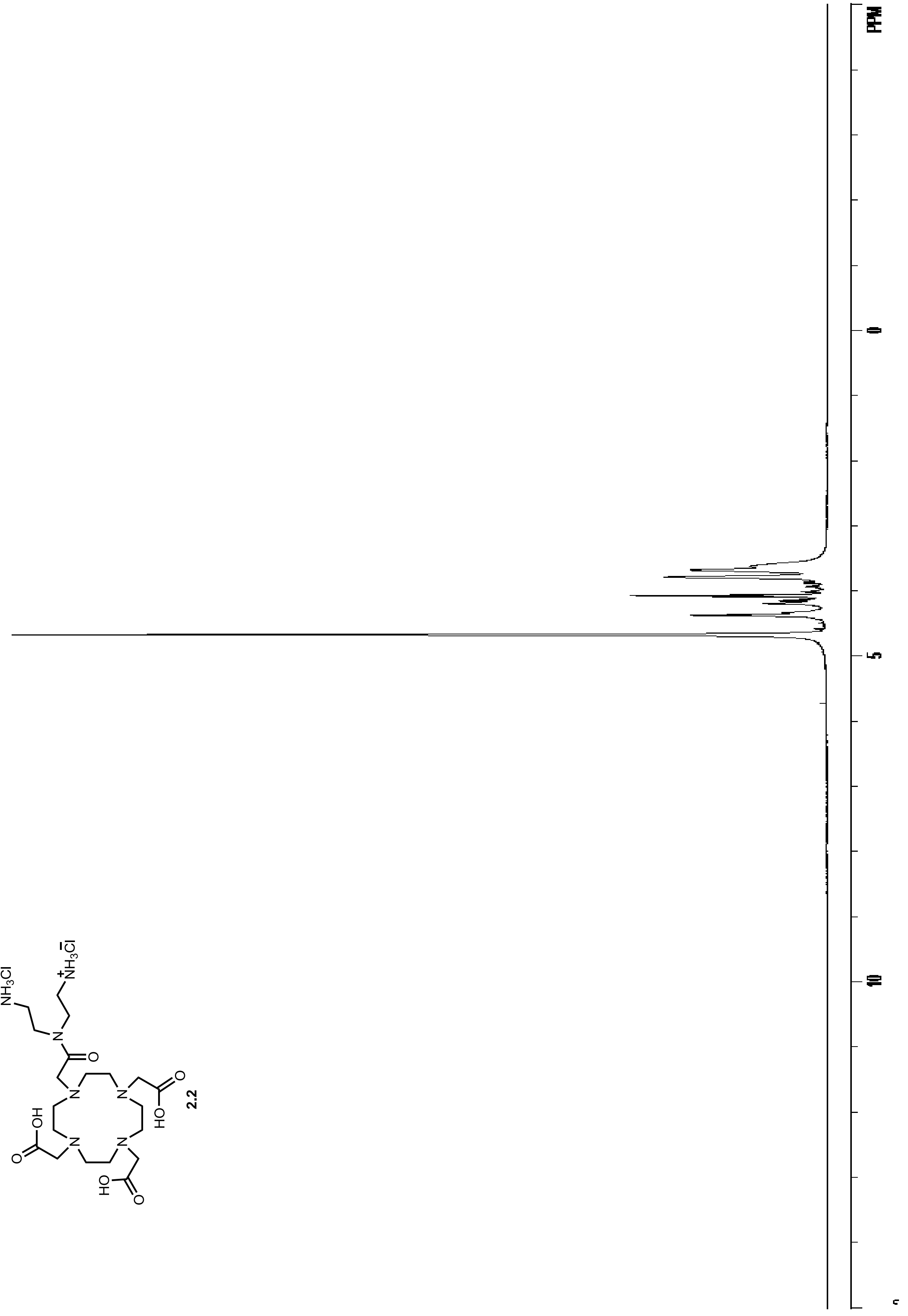

2.2

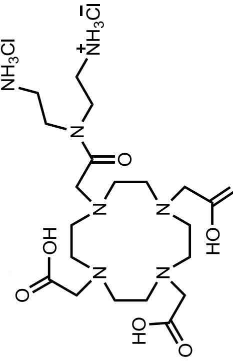

$\overset{+}{N}H_3\bar{C}l$
$\overset{+}{N}H_3\bar{C}l$
N
O
N
N
N
N
OH
O
O
OH
HO
O

2.2

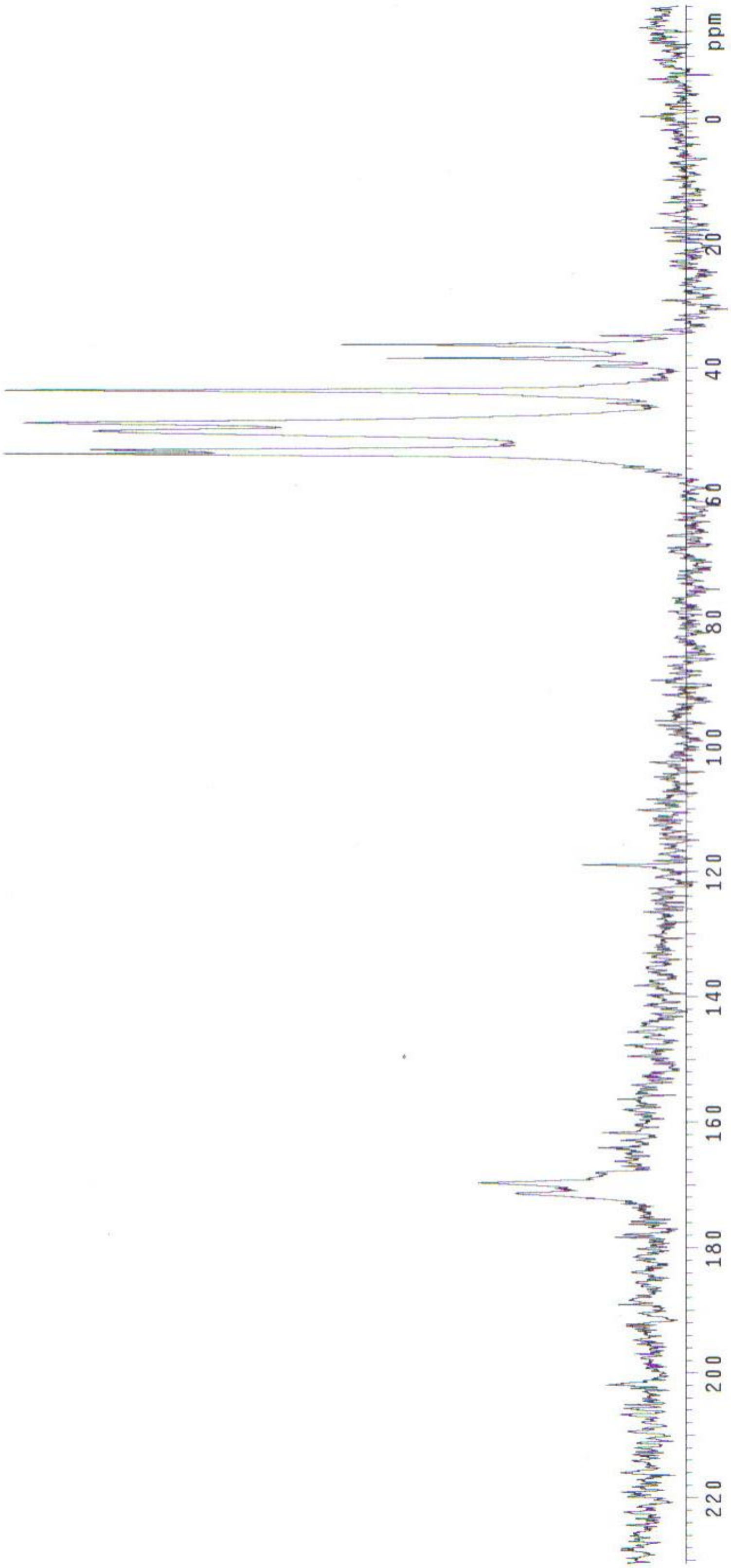

ppm
0
20
40
60
80
100
120
140
160
180
200
220

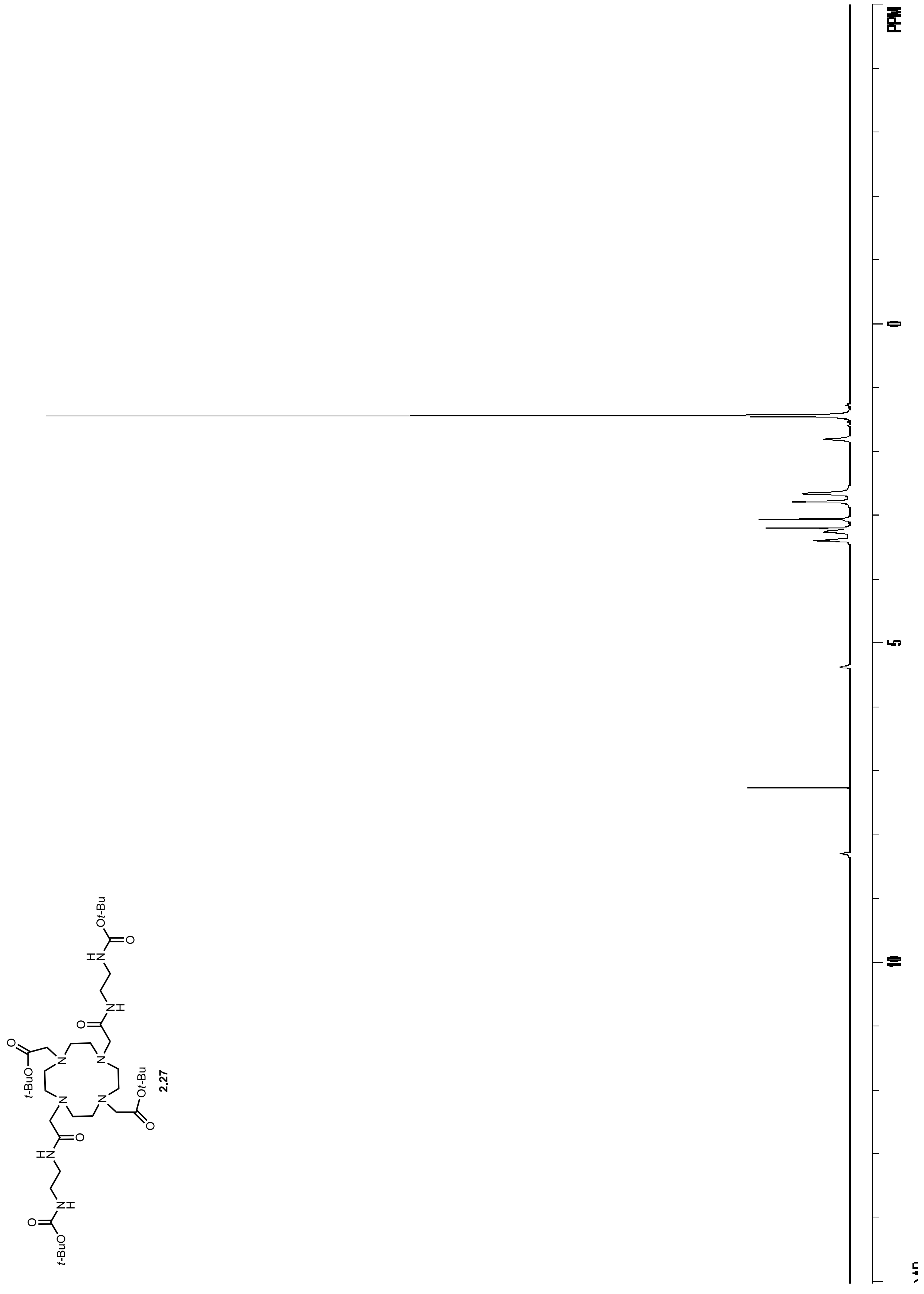

2.27

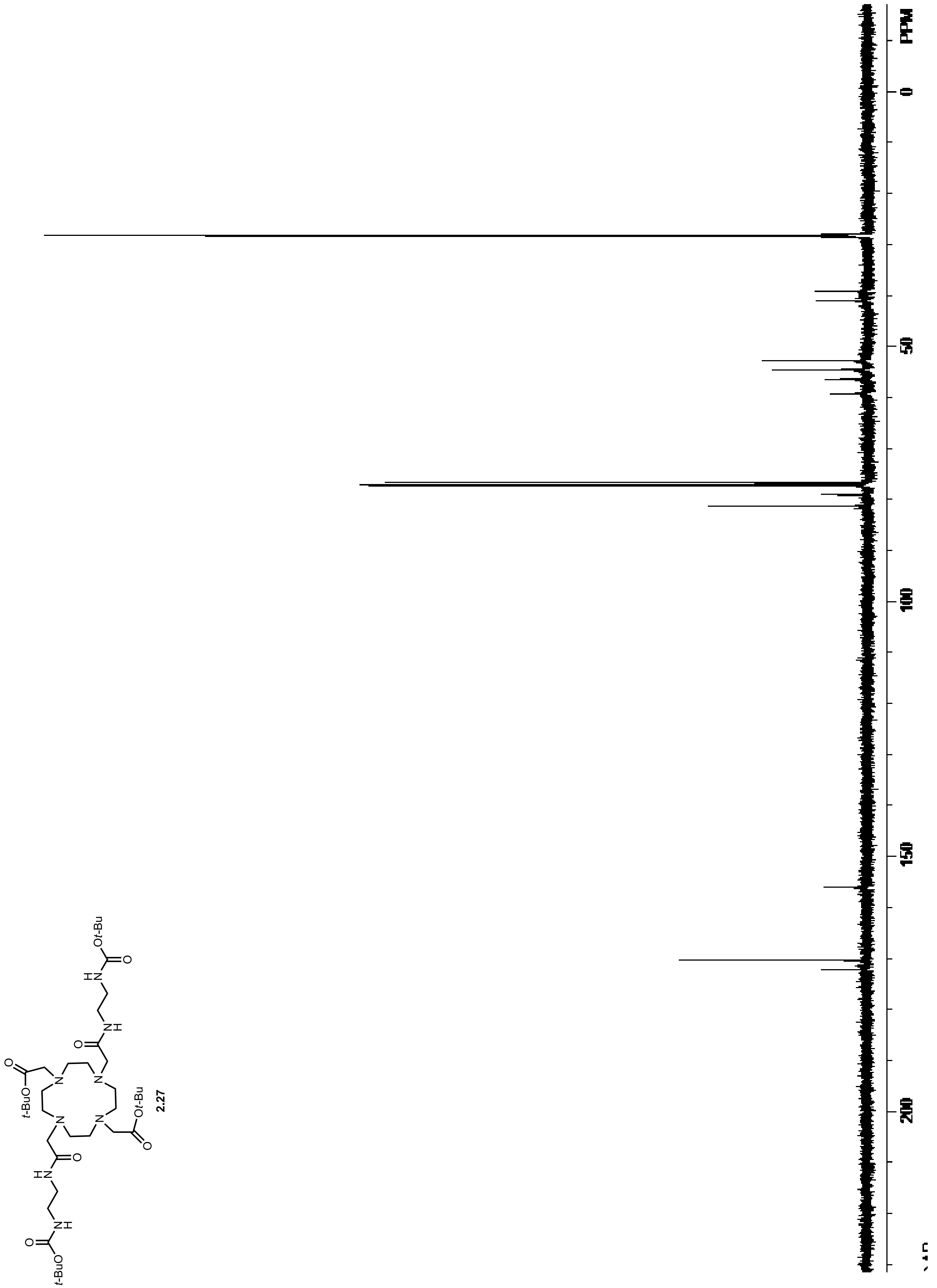

2.27

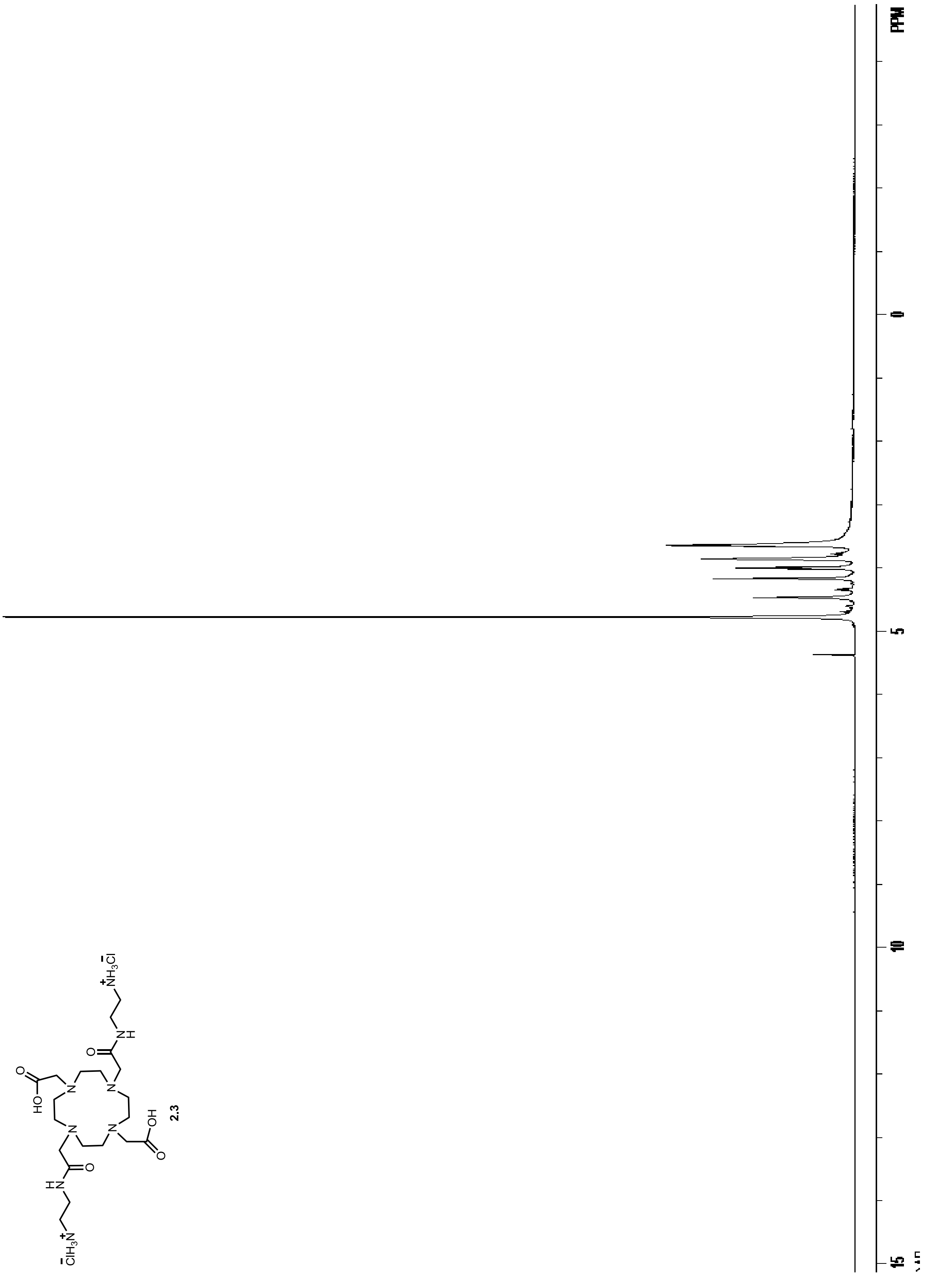
PPM
0
5
10
15
HO
O
N
N
N
N
OH
O
O
H
N
N
H
O
$\bar{C}lH_3\overset{+}{N}$
$\overset{+}{N}H_3\bar{C}l$

2.3

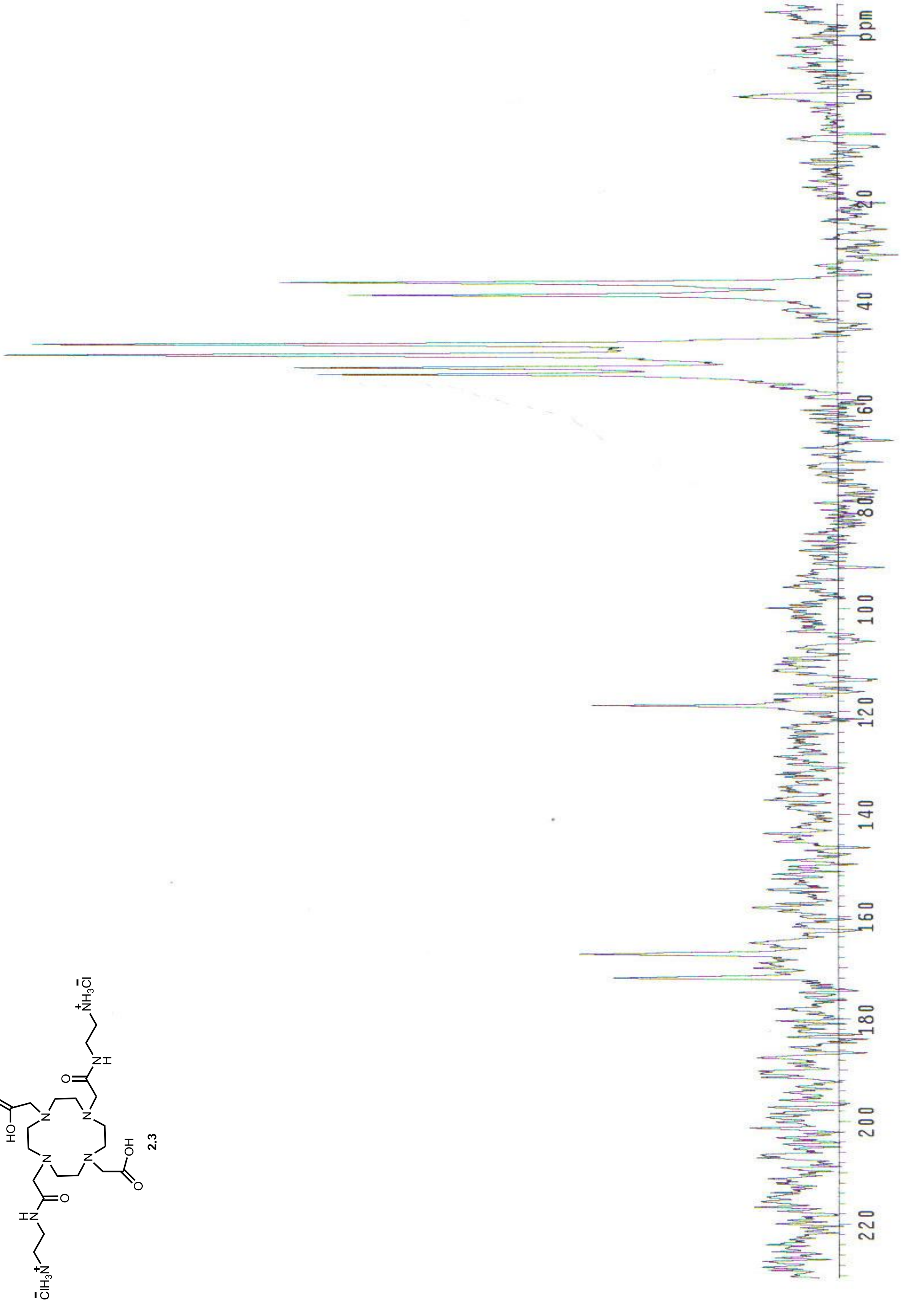
ppm
0
20
40
60
80
100
120
140
160
180
200
220
HO
O
OH
O
N
N
N
N
O
N
H
O
H
N
$\bar{Cl}H_3\overset{+}{N}$
$\overset{+}{N}H_3\bar{Cl}$

2.3

APPENDIX B

2.4

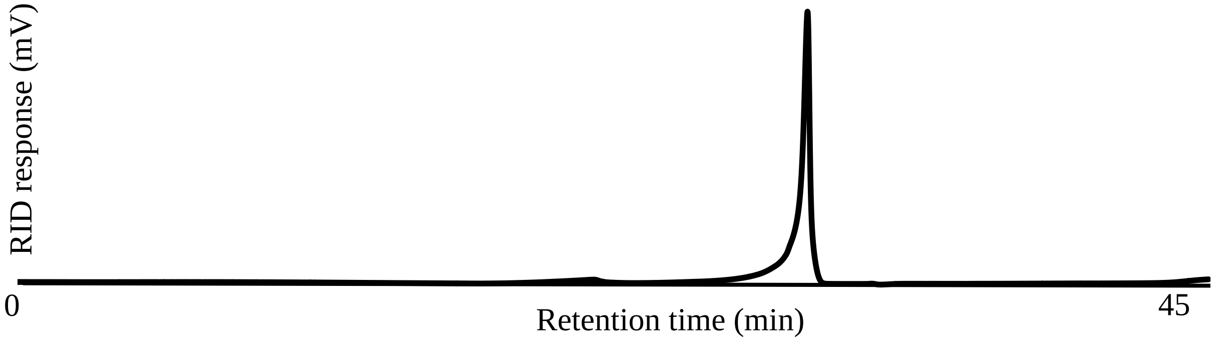

2.5

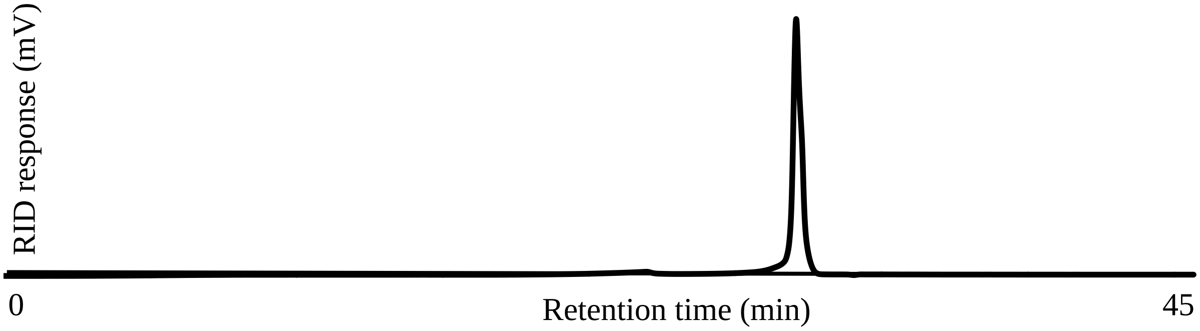

2.6

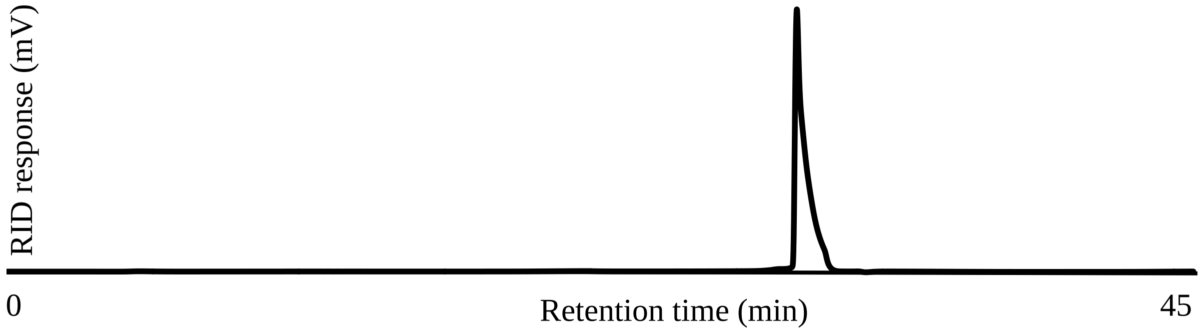

2.13a

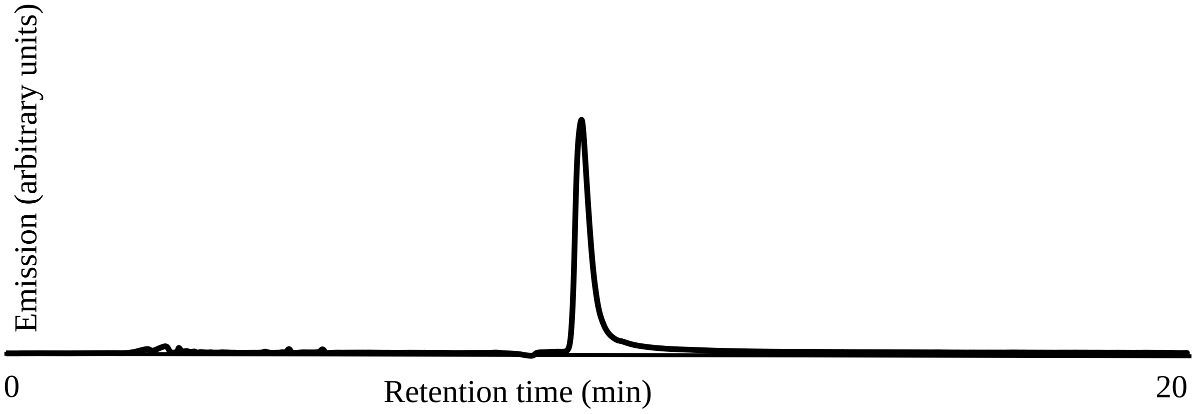

2.14a

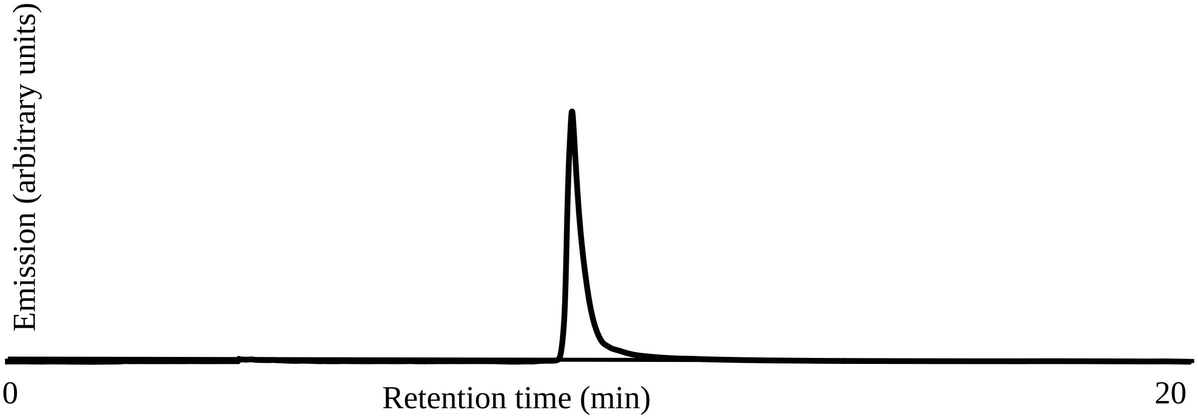

2.15a

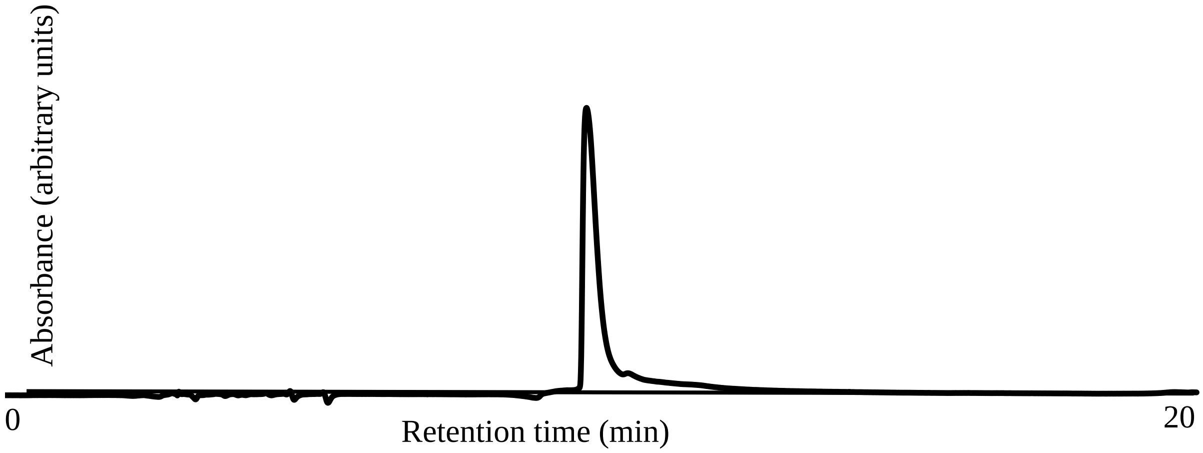

2.13b

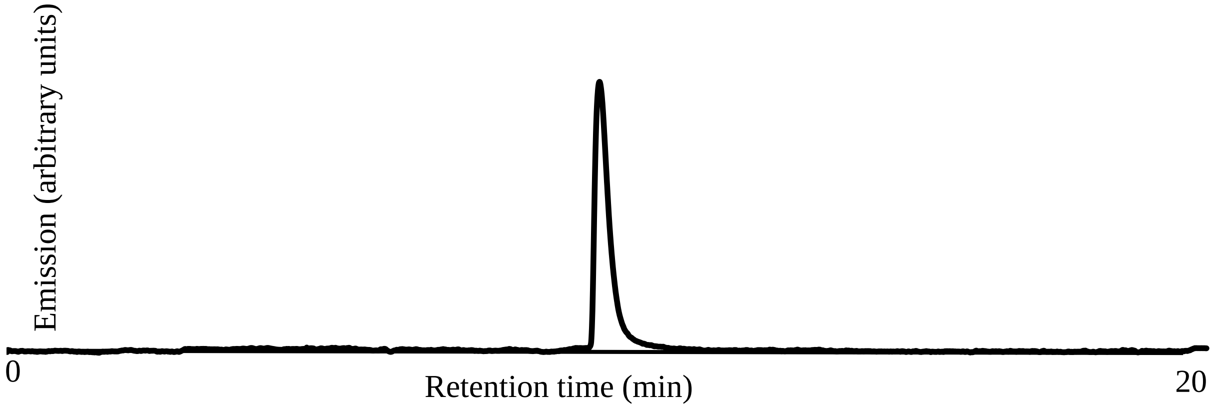

2.14b

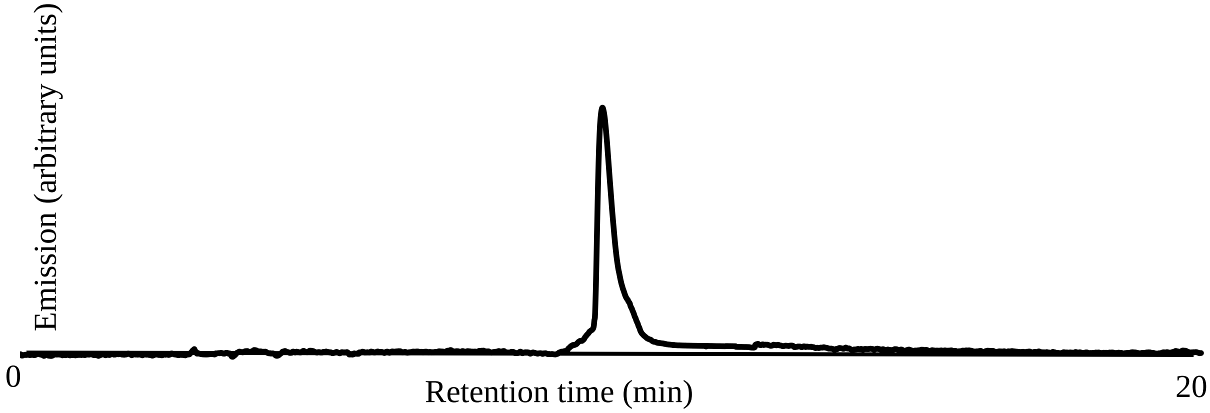

2.15b

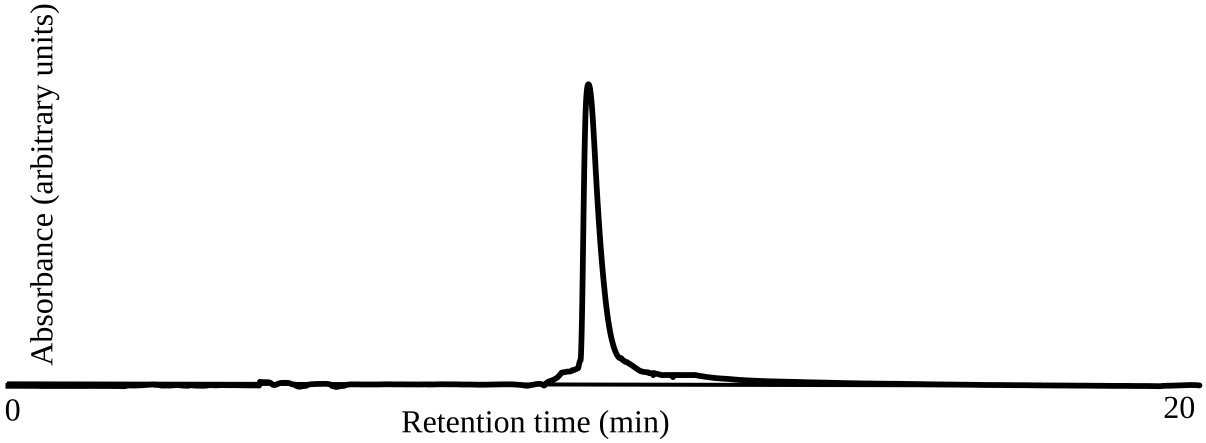

2.13c

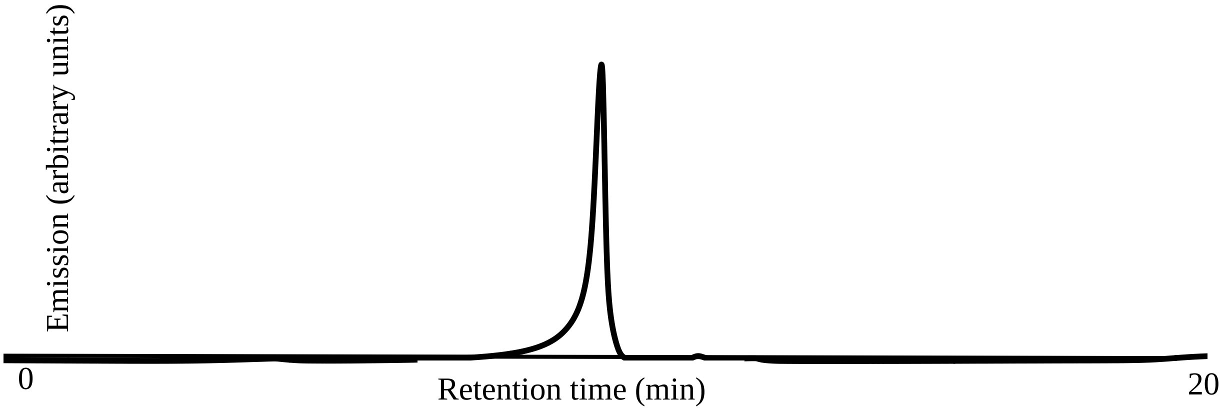

2.14c

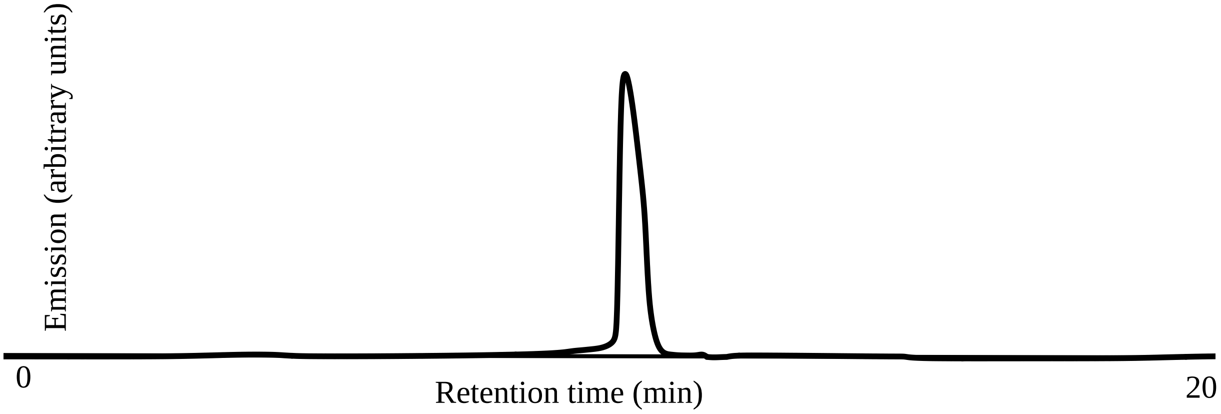

2.15c

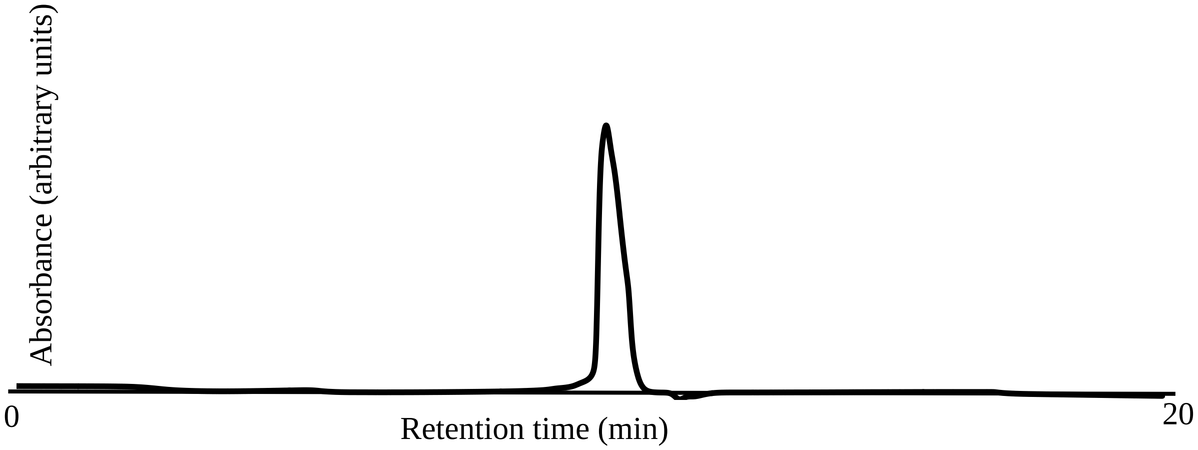

2.13d

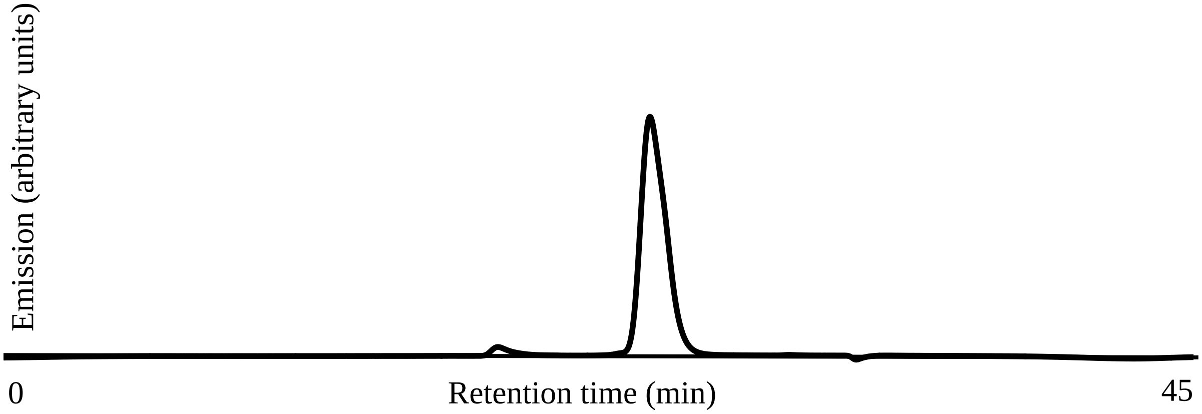

2.14d

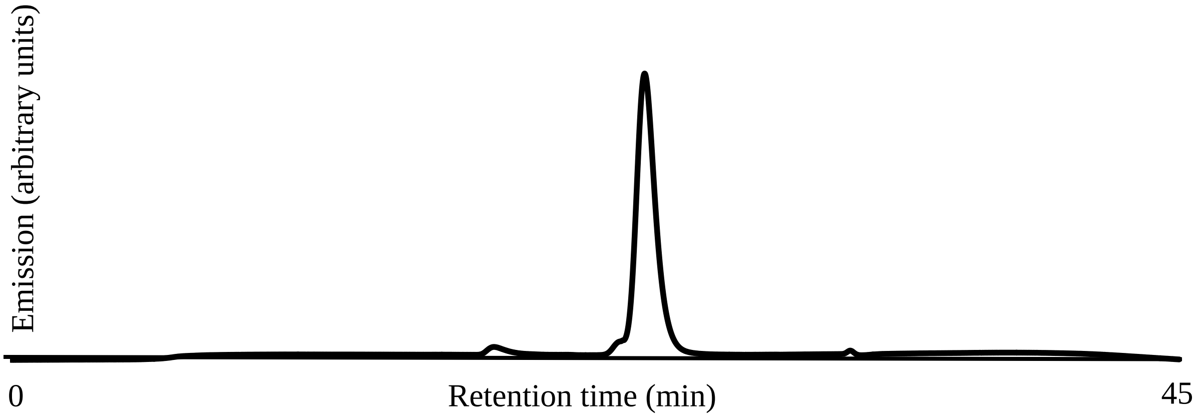

2.15d

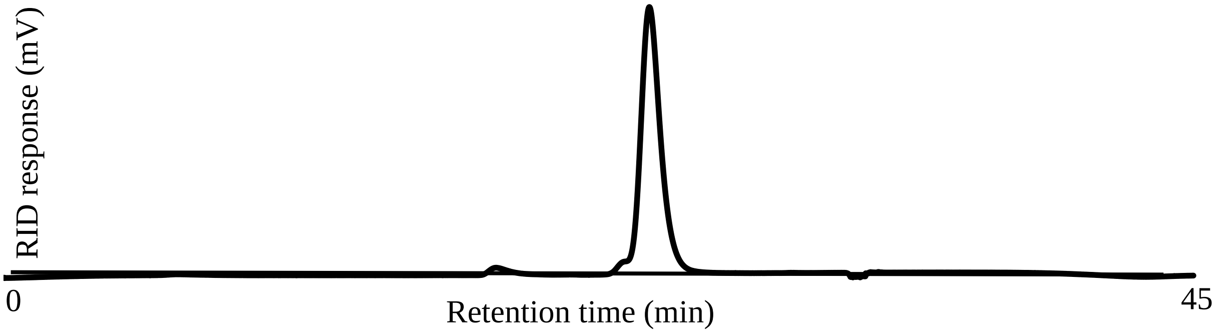

2.7

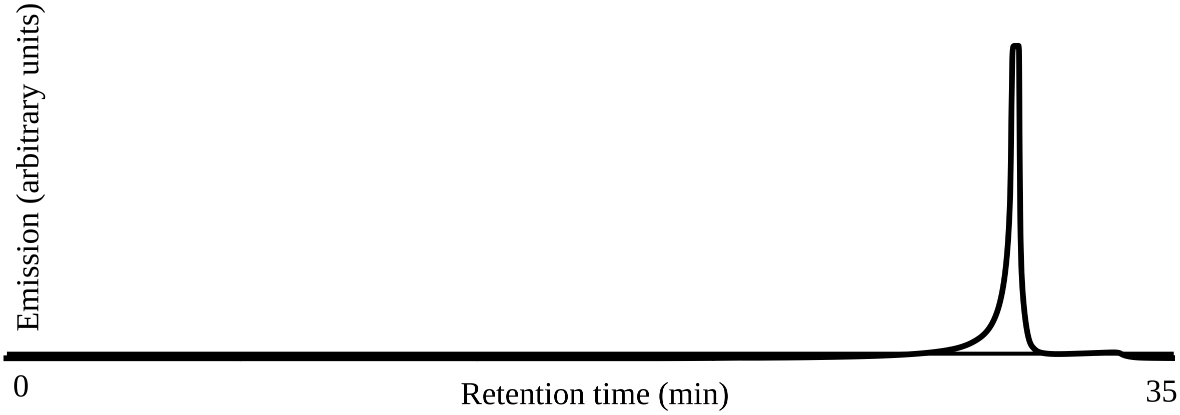
Emission (arbitrary units)
0
Retention time (min)
35

2.8

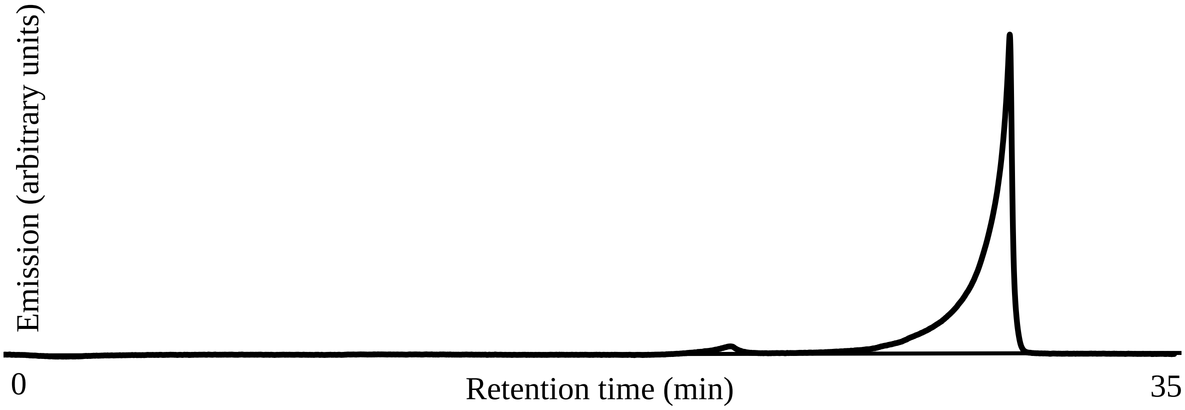
Emission (arbitrary units)
0
Retention time (min)
35

2.9

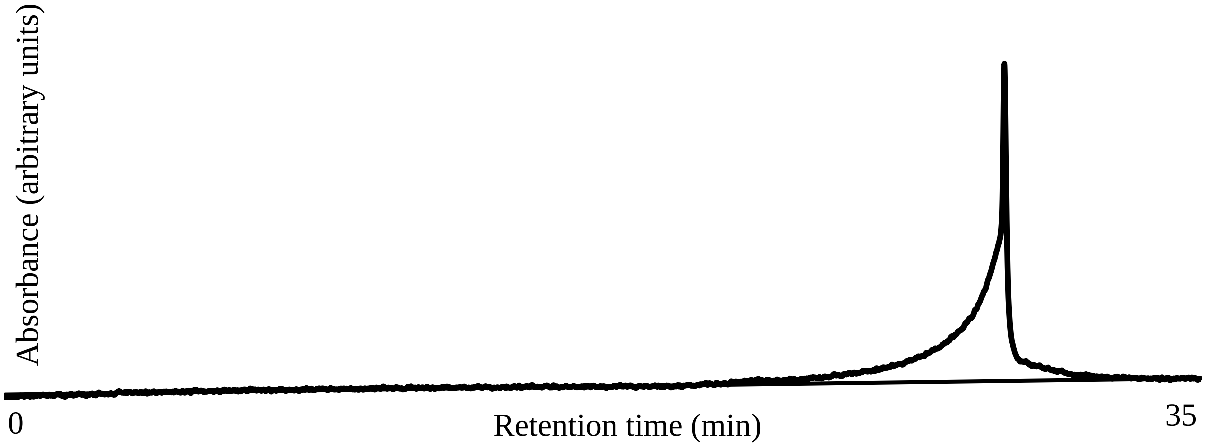
Absorbance (arbitrary units)
0
Retention time (min)
35

2.10

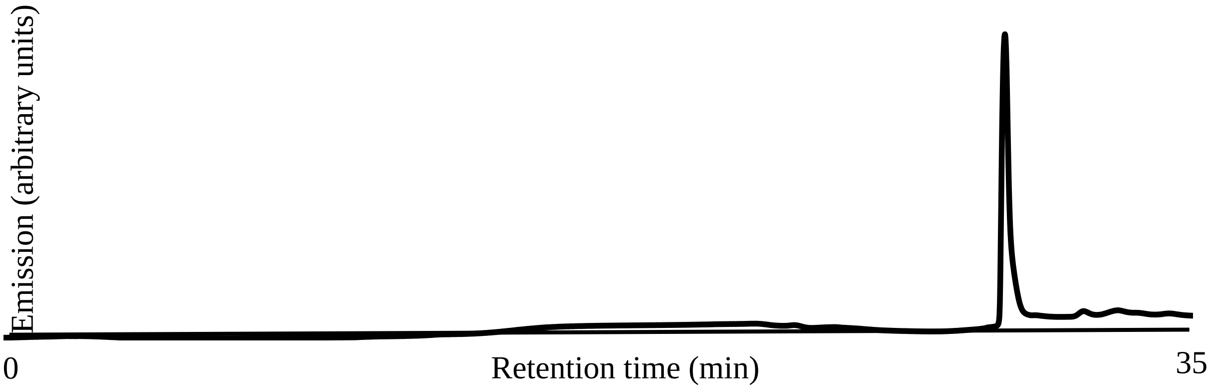
Emission (arbitrary units)
0
Retention time (min)
35

2.11

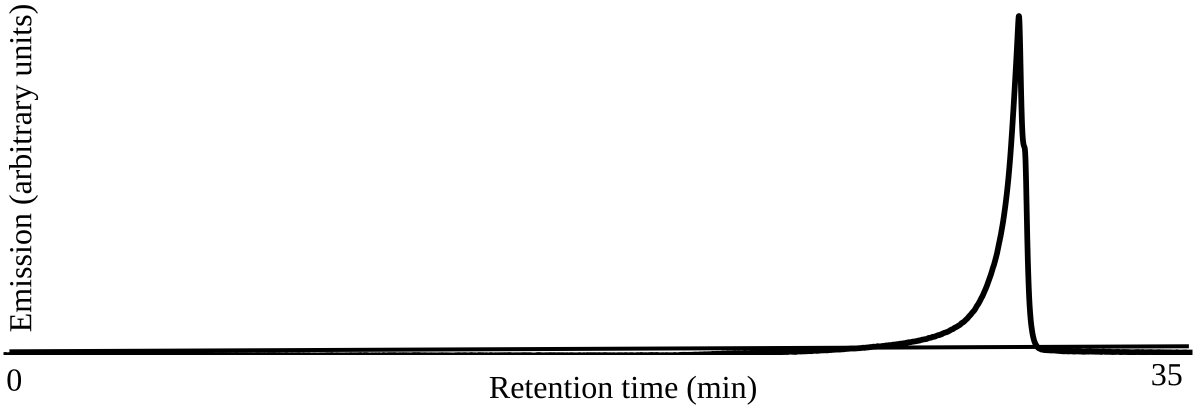
Emission (arbitrary units)
0
Retention time (min)
35

2.12

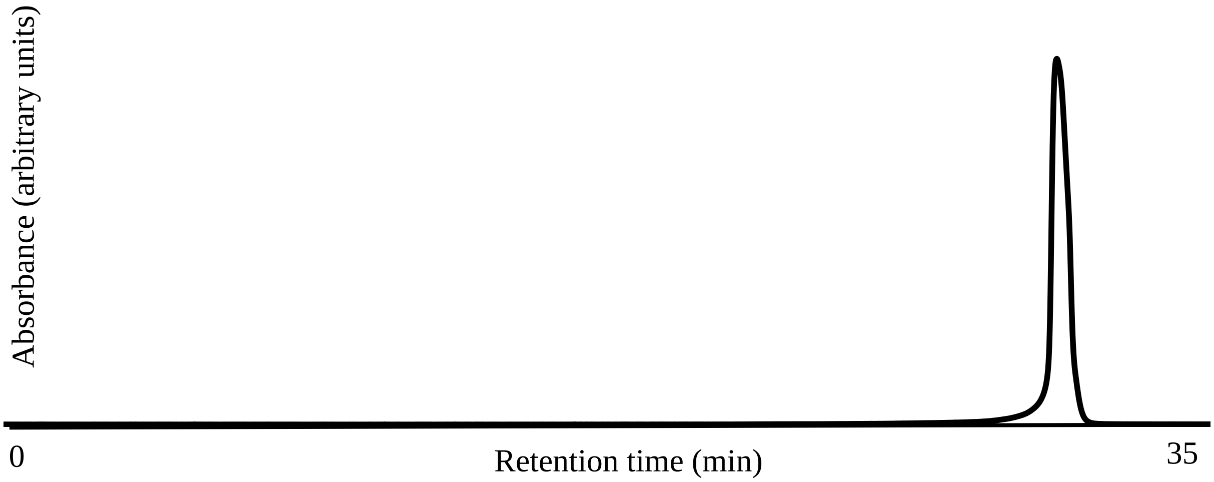
Absorbance (arbitrary units)
0
Retention time (min)
35

APPENDIX C

Table C.1. Water proton relaxation rate data for conjugate **2.13a**.

Trial 1

Concn (mM)	$1/T_1$ (s^{-1})	T_1 (s)
5.70	15.8	0.0633
2.85	7.84	0.128
1.43	4.44	0.225
0.713	2.64	0.379
0.000	0.259	3.87

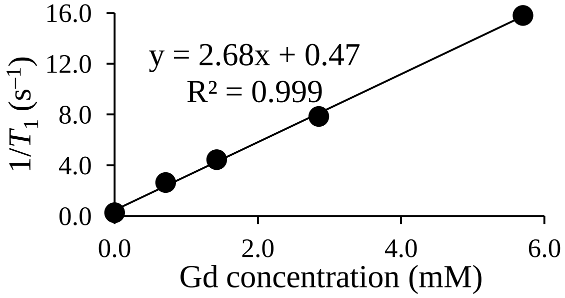

Trial 2

Concn (mM)	$1/T_1$ (s^{-1})	T_1 (s)
5.70	14.5	0.0692
2.85	7.73	0.129
1.43	3.88	0.258
0.713	2.62	0.382
0.000	0.262	3.81

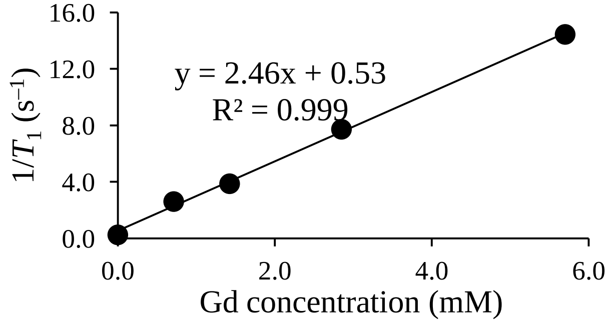

Trial 3

Concn (mM)	$1/T_1$ (s^{-1})	T_1 (s)
5.70	14.5	0.0690
2.85	7.75	0.129
1.43	3.94	0.254
0.713	2.63	0.381
0.000	0.262	3.81

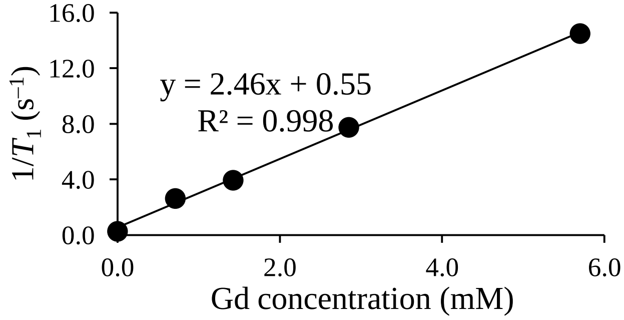

Table C.2. Water proton relaxation rate data for conjugate **2.13b**.

Trial 1

Concn (mM)	$1/T_1$ (s^{-1})	T_1 (s)
7.88	33.0	0.0303
3.94	16.5	0.0606
1.97	8.29	0.121
0.990	4.60	0.217
0.000	0.259	3.87

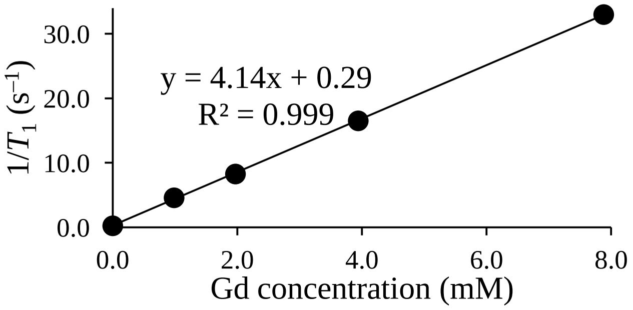

Trial 2

Concn (mM)	$1/T_1$ (s^{-1})	T_1 (s)
7.88	31.4	0.0319
3.94	14.8	0.0675
1.97	8.40	0.119
0.990	4.10	0.244
0.000	0.262	3.81

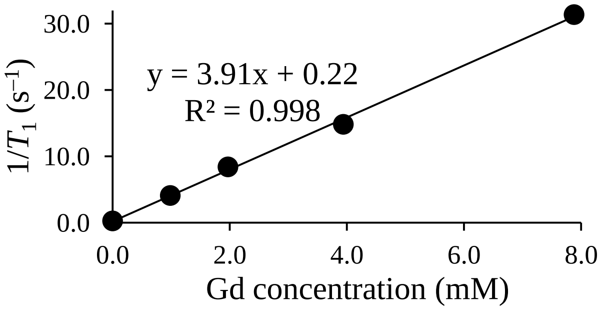

Trial 3

Concn (mM)	$1/T_1$ (s^{-1})	T_1 (s)
7.88	30.9	0.0324
3.94	14.8	0.0675
1.97	8.26	0.121
0.990	4.11	0.244
0.000	0.262	3.81

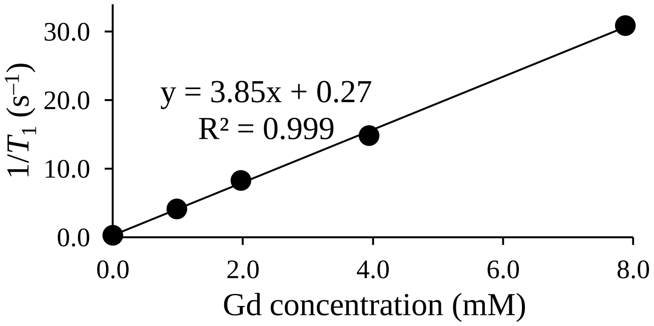

Table C.3. Water proton relaxation rate data for conjugate **2.13c**.

Trial 1

Concn (mM)	$1/T_1$ (s^{-1})	T_1 (s)
1.02	5.68	0.176
0.510	3.03	0.330
0.255	1.42	0.704
0.128	0.790	1.27
0.000	0.260	3.85

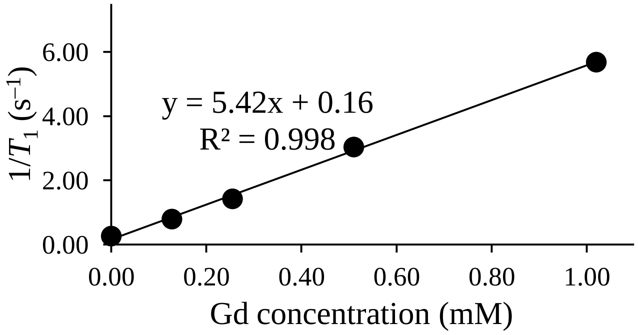

Trial 2

Concn (mM)	$1/T_1$ (s^{-1})	T_1 (s)
1.02	5.68	0.176
0.510	3.03	0.330
0.255	1.42	0.704
0.128	0.790	1.27
0.000	0.262	3.81

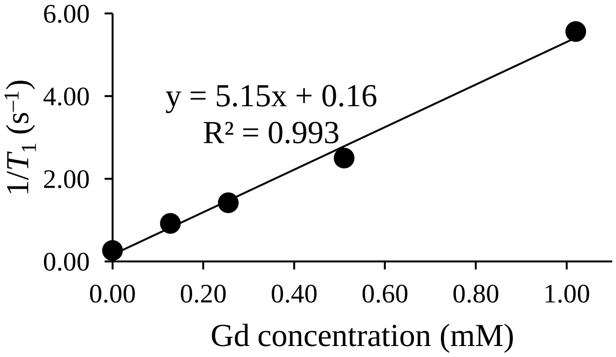

Trial 3

Concn (mM)	$1/T_1$ (s^{-1})	T_1 (s)
1.02	5.68	0.176
0.510	3.03	0.330
0.255	1.42	0.704
0.128	0.790	1.27
0.000	0.262	3.81

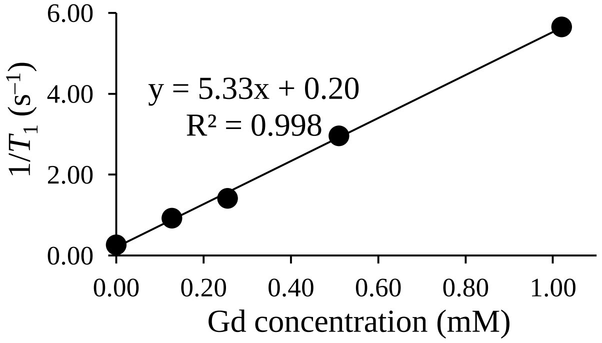

Table C.4. Water proton relaxation rate data for conjugate **2.13d**.

Trial 1

Concn (mM)	$1/T_1$ (s^{-1})	T_1 (s)
0.387	2.61	0.383
0.194	1.41	0.712
0.097	0.842	1.19
0.048	0.547	1.83
0.000	0.260	3.85

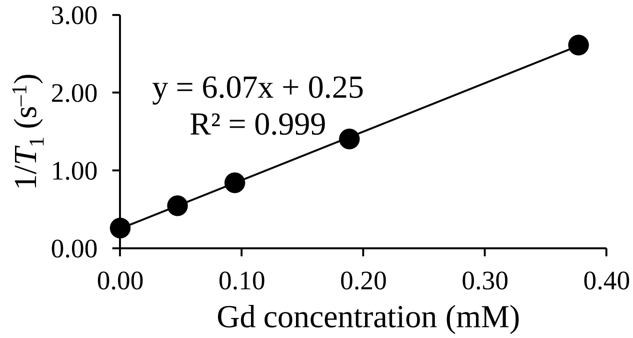

Trial 2

Concn (mM)	$1/T_1$ (s^{-1})	T_1 (s)
0.387	2.72	0.368
0.194	1.46	0.685
0.097	0.867	1.15
0.048	0.555	1.80
0.000	0.262	3.81

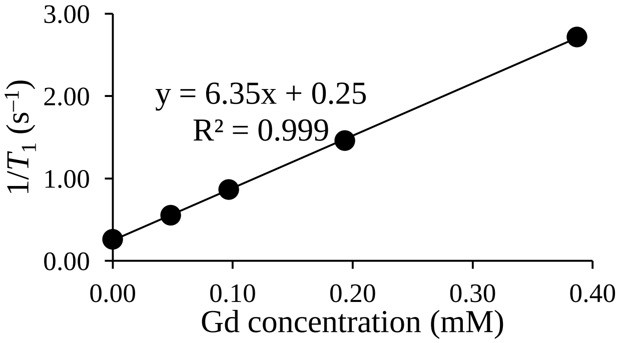

Trial 3

Concn (mM)	$1/T_1$ (s^{-1})	T_1 (s)
0.387	2.71	0.369
0.194	1.46	0.684
0.097	0.870	1.15
0.048	0.554	1.80
0.000	0.262	3.81

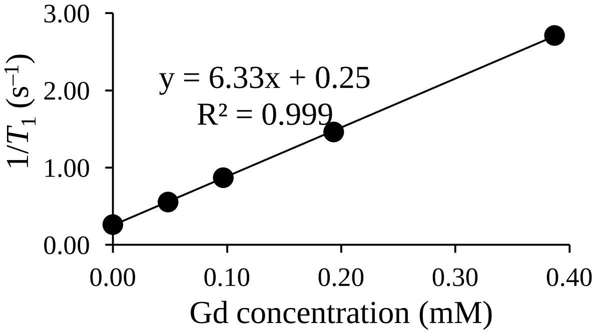

Table C.5. Variable-temperature ^{17}O NMR data for conjugate **2.13a**.

Temperature (°C)	linewidth at half height (Hz)	
	2.13a	**2.15a**
70	114.08	28.87
60	141.92	32.27
50	155.88	37.10
40	151.51	42.31
30	136.03	50.52
25	130.05	58.68

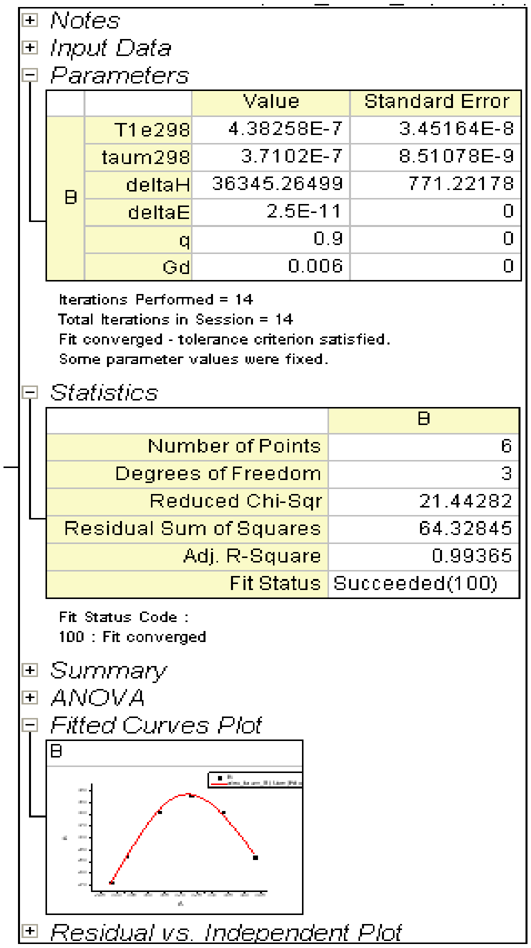

⊞ Notes
⊞ Input Data
⊟ Parameters

		Value	Standard Error
B	T1e298	4.38258E-7	3.45164E-8
	taum298	3.7102E-7	8.51078E-9
	deltaH	36345.26499	771.22178
	deltaE	2.5E-11	0
	q	0.9	0
	Gd	0.006	0

Iterations Performed = 14
Total Iterations in Session = 14
Fit converged - tolerance criterion satisfied.
Some parameter values were fixed.

⊟ Statistics

	B
Number of Points	6
Degrees of Freedom	3
Reduced Chi-Sqr	21.44282
Residual Sum of Squares	64.32845
Adj. R-Square	0.99365
Fit Status	Succeeded(100)

Fit Status Code :
100 : Fit converged

⊞ Summary
⊞ ANOVA
⊟ Fitted Curves Plot

⊞ Residual vs. Independent Plot

Table C.6. Variable-temperature ^{17}O NMR data for conjugate **2.13b**.

Temperature (°C)	linewidth at half height (Hz)	
	2.13b	**2.15b**
70	85.90	30.30
60	102.03	32.84
50	110.20	37.08
40	105.90	42.82
30	97.05	50.93
20	91.20	63.56

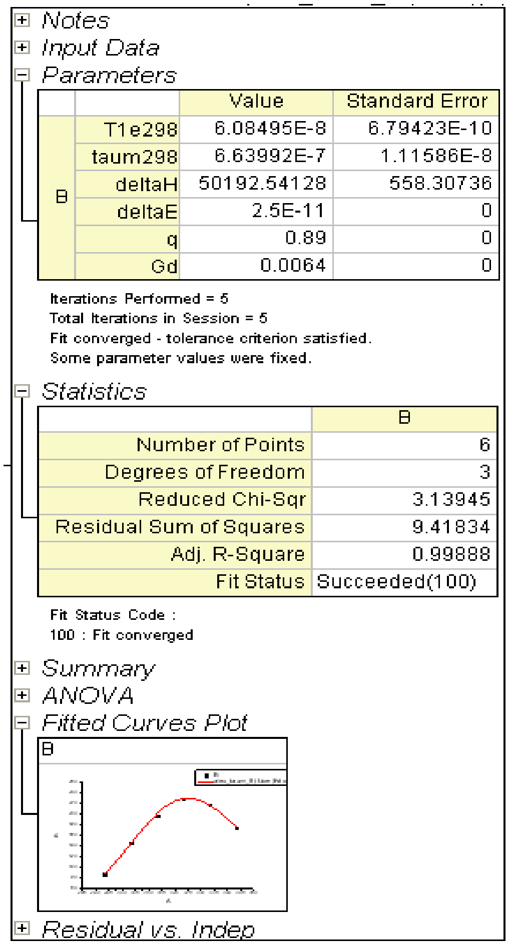
Notes
Input Data
Parameters

		Value	Standard Error
B	T1e298	6.08495E-8	6.79423E-10
	taum298	6.63992E-7	1.11586E-8
	deltaH	50192.54128	558.30736
	deltaE	2.5E-11	0
	q	0.89	0
	Gd	0.0064	0

Iterations Performed = 5
Total Iterations in Session = 5
Fit converged - tolerance criterion satisfied.
Some parameter values were fixed.

Statistics

	B
Number of Points	6
Degrees of Freedom	3
Reduced Chi-Sqr	3.13945
Residual Sum of Squares	9.41834
Adj. R-Square	0.99888
Fit Status	Succeeded(100)

Fit Status Code :
100 : Fit converged

Summary
ANOVA
Fitted Curves Plot
B
Residual vs. Indep

Table C.7. Variable-temperature ^{17}O NMR data for conjugate **2.13c**.

Temperature (°C)	linewidth at half height (Hz)	
	2.13c	**2.13c**
70	42.16	29.56
60	48.22	32.88
50	53.56	37.10
40	57.82	43.01
30	62.26	51.34
20	71.26	63.73

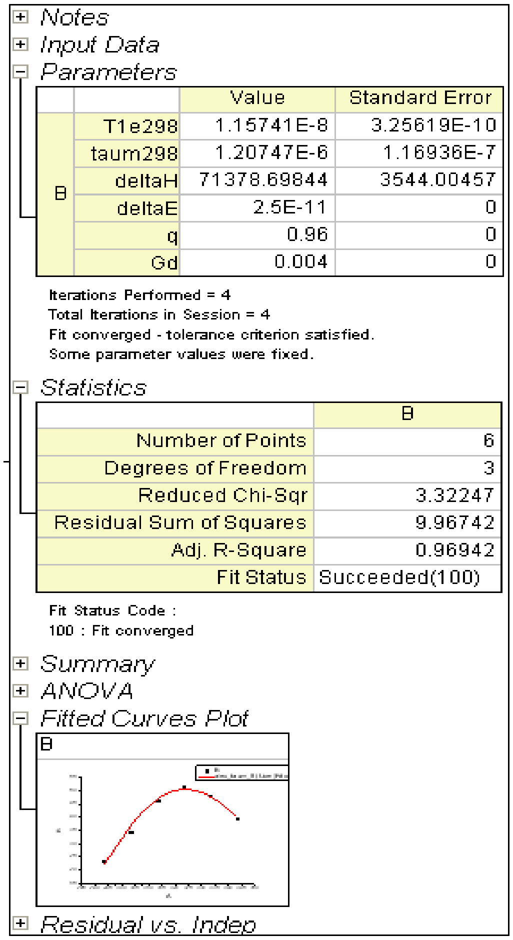

⊞ Notes
⊞ Input Data
⊟ Parameters

		Value	Standard Error
B	T1e298	1.15741E-8	3.25619E-10
	taum298	1.20747E-6	1.16936E-7
	deltaH	71378.69844	3544.00457
	deltaE	2.5E-11	0
	q	0.96	0
	Gd	0.004	0

Iterations Performed = 4
Total Iterations in Session = 4
Fit converged - tolerance criterion satisfied.
Some parameter values were fixed.

⊟ Statistics

	B
Number of Points	6
Degrees of Freedom	3
Reduced Chi-Sqr	3.32247
Residual Sum of Squares	9.96742
Adj. R-Square	0.96942
Fit Status	Succeeded(100)

Fit Status Code :
100 : Fit converged

⊞ Summary
⊞ ANOVA
⊟ Fitted Curves Plot

⊞ Residual vs. Indep

Table C.8. Variable-temperature ^{17}O NMR data for conjugate **2.13d**.

Temperature (°C)	linewidth at half height (Hz)	
	2.13d	**2.13d**
70	46.59	30.11
60	53.57	34.15
50	59.60	38.95
40	65.80	45.61
30	72.63	54.55
20	79.79	68.18

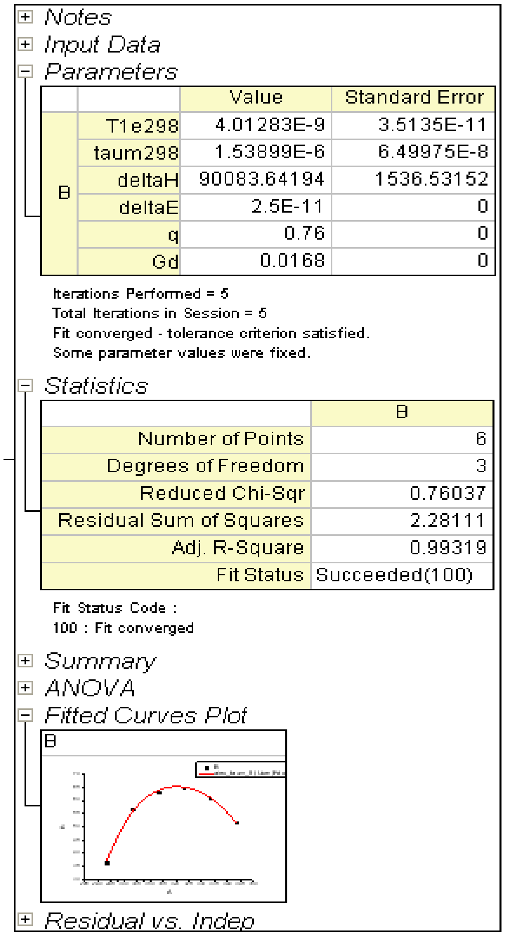

⊞ Notes

⊞ Input Data

⊟ Parameters

		Value	Standard Error
B	T1e298	4.01283E-9	3.5135E-11
	taum298	1.53899E-6	6.49975E-8
	deltaH	90083.64194	1536.53152
	deltaE	2.5E-11	0
	q	0.76	0
	Gd	0.0168	0

Iterations Performed = 5
Total Iterations in Session = 5
Fit converged - tolerance criterion satisfied.
Some parameter values were fixed.

⊟ Statistics

	B
Number of Points	6
Degrees of Freedom	3
Reduced Chi-Sqr	0.76037
Residual Sum of Squares	2.28111
Adj. R-Square	0.99319
Fit Status	Succeeded(100)

Fit Status Code :
100 : Fit converged

⊞ Summary

⊞ ANOVA

⊟ Fitted Curves Plot

⊞ Residual vs. Indep

Table C.9. Luminescence-decay rate data for conjugates **2.14a–d**.

Complex	Luminescence-decay rates (s^{-1})					
	Trial 1		Trial 2		Trial 3	
	in H_2O	in D_2O	in H_2O	in D_2O	in H_2O	in D_2O
2.14a	1.48	0.419	1.46	0.428	1.48	0.428
2.14b	1.46	0.427	1.48	0.434	1.47	0.432
2.14c	1.52	0.404	1.52	0.404	1.48	0.419
2.14d	1.33	0.422	1.32	0.422	1.39	0.421

2.13a

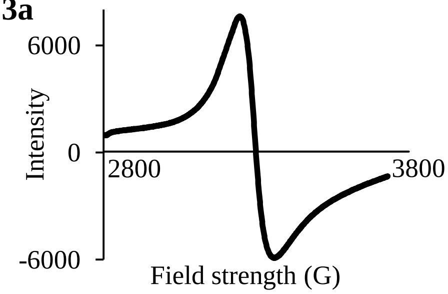

2.13b

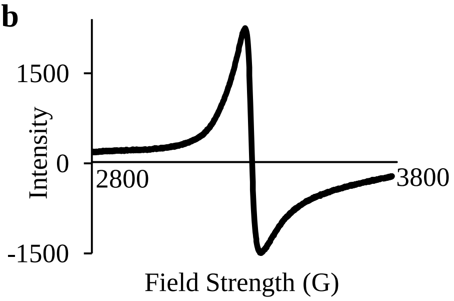

2.13c

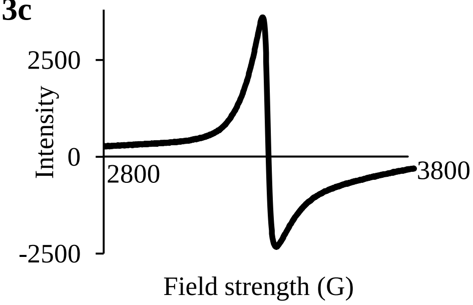

2.13d

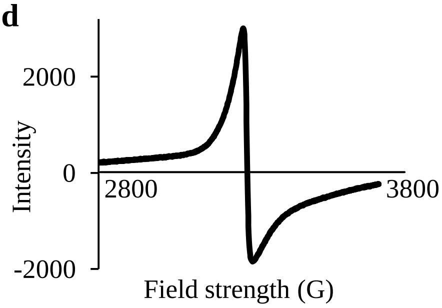

Table C.10. Peak-to-peak line widths, ΔH_{pp} obtained from EPR spectra for conjugates **2.13a–d**.

Complex	ΔH_{pp} (G)
2.13a	118
2.13b	53.8
2.13c	43.0
2.13d	33.2

Estimation of Rotational Correlation Time *(τ_R)*

To obtain an estimation of τ_R, equation 1 was used that relates observed relaxivity, r_1^{obs}, to inner- and outer-sphere relaxivities, r_1^{IS} and r_1^{OS}, respectively, at 1.4 T (60 MHz).

$$r_1^{obs} = r_1^{IS} + r_1^{OS} \qquad \text{equation 1}$$

Assuming that complexes **2.13a–d** behave similarly to small molecular contrast agents, r_1^{obs} is composed of approximately equal contributions from r_1^{IS} and r_1^{OS}.[8] Therefore, r_1^{IS} can be expressed as half of r_1^{obs} as shown in equation 2.

$$0.5r_1^{obs} = r_1^{IS} \qquad \text{equation 2}$$

The term r_1^{IS} is related to the number of coordinated water molecules (q), the longitudinal relaxation time of the coordinated water proton (T_{1m}), and the residence lifetime of the coordinated water molecule in the inner-sphere (τ_m, reciprocal of water-exchange rate, k_{ex}) as expressed in equation 3.

$$r_1^{IS} = \frac{q}{55{,}500}\left[\frac{1}{T_{1m} + \tau_m}\right] \qquad \text{equation 3}$$

Equations 2 and 3 can be combined to obtain equation 4, which enables the calculation of T_{1m} by substituting r_1^{obs}, τ_m, and q with values obtained experimentally for complexes **2.13a–d** (r_1^{obs} and τ_m) and **2.14a–d** (q).

$$T_{1m} = \frac{q}{27{,}750r_1^{obs}} - \tau_m \qquad \text{equation 4}$$

The term T_{1m} is composed of a dipole–dipole contribution (*DD)* and a scalar (*SC*) contribution to longitudinal proton relaxation as shown in equation 5.

$$\frac{1}{T_{1m}} = \frac{1}{T_1^{DD}} + \frac{1}{T_1^{SC}} \qquad \text{equation 5}$$

The scalar contribution to overall longitudinal proton relaxation is negligible at field strengths greater than 10 MHz.[8] Therefore, at field strengths above 10 MHz, the longitudinal proton relaxation becomes equal to the *DD* contribution that can be expressed as shown in equation 6.

$$\frac{1}{T_{1m}} = \frac{1}{T_1^{DD}} = \frac{2}{15}\left(\frac{\gamma_I^2 g^2 \mu_B^2}{r_{GdH}^6}\right) S(S+1) \left(\frac{\mu_0}{4\pi}\right)^2 \left(7\frac{\tau_{C2}}{1+\omega_S^2\tau_{C2}^2} + 3\frac{\tau_{C1}}{1+\omega_I^2\tau_{C1}^2}\right) \qquad \text{equation 6}$$

In equation 6, γ_I is the nuclear gyromagnetic ratio (2.67×10^8 s^{-1} T^{-1}), *g* is the electron *g*-factor obtained for complexes **2.13a–d** from EPR spectra, μ_B is the Bohr magneton (9.274×10^{-24} J T^{-1}), μ_0 is the vacuum permeability ($4\pi \times 10^{-7}$ T mA^{-1}), r_{GdH}, is the electron spin-proton distance (3.1×10^{-10} m, from reference 8 for DOTA-type Gd$^{\mathrm{III}}$-containing complexes), and *S* is the electron spin for Gd$^{\mathrm{III}}$ (3.5). Terms ω_S and ω_I are the electron and nuclear Larmor frequencies, respectively at magnetic field strength, *B* (1.4 T). ω_S and ω_I are related to γ_S (electron gyromagnetic ratio = 1.76×10^{11} s^{-1} T^{-1}), γ_I, and B as shown in equations 7 and 8.

$$\omega_S = \gamma_S B \qquad \text{equation 7}$$

$$\omega_I = \gamma_I B \qquad \text{equation 8}$$

Correlation times τ_{C1} and τ_{C2} are related to the rotational correlation time, τ_R, the residency lifetime of coordinated water, τ_m, longitudinal electron spin relaxation time, T_{1e}, and transverse electron spin relaxation time, T_{2e} as shown in equations 9 and 10.

$$\frac{1}{\tau_{C_2}} = \frac{1}{\tau_R} + \frac{1}{\tau_m} + \frac{1}{T_{2e}} \qquad \text{equation 9}$$

$$\frac{1}{\tau_{C_1}} = \frac{1}{\tau_R} + \frac{1}{\tau_m} + \frac{1}{T_{1e}} \qquad \text{equation 10}$$

T_{1e} (obtained from the fitting of ^{17}O NMR data) and T_{2e} (obtained from EPR spectra) for complexes **2.13a–d** were used in equations 9 and 10 that were combined with equation 6 to solve for τ_R for complexes **2.13a–d**.

Table C.11. Estimated T_{1m} and τ_R values for conjugates **2.13a–d**.

Complex	$T_{1m} \times 10^{-6}$ (s)	$\tau_R \times 10^{-12}$ (s)
2.13a	13	46
2.13b	2.9	79
2.13c	5.3	110
2.13d	7.4	220

Estimation of Relaxivity, r_1^{obs}, Based on τ_R

Estimated relaxivity values for complex **2.13a** were obtained using τ_R values from complexes **2.13a–d**, and τ_m and q values from complex **2.13a**: $\tau_m = 3.7 \times 10^{-7}$ s and $q = 0.9$. Values of τ_{C1} and τ_{C2} were calculated for **2.13a** by substituting τ_m, T_{1e}, and T_{2e} obtained for **2.13a** and τ_R from **2.13a–d**. The calculated τ_{C1} and τ_{C2} values together with other constants were used to calculate a value for T_{1m} using equation 6.

The calculated T_{1m} values for **2.13a** and fixed τ_m and q values were substituted in equation 3 to obtain r_1^{IS} that was in turn used in equation 2 to obtain r_1^{obs}, which are the expected relaxivity values for **2.13a** based on changes in τ_R associated with complexes **2.13a–d**.

Table C.12. Observed r_1 values for conjugates **2.13a–d** and estimated r_1 values for conjugate **2.13a** using τ_R values from conjugates **2.13a–d**.

Complex	Observed r_1 (mM^{-1} s^{-1})	Complex	Estimated r_1 (mM^{-1} s^{-1})
2.13a	2.5	**2.13a**	2.5
2.13b	4.0	**2.13a** with τ_R from **2.13b**	4.2
2.13c	5.3	**2.13a** with τ_R from **2.13c**	5.7
2.13d	6.3	**2.13a** with τ_R from **2.13d**	11

APPENDIX D

Permission for *Dalton Trans*. 2013, *42*, 6724–6727.

Date: Fri, 20 Dec 2013 09:44:12 +0000 [12/20/2013 04:44:12 AM EST]
From: CONTRACTS-COPYRIGHT (shared) <Contracts-Copyright@rsc.org>
To: 'buddhima@chem.wayne.edu' <buddhima@chem.wayne.edu>
Subject: RE: Reuse of my Dalton Trans. paper in my dissertation

Dear Buddhima

The Royal Society of Chemistry (RSC) hereby grants permission for the use of your paper(s) specified below in the printed and microfilm version of your thesis. You may also make available the PDF version of your paper(s) that the RSC sent to the corresponding author(s) of your paper(s) upon publication of the paper(s) in the following ways: in your thesis via any website that your university may have for the deposition of theses, via your university's Intranet or via your own personal website. We are however unable to grant you permission to include the PDF version of the paper(s) on its own in your institutional repository. The Royal Society of Chemistry is a signatory to the STM Guidelines on Permissions (available on request).

Please note that if the material specified below or any part of it appears with credit or acknowledgement to a third party then you must also secure permission from that third party before reproducing that material.

Please ensure that the thesis states the following:
Reproduced by permission of The Royal Society of Chemistry
and include a link to the paper on the Royal Society of Chemistry's website.
Please ensure that your co-authors are aware that you are including the paper in your thesis.

Regards
Gill Cockhead
Publishing Contracts & Copyright Executive
Royal Society of Chemistry,
Thomas Graham House,
Science Park, Milton Road,
Cambridge, CB4 0WF, UK
Tel +44 (0) 1223 432134
Follow the Royal Society of Chemistry:
www.rsc.org/follow<http://www.rsc.org/follow>
Winner of The Queen's Award for Enterprise, International Trade 2013

----Original Message-----

From: buddhima@chem.wayne.edu [mailto:buddhima@chem.wayne.edu]
Sent: 17 December 2013 00:25
To: CONTRACTS-COPYRIGHT (shared)
Subject: Reuse of my Dalton Trans. paper in my dissertation

Dear Mrs. Cockhead,

I am writing to ask for permission to use the following paper in my dissertation:

Modulating water-exchange rates of lanthanide(III)-containing polyaminopolycarboxylate-type complexes using polyethylene glycol Siriwardena-Mahanama, B. N.; Allen, M. J.* *Dalton Trans*. 2013, *42*, 6724–6727.
DOI: 10.1039/C3DT50885D
I am the author of the original work and I would like to use the entire article in my dissertation.
Also, I will not be translating and the format and distribution are given below.
Format: print and electronic
Distribution: about 10

Thank you,
Buddhima
Buddhima N. Siriwardena Mahanama
Prof. Matthew J. Allen's Research Group
Department of Chemistry
Wayne State University
5101 Cass Avenue
Detroit, MI 48202
Phone: 313-577-2042
E-mail: buddhima@chem.wayne.edu

Permission for *Molecules* 2013, *18*, 9352–9381.

Date: Mon, 23 Dec 2013 09:51:18 +0800 [12/22/2013 08:51:18 PM EST]
From: Molecules Editorial Office <molecules@mdpi.com>
To: buddhima@chem.wayne.edu
Reply-To: molecules@mdpi.com
Subject: Re: Reuse of my Molecules review article in my dissertation

Dear Dr. Siriwardena Mahanama,

Thank you very much for your request. As we are online journal, we follow the Creative Commons Attribution License 3.0. This means you may use these materials freely from our side, on condition that "proper
accreditation of the source and original publisher" is made.

Moreover, the copyright still stays with the authors, thus you are free to use it. We wish you success in the dissertation. Please feel free to let us know if we can provide any further assistance.

Kind regards,
Jessica Bai
Assistant Editor
Molecules (http://www.mdpi.com/journal/molecules)

Ms. Jessica Bai, M. Sc.
MDPI Branch Office, Beijing
Ruidu International Center, No. 1 Cuijingbeili, Tongzhou
District, Beijing 101121, China
E-mail: jessica.bai@mdpi.com
Skype: jessica.bai.mdpi
Tel./Fax: +86 10 8152 1170

MDPI AG
Molecules Editorial Office
Klybeckstrasse 64, 2nd Floor, Basel CH-4057, Switzerland
Tel. +41 61 683 77 34; Fax: +41 61 302 89 18
E-Mail: molecules@mdpi.com
http://www.mdpi.com/journal/molecules

On 12/20/2013 11:15 PM, buddhima@chem.wayne.edu wrote:

Hi!

I am writing to ask for permission to use the following review article in my dissertation:

Strategies for Optimizing Water-Exchange Rates of Lanthanide-Based Contrast Agents for Magnetic Resonance Imaging, Siriwardena-Mahanama, B. N.; Allen, M. J.* Molecules 2013, *18* (*8*), 9352–9381.
DOI: 10.3390/molecules18089352

I would like to use the entire article in my dissertation. Also, I will not be translating and the format and distribution are given below.
Format: print and electronic
Distribution: about 10

Thank you,
Buddhima
Buddhima N. Siriwardena Mahanama
Prof. Matthew J. Allen's Research Group
Department of Chemistry
Wayne State University
5101 Cass Avenue
Detroit, MI 48202
Phone: 313-577-2042
E-mail: buddhima@chem.wayne.edu

REFERENCES

(1) Hermann, P.; Kotek, J.; Kubíček, V.; Lukeš, I. *Dalton Trans.* **2008**, 3027–3047.

(2) Caravan, P. *Chem. Soc. Rev.* **2006**, *35*, 512–523.

(3) Terreno, E.; Castelli, D.D.; Viale, A.; Aime, S. *Chem. Rev*. **2010**, *110*, 3019–3042.

(4) Laurent, S.; Henoumont, C.; Vander Elst, L.; Muller, R.N. *Eur. J. Inorg. Chem*. **2012**, *2012*, 1889–1915.

(5) Dastrù, W.; Longo, D.; Aime, S. *Drug Discov. Today* **2011**, *8*, e109–e115.

(6) Weise, G.; Basse-Lüsebrink, T.C.; Kleinschnitz, C.; Kampf, T.; Jakob, P.M.; Stoll, G. *PLoS One* **2011**, *6*, e28143.

(7) Caravan, P.; Farrar, C.T.; Frullano, L.; Uppal, R. *Contrast Media Mol. Imaging* **2009**, *4*, 89–100.

(8) Caravan, P.; Ellison, J.J.; McMurry, T.J.; Lauffer, R.B. *Chem. Rev.* **1999**, *99*, 2293–2352.

(9) *The Chemistry of Contrast Agents in Medical Magnetic Resonance Imaging*, 2nd ed.; Merbach, A.E.; Helm, L.; Tóth, É.; Eds.; John Wiley & Sons, Ltd.: Chichester, U.K.; 2013.

(10) Ruloff, R.; Tóth, É.; Scopelliti, R.; Tripier, R.; Handel, H.; Merbach, A.E. *Chem. Commun*. **2002**, 2630–2631.

(11) Aime, S.; Barge, A.; Botta, M.; Parker, D.; De Sousa, A.S. *J. Am. Chem. Soc.* **1997**, *119*, 4767–4768.

(12) Woods, M.; Woessner, D.E.; Sherry, A.D. *Chem. Soc. Rev.* **2006**, *35*, 500–511.

(13) Viswanathan, S.; Kovacs, Z.; Green, K.N.; Ratnakar, S.J.; Sherry, A.D. *Chem. Rev.* **2010**, *110*, 2960–3018.

(14) Dorazio, S.J.; Morrow, J.R. *Eur. J. Inorg. Chem.* **2012**, *2012*, 2006–2014.

(15) Mani, T.; Tircsó, G.; Togao, O.; Zhao, P.; Soesbe, T.C.; Takahashi, M.; Sherry, A.D. *Contrast Media Mol. Imaging* **2009**, *4*, 183–191.

(16) Terreno, E.; Castelli, D.D.; Cravotto, G.; Milone, L.; Aime, S. *Invest. Radiol.* **2004**, *39*, 235–243.

(17) Opina, A.C.L.; Wu, Y.; Zhao, P.; Kiefer, G.; Sherry, A.D. *Contrast Media Mol. Imaging* **2011**, *6*, 459–464.

(18) Powell, D.H.; Favre, M.; Graeppi, N.; Dhubhghaill, O.M.N.; Pubanz, D.; Merbach, A.E. *J. Alloys Compd*. **1995**, *225*, 246–252.

(19) Aime, S.; Botta, M.; Fasano, M.; Crich, S.G.; Terreno, E. *Coord. Chem. Rev.* **1999**, *185–186*, 321–333.

(20) Helm, L.; Nicolle, G.M.; Merbach, A.E. *Adv. Inorg. Chem.* **2005**, *57*, 327–379.

(21) Aime, S.; Botta, M.; Fasano, M.; Terreno, E. *Acc. Chem. Res.* **1999**, *32*, 941–949.

(22) Sherry, A.D.; Wu, Y. *Curr. Opin. Chem. Biol.* **2013**, *17*, 1–8.

(23) Helm, L.; Merbach, A.E. *Chem. Rev.***2005**, *105*, 1923–1959.

(24) Cossy, C.; Helm, L.; Merbach, A.E. *Inorg. Chem.* **1988**, *27*, 1973–1979.

(25) Graeppi, N.; Powell, D.H.; Laurenczy, G.; Zékány, L.; Merbach, A.E. *Inorg. Chim. Acta* **1995**, *235*, 311–326.

(26) Pubanz, D.; González, G.; Powell, D.H.; Merbach, A.E. *Inorg. Chem.* **1995**, *34*, 4447–4453.

(27) Zhang, S.; Sherry, A.D. *J. Solid State Chem.* **2003**, *171*, 38–43.

(28) Cohen, S.M.; Xu, J.; Radkov, E.; Raymond, K.N.; Botta, M.; Barge, A.; Aime, S. *Inorg. Chem.* **2000**, *39*, 5747–5756.

(29) Thompson, M.K.; Botta, M.; Nicolle, G.; Helm, L.; Aime, S.; Merbach, A.E; Raymond, K.N. *J. Am.Chem. Soc.* **2003**, *125*, 14274–14275.

(30) Pierre, V.C.; Botta, M.; Aime, S.; Raymond, K.N. *J. Am.Chem. Soc.* **2006**, *128*, 5344–5345.

(31) Powell, D.H.; Dhubhghaill, O.M.N.; Pubanz, D.; Helm, L.; Lebedev, Y.S.; Schlaepfer, W.; Merbach, A.E. *J. Am. Chem. Soc.* **1996**, *118*, 9333−9346.

(32) Aime, S.; Botta, M.; Frullano, L.; Crich, S.G.; Giovenzana, G.; Pagliarin, R.; Palmisano, G.; Sirtori, F.R.; Sisti, M. *J. Med. Chem*. **2000**, *43*, 4017–4024.

(33) Micskei, K.; Powell, D.H.; Helm, L.; Brücher, E.; Merbach, A.E. *Magn. Reson. Chem.* **1993**, *31*, 1011–1020.

(34) Tirscó, G.; Kálmán, F.K.; Pál, R.; Bányai, I.; Varga, T.R.; Király, R.; Lázár, I.; Québatte, L.; Merbach, A.E.; Tóth, É.; *et al. Eur. J. Inorg. Chem*. **2012**, *2012*, 2062–2073.

(35) Mato-Iglesias, M.; Platas-Iglesias, C.; Djanashvili, K.; Peters, J.A.; Tóth, É.; Balogh, E.; Muller, R.N.; Vander Elst, L.; De Blas, A.; Rodríguez-Blas, T. *Chem. Commun*. **2005**, 4729–4731.

(36) Balogh, E.; Mato-Iglesias, M.; Platas-Iglesias, C.; Tóth, É.; Djanashvili, K.; Peters, J.A.; De Blas, A.; Rodríguez-Blas, T. *Inorg. Chem.* **2006**, *45*, 8719–8728.

(37) Pálinkás, Z.; Roca-Sabio, A.; Mato-Iglesias, M.; Esteban-Gómez, D.; Platas-Iglesias, C.; de Blas, A.; Rodríguez-Blas, T.; Tóth, É. *Inorg. Chem.* **2009**, *48*, 8878–8889.

(38) Botteman, F.; Nicolle, G.M.; Vander Elst, L.; Laurent, S.; Merbach, A.E.; Muller, R.N. *Eur. J. Inorg. Chem.* **2002**, *2002*, 2686–2693.

(39) Tóth, É.; Burai, L.; Brücher, E.; Merbach, A.E. *J. Chem. Soc., Dalton Trans.* **1997**, 1587–1594.

(40) Zhang, S.; Merritt, M.; Woessner, D.E.; Lenkinski, R.E.; Sherry, A.D. *Acc. Chem. Res.* **2003**, *36*, 783–790.

(41) Lebdušková, P.; Hermann, P.; Helm, L.; Tóth, É.; Kotek, J.; Binnemans, K.; Rudovský, J.; Lukeš, I.; Merbach, A.E. *Dalton Trans*. **2007**, 493–501.

(42) Polasek, M.; Caravan, P. *Inorg. Chem.* **2013**, *52*, 4084–4096.

(43) Jászberényi, Z.; Tóth, É.; Kálai, T.; Király, R.; Burai, L.; Brücher, E.; Merbach, A.E.; Hideg, K. *Dalton Trans.* **2005**, 694–701.

(44) Rojas-Quijano, F.A.; Benyó, E.T.; Tirscó, G.; Kálmán, F.K.; Baranyai, Z.; Aime, S.; Sherry, A.D.; Kovács, Z. *Chem. Eur. J.* **2009**, *15*, 13188–13200.

(45) Terreno, E.; Boniforte, P.; Botta, M.; Fedeli, F.; Milone, L.; Mortillaro, A.; Aime, S. *Eur. J. Inorg. Chem.* **2003**, *2003*, 3530–3533.

(46) Botta, M.; Aime, S.; Barge, A.; Bobba, G.; Dickins, R.S.; Parker, D.; Terreno, E. *Chem. Eur. J.* **2003**, *9*, 2102–2109.

(47) Ratnakar, S.J.; Woods, M.; Lubag, A.J.M.; Kovács, Z.; Sherry A.D. *J. Am. Chem. Soc.* **2008**, *130*, 6–7.

(48) Viswanathan, S.; Ratnakar, S.J.; Green, K.N.; Kovacs, Z.; De León-Rodríguez, L.M; Sherry, A.D. *Angew. Chem. Int. Ed.* **2009**, *48*, 9330–9333.

(49) Green, K.N.; Viswanathan, S.; Rojas-Quijano, F.A.; Kovacs, Z.; Sherry, A.D. *Inorg. Chem.* **2011**, *50*, 1648–1655.

(50) Jászberényi, Z.; Sour, A.; Tóth, É.; Benmelouka, M.; Merbach, A.E. *Dalton Trans.* **2005**, 2713–2719.

(51) Congreve, A.; Parker, D.; Gianolio, E.; Botta, M. *Dalton Trans.* **2004**, 1441–1445.

(52) Tóth, É.; Pubanz, D.; Vauthey, S.; Helm, L.; Merbach, A.E. *Chem. Eur. J.* **1996**, *2*, 1607–1615.

(53) Tei, L.; Gugliotta, G.; Baranyai, Z.; Botta, M. *Dalton Trans.* **2009**, 9712–9714.

(54) Nonat, A.; Giraud, M.; Gateau, C.; Fries, P.H.; Helm, L.; Mazzanti, M. *Dalton Trans.* **2009**, 8033–8046.

(55) Laus, S.; Ruloff, R.; Tóth, É.; Merbach, A.E. *Chem. Eur. J.* **2003**, *9*, 3555–3566.

(56) Yerly, F.; Hardcastle, K.I.; Helm, L.; Aime, S.; Botta, M.; Merbach, A.E. *Chem. Eur. J.* **2002**, *8*, 1031–1039.

(57) Laurent, S.; Botteman, F.; Vander Elst, L.; Muller, R.N. *MAGMA* **2004**, *16*, 235–245.

(58) Forgács, A.; Giovenzana, G.B.; Botta, M.; Brücher, E.; Tóth, I.; Baranyai, Z. *Eur. J. Inorg. Chem.* **2012**, *2012*, 2074–2086.

(59) Kotek, J.; Lebdušková, P.; Hermann, P.; Vander Elst, L.; Muller, R.N.; Geraldes, C.F.G.C.; Maschmeyer, T.; Lukeš, I.; Peters, J.A. *Chem. Eur. J.* **2003**, *9*, 5899–5915.

(60) Tei, L.; Baranyai, Z.; Cassino, C.; Fekete, M.; Kálmán, F.K.; Botta, M. *Dalton Trans.* **2012**, *41*, 12797–12806.

(61) Port, M.; Raynal, I.; Vander Elst, L.; Muller, R.N.; Dioury, F.; Ferroud, C.; Guy, A. *Contrast Med. Mol. Imaging* **2006**, *1*, 121–127.

(62) Roca-Sabio, A.; Bonnet, C.S.; Mato-Iglesias, M.; Esteban-Gómez, D.; Tóth, É.; de Blas, A.; Rodríguez-Blas, T.; Platas-Iglesias, C. *Inorg. Chem.* **2012**, *51*, 10893–10903.

(63) Aime, S.; Barge, A.; Batsanov, A.S.; Botta, M.; Castelli, D.D.; Fedeli, F.; Mortillaro, A.; Parker, D.; Puschmann, H. *Chem. Commun.* **2002**, 1120–1121.

(64) Zhang, S.; Jiang, X.; Sherry, A.D. *Helv. Chim. Acta* **2005**, *88*, 923–935.

(65) Aime, S.; Barge, A.; Bruce, J.I.; Botta, M.; Howard, J.A.K.; Moloney, J.M.; Parker, D.; de Sousa, A.S.; Woods, M. *J. Am. Chem. Soc.***1999**, *121*, 5762–5771.

(66) Zhang, S.; Wu, K.; Sherry, A.D. *Invest. Radiol.* **2001**, *36*, 82–86.

(67) Thompson, M.K.; Doble, D.M.J.; Tso, L.S.; Barra, S.; Botta, M.; Aime, S.; Raymond, K.N. *Inorg. Chem.* **2004**, *43*, 8577–8586.

(68) Doble, D.M.J.; Botta, M.; Wang, J.; Aime, S.; Barge, A.; Raymond K.N. *J. Am. Chem. Soc.* **2001**, *123*, 10758–10759.

(69) Dunand, F.A.; Aime. S.; Merbach, A.E. *J. Am. Chem. Soc.* **2000**, *122*, 1506–1512.

(70) Zhang, S.; Kovacs, Z.; Burgess, S.; Aime, S.; Terreno, E.; Sherry, A.D. *Chem. Eur. J.* **2001**, *7*, 288–296.

(71) Rudovský, J.; Cígler, P.; Kotek, J.; Hermann, P.; Vojtíšek, P.; Lukeš, I.; Peters, J.A.; Vander Elst, L.; Muller, R.N. *Chem. Eur. J.* **2005**, *11*, 2373–2384.

(72) Rudovský, J.; Kotek, J.; Hermann, P.; Lukeš, I.; Mainero, V.; Aime, S. *Org. Biomol. Chem.* **2005**, *3*, 112–117.

(73) Rodríguez-Rodríguez, A.; Esteban-Gómez, D.; de Blas, A.; Rodríguez-Blas, T.; Fekete, M.; Botta, M.; Tripier, R.; Platas-Iglesias, C. *Inorg. Chem.* **2012**, *51*, 2509–2521.

(74) Woods, M.; Aime, S.; Botta, M.; Howard, J.A.K.; Moloney, J.M.; Navet, M.; Parker, D.; Port, M.; Rousseaux, O. *J. Am. Chem. Soc.* **2000**, *122*, 9781–9792.

(75) Woods, M.; Kovacs, Z.; Kiraly, R.; Brücher, E.; Zhang, S.; Sherry, A.D. *Inorg. Chem.* **2004**, *43*, 2845–2851.

(76) Woods, M.; Kovacs, Z.; Zhang, S.; Sherry, A.D. *Angew. Chem. Int. Ed.* **2003**, *42*, 5889–5892.

(77) Pollet, R.; Nair, N.N.; Marx, D. *Inorg. Chem.* **2011**, *50*, 4791–4797.

(78) Castelli, D.D.; Caligara, M.C.; Botta, M.; Terreno, E.; Aime, S. *Inorg. Chem.* **2013**, *52*, 7130–7138.

(79) Aime, S.; Barge, A.; Botta, M.; De Sousa, A.S.; Parker, D. *Angew. Chem. Int. Ed.* **1998**, *37*, 2673–2675.

(80) Miller, K.J.; Saherwala, A.A.; Webber, B.C.; Wu, Y.; Sherry, A.D.; Woods, M. *Inorg. Chem.* **2010**, *49*, 8662–8664.

(81) Zhang, S.; Wu, K.; Biewer, M.C.; Sherry, A.D. *Inorg. Chem*. **2001**, *40*, 4284–4290.

(82) Marques, M.P.M.; Geraldes, C.F.G.C.; Sherry, A.D.; Merbach, A.E.; Powell, H.; Pubanz, D.; Aime, S.; Botta, M. *J. Alloy. Compd.* **1995**, *225*, 303–307.

(83) Ranganathan, R.S.; Fernandez, M.E.; Kang, S.I.; Nunn, A.D.; Ratsep, P.C.; Pillai, K.M.; Zhang, X.; Tweedle, M.F. *Invest. Radiol.* **1998**, *33*, 779–797.

(84) Rudovský, J.; Botta, M.; Hermann, P.; Koridze, A.; Aime, S. *Dalton Trans.* **2006**, 2323–2333.

(85) Tei , L.; Gugliotta, G.; Avedano, S.; Giovenzana, G.B.; Botta, M. *Org. Biomol. Chem.* **2009**, *7*, 4406–4414.

(86) Andrews, M.; Amoroso, A.J.; Harding, L.P.; Pope, S.J.A. *Dalton Trans.* **2010**, *39*, 3407–3411.

(87) Bünzli, J.-C.G. *Acc. Chem. Res.* **2006**, *39*, 53–61.

(88) Belcheva, N.; Baldwin, S.P.; Saltzman, W.M. *J. Biomater. Sci. Polym. Ed.* **1998**, *9*, 207–226.

(89) Belcheva, N.; Woodrow-Mumford, K.; Mahoney, M.J.; Saltzman, W.M. *Bioconjugate Chem.* **1999**, *10*, 932–937.

(90) Lee, J.H.; Lee, H.B.; Andrade J.D. *Prog. Poly. Sci.* **1995**, *20*, 1043–1079.

(91) Still, W.C.; Kahn, M.; Mitra, A. *J. Org. Chem.* **1978**, *43*, 2923–2925.

(92) Fanning, A.-M.; Plush, S.E.; Gunnlaugsson, T. *Chem. Commun.* **2006**, 3791–3793.

(93) De León-Rodríguez, L.M.; Kovacs, Z.; Esqueda-Olivaa, A.C.; Miranda-Olveraa, A.D. *Tetrahedron Lett.* **2006**, *47*, 6937–6940.

(94) Kovacs, Z.; Sherry, A.D. *Synthesis* **1997**, *7*, 759–763.

(95) Dadabhoy, A.; Faulkner, S.; Sammes, P.G. *J. Chem. Soc., Perkin Trans. 2* **2002**, 348–357.

(96) Avedano, S.; Tei, L.; Lombardi, A.; Giovenzana, G.B.; Aime, S.; Longo, D.; Botta, M. *Chem. Commun.* **2007**, 4726–4728.

(97) Aime, S.; Botta, M.; Bruce, J.I.; Mainero, V.; Parker, D.; Terreno, E. *Chem. Commun.* **2001**, 115–116.

(98) Caravan, P.; *Acc. Chem. Res.* **2009**, *42*, 851–862.

(99) Torres, S.; Martins, J.A.; André, J.P.; Geraldes, C.F.G.C.; Merbach, A.E.; Tóth, É. *Chem Eur. J.* **2006**, *12*, 940–948.

(100) Manus, L.M.; Strauch, R.C.; Hung, A.H.; Eckermann, A.L.; Meade, T.J. *Anal. Chem.* **2012**, *84*, 6278–6287.

(101) Ali, M.M.; Liu, G.; Shah, T.; Flask, C.A.; Pagel, M.D. *Acc. Chem. Res.* **2009**, *42*, 915–924.

(102) Aime, S.; Botta, M.; Fasano, M.; Terreno, E. *Chem. Soc. Rev.* **1998**, *27*, 19–29.

(103) Que, E.L.; Chang, C.J. *Chem. Soc. Rev.* **2010**, *39*, 51–60.

(104) Thompson, A.L.; Parker, D.; Fulton, D.A.; Howard, J.A.K.; Pandya, S.U.; Puschmann, H.; Senanayake, K.; Stenson, P.A.; Badari, A; Botta, M.; Avedano, S.; Aime, S. Dalton Trans. 2006, 5605–5616.

(105) Pierre, V.C.; Botta, M.; Aime, S.; Raymond, K.N. *Inorg. Chem.* **2006**, *45*, 8355–8364.

(106) Werner, E.J.; Kozhukh, J.; Botta, M.; Moore, E.G.; Avedano, S.; Aime, S.; Raymond, K.N. *Inorg. Chem.* **2009**, *48*, 277–286.

(107) Garcia, J.; Neelavalli, J.; Haacke, E. M.; Allen, M. J. *Chem. Commun.* **2011**, *47*,12858–12860.

(108) Supkowski, R.M.; Horrocks Jr., W.D. *Inorg. Chim. Acta* 2002, 340, 44–4.

(109) Caravan, P.; Cloutier, N.J.; Greenfield, M.T.; McDermid, S.A.; Dunham, S.U.; Butle, J.W.M.; Amedio Jr., J.C.; Looby, R.J.; Supkowski, R.M.; Horrocks Jr., W.D.; McMurry, T.J.; Lauffer, R.B. J. Am. Chem. Soc. 2002, 124, 3152–3162.

ABSTRACT

MODULATION OF WATER-EXCHANGE RATES OF LANTHANIDE(III)-CONTAINING COMPLEXES USING POLYETHYLENE GLYCOL

by

BUDDHIMA N. SIRIWARDENA-MAHANAMA

May 2014

Advisor: Dr. Matthew J. Allen

Major: Chemistry

Degree: Doctor of Philosophy

A modular system of lanthanide(III)-containing polyethylene glycol (PEG) conjugates was synthesized and characterized to investigate the influence of length and density of PEG on water-exchange rates of lanthanide(III)-containing complexes. The water-exchange rates of lanthanide(III)-containing complexes contribute to the efficiency of these complexes as T_1-shortening and paramagnetic chemical exchange saturation transfer (PARACEST) contrast agents for magnetic resonance imaging (MRI). Because the mechanism of these two MRI methods is vastly different, there is a need to tune the water-exchange rates of lanthanide(III)-containing complexes over a broad range: towards fast rates (10^8 s^{-1}) for T_1-shortening agents and slow rates (10^3 s^{-1}) for PARACEST agents. As a result, extensive research efforts have contributed to tuning water-exchange rates of both types of contrast agents using coordination-chemistry-based strategies. These studies reveal that small modifications in the structure of lanthanide(III)-containing complexes lead to considerable changes in water-exchange rates. This thesis tests the hypothesis that hydrophilic PEG alters the accessibility of bulk water and the extent of hydrogen bonding between lanthanide(III)-coordinated and bulk water. To test this hypothesis, a PEG-based lanthanide(III)-containing model system was designed and synthesized

to investigate the influence of length and density of PEG on the water-exchange rates of lanthanide(III)-containing complexes. Properties of the new complexes that are relevant to MRI, including water-exchange rates, were determined using relaxometric and spectroscopic techniques. The modular lanthanide(III)-containing system designed to investigate the influence of length of PEG demonstrated that PEG is able to tune water-exchange rates of lanthanide(III)-containing polyaminopolycarboxylate-type complexes toward slower rates. The ability of PEG to tune water-exchange rates toward slower rates as a function of the length of PEG is likely due to the variation in extent of hydrogen bonding between coordinated and bulk water. These findings provide insight into the influence of length and density of PEG on water-exchange rate and contrast agent efficiency and are expected to be useful in the design of contrast agents with optimum water-exchange rates.

AUTOBIOGRAPHICAL STATEMENT

Education

Wayne State University, Detroit, MI, USA: Chemistry, Ph.D. 2008–2014
University of Colombo, Colombo 3, Sri Lanka: Chemistry, B.Sc. 2002–2006

Research Experience

Wayne State University	May 2009–May 2014	(Graduate Student)

Advisor: Prof. Matthew J. Allen
Modulation of water-exchange rates of lanthanide(III)-containing complexes using polyethylene glycol

University of Colombo	August 2005–August 2006	(Undergraduate)

Advisor: Prof. Dhammike P. Dissanayake
Oxidation of halogen-containing volatile organic compounds

Awards

Best Poster Award, The Midland Section of the American Chemical Society Fall Scientific Meeting: October 2013
Departmental Citation for Excellence in Teaching Service, Wayne State University: April 2012

Professional Affiliations

American Chemical Society—Member	2012–Present
Phi Lambda Upsilon (Chemistry Honors Society)	2010–Present
Chemical Society, University of Colombo—Assistant Secretary	2006–2007
Chemical Society, University of Colombo—Member	2004–2006
The Chartered Institute of Marketing, UK—Member	2004–2007

Publications

Siriwardena-Mahanama, B. N.; Allen, M. J. *Dalton Trans*. **2013,** *42,* 6724–6727.
Siriwardena-Mahanama, B. N.; Allen, M. J. *Molecules* **2013,** *18, 9352–9381*.
Averill, D. J.; Garcia, J.; **Siriwardena-Mahanama, B. N.**;* Vithanarachchi, S. M.; Allen, M. J. *J. Vis. Exp.* **2011,** *53,* e2844. (* co-first author)

Presentations/Conferences Attended

The Midland Section of the American Chemical Society Fall Scientific Meeting. Delta College, Midland, MI. October 5, 2013; Poster.
15th Annual Chemistry Graduate Research Symposium 2013. Wayne State University, Detroit, MI. September 28, 2013; Poster.
Ohio Inorganic Weekend 2012. Wayne State University, Detroit, MI. October 19–20, 2012; Poster.
14th Annual Chemistry Graduate Research Symposium 2012. Wayne State University, Detroit, MI. October 13, 2012; Poster.
244thAmerican Chemical Society National Meeting & Exposition. Philadelphia, PA. August 19–23, 2012; Poster.
Proteases and Cancer Program Annual Retreat 2011. Wayne State University, Detroit, MI. December 1, 2011; Poster.
Ohio Inorganic Weekend 2011. University of Cincinnati, Cincinnati, OH. October 28–29, 2011; Talk.
Schaap Chemistry Symposium. Wayne State University, Detroit, MI. September 17, 2011; Poster.
Ohio Inorganic Weekend 2010. The Ohio State University, Columbus, OH. October 29–30, 2010; Poster.
12th Annual Chemistry Graduate Research Symposium 2010. Wayne State University, Detroit, MI. October 9, 2010; Poster.
Ohio Inorganic Weekend 2009. Case Western Reserve University, Cleveland, OH. November 13–14, 2009; Poster.
11th Annual Chemistry Graduate Research Symposium 2009. Wayne State University, Detroit, MI. October 3, 2009; Poster.